Climate Change Impacts on River Floods: Uncertainty and Adaptation

Lu Wang

Climate Change Impacts on River Floods: Uncertainty and Adaption

Proefschrift

ter verkrijging van de graad van doctor
aan de Technische Universiteit Delft,
op gezag van de Rector Magnificus prof. ir. K.C.A.M. Luyben,
voorzitter van het College voor Promoties,
in het openbaar te verdedigen op donderdag 30 April 2015 om 12.30 uur

door

Lu Wang

Master of Science in Hydrology and Water Resources Engineering
Hohai University, China
geboren te Handan, China.

This dissertation has been approved by the
promotors: Prof. drs. ir. J.K. Vrijling and
            Prof. dr. ir. P.H.A.J.M. van Gelder

Composition of the doctoral committee:

Rector Magnificus
Prof. drs. ir. J.K. Vrijling   promotor
Prof. dr. ir. P.H.A.J.M. van Gelder   promotor

Independent members:
Prof. dr. ir. S.N. Jonkman   CiTG, TU Delft
Prof. dr. W. Wang   Hohai University, China
Prof. dr. R. Ranasinghe   UNESCO IHE/The Australian National University
Dr. S. Maskey   UNESCO IHE
Dr. R. Jongejan   Jongejan RMC
Substitute member:
Prof. dr. ir. M.J.F. Stive   CiTG, TU Delft

Summary

The modelling frameworks, which include greenhouse gas emission scenarios, climate models, downscaling methods and hydrological models, are generally used to assess climate change impacts on river floods. In this research, the uncertainty associated with each component of the modelling framework is analysed with particular reference to climate change impacts on flood frequency. A method of risk-averse economic optimisation has been proposed for adapting river dikes to climate change under uncertainty. The Huai River Basin in China has been selected as a case study.

The outputs of climate models, i.e., General Circulation Models (GCMs), under greenhouse gas emission scenarios have been commonly used as fundamental inputs of the climate change impact assessments. The analysis in this thesis employed the climate model projections of the WCRP CMIP3 and CMIP5 datasets. In Chapter 2, a brief introduction of emission scenarios, as well as a preliminary analysis of the simulative ability and future projections of the participating climate models, is provided. The results confirm the necessity to bias-correct and downscale the climate model outputs before being used in impact-related studies. The annual mean temperature in the study area is suggested to increase up to 8°C at the end of this century under a high greenhouse gas emission scenario without mitigation measures. The standard deviation of precipitation intensity is suggested to increase, especially in summer, which may in the future lead to high-magnitude floods.

Empirical statistical downscaling methods are becoming increasingly popular in climate change impact assessments that require downscaling multi-GCM projections. In Chapter 3 empirical statistical downscaling methods are classified based on calibration strategies and statistical transformations. Ten combinations of calibration strategies and transformation methods were used to represent a range of empirical statistical downscaling methods. To test the performance of these methods in downscaling daily precipitation and temperature, an inter-model cross validation was carried out using an ensemble of 16 GCMs. These downscaling methods were further applied to downscale the climate for the future period to assess the associated uncertainties. The results show that the change factor based methods outperform the bias correction based methods in projecting the probability distribution of downscaled daily temperature. With the change factor calibration strategy, simply adding (for temperature) or multiplying (for precipitation) the mean change factor is sufficient to represent most of the relative changes projected by GCMs. The use of quantile based methods appear to be advantageous only at the tails of the distribution. More sophisticated bias correction based methods are needed to remove the biases in the higher-order statistics of the GCM outputs. The two calibration strategies led to fundamentally different temporal structures and spatial variability of the downscaled climatic variables. Bias correction based methods produced larger uncertainty bounds of inter-annual variability than the change factor methods. For downscaled precipitation, the uncertainty arising from the downscaling methods is comparable to the uncertainty arising from GCMs, while more uncertainty is introduced by calibration strategies than statistical transformation methods.

There is a growing consensus that the performance of hydrological models should be routinely evaluated before being used in impact-related studies. The uncertainty, which stems from transferring calibrated models to a changing future climate, is receiving increasing attention. Chapter 4 assesses the uncertainties associated with the parameter calibration of the lumped Xinanjiang hydrological model when assessing the climate change impacts on river flow. The transferability of model parameters was tested in the context of historical climate variability using the differential split-sample test. The parameters calibrated from the periods representing differing climatic conditions were used to project future river flow in a changing climate. The uncertainties in projected future river flows stemming from the choice of calibration periods and parameter equifinality were compared. The results show that the transferability of the parameters calibrated from a wet period to a dry period is poorer than the other way around. The model error as well as the variability in the simulations due to equifinality increase with the increase of the difference in rainfall between the calibration and validation periods. The uncertainty due to the choice of calibration periods takes the majority of the total parameter uncertainty in the projected future mean discharge. When the calibration period contains enough information on climate variability, the equifinality effect and the choice of calibration periods contribute comparable magnitudes of uncertainty in terms of extreme discharge.

Five sources of uncertainty mentioned above were compared in Chapter 5, i.e. GCM structure, greenhouse gas emission scenario, downscaling method, choice of period for calibrating the hydrological model, and non-uniqueness of hydrological parameters. Multiple samples of flood frequency curves were generated through the combinations of different emission scenarios, GCMs, downscaling methods and hydrological model settings. All samples were given equal weights in the analysis. The results show that the future flood magnitude is expected to increase, not only due to the increase in mean precipitation, but also due to the increase in variation of precipitation. Nonetheless, there is still a small likelihood that the flood quantiles with a high return period (above 20 years) will decrease in the future. The results of uncertainty comparison suggest that the GCM structure is the dominant source of uncertainty, emission scenarios and empirical statistical downscaling methods also result in considerable uncertainty, and the uncertainties related to hydrological model are less than those related to other uncertainty sources.

To guarantee a safe flood defence in a changing environment, the adaptation to climate change needs to be considered in the design of river dikes. However, the large uncertainty in the projections of the future climate leads to varied estimations of future flood probability. How to cope with the uncertainties in future flood probability under climate change is an inevitable question in adaptation decision-makings. In Chapter 6, the uncertainty introduced by climate projections was integrated into the 'expected predictive flood probability', and the risk-aversion attitude was introduced in the adaptation of river dikes. The uncertainty in the climate change projections on flood probability was represented by the uncertainty in the parameters of the probabilistic model. This parameter uncertainty was estimated based on the outputs from the GCMs participating in IPCC AR4. The parameter uncertainty, estimated from the selected GCMs under different scenarios, was integrated into the expected predictive probability of flooding, which was then used in the risk-averse economic optimization. Different optimal results were obtained based on varied values of the risk-aversion index which represents the risk-averse altitude of decision makers. The case of a dike ring area in the Bengbu City in the Huai River Basin is studied as an example using the proposed approach. The results show that the uncertainty of climate change decreases the optimal safety level and increases the optimal dike heightening up to 8.23 m (with the risk-aversion index of 1.5) in a gradually changing climate. The value would be even larger if the climate will change sooner. Integrated adaptive measures rather than only dike heightening are needed to respond to the uncertain impacts in the future. The proposed approach enables decision makers to cope with climate change and the associated uncertainty by adjusting the level of risk aversion.

Lu Wang

December 2014 in Delft

Samenvatting

In de beoordeling van de gevolgen van klimaatverandering op rivieroverstromingen wordt over het algemeen het procesmatig modelleringskader gebruikt. Het modelleringskader bevat prognoses van klimaatmodellen onder invloed van broeikasgas scenario's, downscaling methoden en hydrologische modellen. In dit onderzoek wordt de onzekerheid, die gekoppeld is aan elke component van het modelleringskader, geanalyseerd en wordt bijzondere aandacht gegeven aan de gevolgen van klimaatverandering op overstromingsfrequentie. Een methode van risicomijdende economische optimalisatie wordt voorgesteld voor de aanpassing van de rivierdijken aan klimaatverandering onder onzekerheid. Het Huai Rivier bekken in China is geselecteerd als een casestudie.

De uitkomsten van de klimaatmodellen onder scenario's van broeikasgasuitstoot zijn gebruikt om basisinformatie te verstrekken in de beoordelingen van de effecten van klimaatverandering. In dit proefschrift worden de prognoses van klimaatmodellen gebruikt aan de hand van de WCRP CMIP3 en CMIP5 datasets. In hoofdstuk 2 wordt een korte inleiding gegeven over zowel de emissie scenario's als een voorlopige analyse van het simulatie vermogen, en wordt een toekomstige prognose van de onderzochte klimaatmodellen verstrekt. De resultaten bevestigen de noodzaak van bias-correctie en downscaling van uitkomsten van het klimaatmodel, alvorens het gebruik in effect-

gerelateerde evaluaties. De jaarlijkse gemiddelde temperatuur in het studiegebied wordt verhoogd tot 8oC aan het eind van deze eeuw, onder het hoge emissie scenario en zonder risico beperkende maatregelen. De standaarddeviatie van neerslag intensiteit wordt verhoogd, met name in de zomer, wat in de toekomst tot overstromingen van grote omvang kan leiden.

Empirisch-statistische downscalingmethoden worden steeds populairder in de beoordelingen van de gevolgen van klimaatverandering die downscaling van multi-GCM projecties vereisen. In hoofdstuk 3 worden empirische statistische downscalingmethoden ingedeeld op basis van ijkingsstrategieën en statistische transformaties. Tien combinaties van ijkingsstrategieën en transformatie methoden werden gebruikt om een aantal empirische statistische downscalingmethoden weer te geven. Een kruisvalidatie tussen de modellen onderling is uitgevoerd om de prestaties van deze methoden van downscaling van dagelijkse neerslag en temperatuur, met behulp van een ensemble van 16 GCMs, te testen. Deze downscalingmethoden werden verder toegepast op downscaling van klimaat in de toekomst om de bijbehorende onzekerheden te beoordelen. De resultaten tonen aan dat, methoden gebaseerd op veranderingsfactoren, de methoden overtreffen op basis van bias correctie in de projectie van de kansverdeling van downscaling van dagelijkse temperatuur. Met de strategie van verandering van kalibratiefactor, door simpele toevoeging (voor temperatuur) of vermenigvuldiging (voor neerslag), is de gemiddelde veranderingsfactor voldoende om de relatieve, door GCMs geprojecteerde veranderingen, te vertegenwoordigen. Het gebruik van op kwantiel gebaseerde methoden lijkt alleen aan het einde van de verdeling gunstig te zijn. Meer geavanceerde op bias correctie gebaseerde methoden zijn nodig om de afwijkingen van de GCM uitkomsten, die samengaan met de statistieken van hogere orde, weg te nemen. De twee ijkingsstrategieën hebben geleid tot fundamenteel verschillende temporele structuren en ruimtelijke variabiliteit van de ingekrompen klimatologische variabelen. De op bias correctie gebaseerde methoden hebben aanzienlijke grotere onzekerheidsbeperkingen van intra-jaarlijkse variabiliteit geproduceerd dan de methoden van veranderingsfactor. Voor ingekrompen neerslag is de onzekerheid als gevolg van downscalingmethoden vergelijkbaar met de onzekerheid als gevolg van GCMs, terwijl meer onzekerheid wordt geïntroduceerd door kalibrerings-strategieën dan statistische transformatie methoden.

Er is een groeiende consensus dat de prestaties van hydrologische modellen regelmatig moeten worden geëvalueerd alvorens te worden gebruikt in effect-gerelateerde evaluaties. De onzekerheid die voortkomt uit de overdracht van gekalibreerde modellen op een gewijzigd toekomstig klimaat krijgt steeds meer aandacht. Hoofdstuk 4 beoordeelt de onzekerheden in verband met de kalibreringsvariabele van het 'lumped' Xinanjiang hydrologische model bij de beoordeling van de gevolgen van klimaatverandering op de afvoer van de rivier. De overdracht van de variabelen van het model is getest in de context van historische klimaatvariaties met behulp van de differentiële split-proef test. De gekalibreerde variabelen uit de perioden die verschillende klimatologische omstandigheden

vertegenwoordigen, worden gebruikt om toekomstige rivier afvoer in een veranderend klimaat te projecteren. De onzekerheden in de verwachte toekomstige rivierafvoer, die voortvloeien uit de keuze van de kalibratie periode en de variabele van equifinaliteit, worden vergeleken. Uit de resultaten blijkt dat de overdracht van de variablen die gekalibreerd zijn vanuit een natte naar een droge periode, zwakker zijn dan andersom. De modelfouten, evenals de variabiliteit in de simulatie als gevolg van equifinaliteit, nemen toe met de verhoging van het verschil in neerslag tussen de kalibrerings- en validatieperiodes. De onzekerheid als gevolg van de keuze van kalibreringsperioden vormt het merendeel van de totale onzekerheid in de geprojecteerde toekomstige gemiddelde neerslag. Wanneer de kalibreringsperiode voldoende informatie over klimaatvariatie bevat, dragen het equifinaliteitseffect en de keuze van kalibreringsperioden aan een vergelijkbare omvang van onzekerheid bij, in termen van extreme neerslag.

Vijf bronnen van onzekerheid worden in hoofdstuk 5 vergeleken: GCM structuur, broeikasgas emissie scenario, downscalingmethode, keuze van de periode voor het kalibreren van hydrologische model, en niet uniekheid van hydrologische parameters. Meerdere reeksen van overstroming frequentie curves zijn gegenereerd door combinaties van verschillende emissie scenario's, GCMs, downscalingmethoden en hydrologische model instellingen toe te passen. Alle hebben in de analyse hetzelfde gewicht. Uit de resultaten blijkt dat de omvang van toekomstige overstroming toename niet alleen te wijten is aan de stijging van de gemiddelde neerslag, maar ook een gevolg is van een toename van variatie in neerslag. Er is echter nog een kleine kans dat de overstromingsquantielen met een grotere herhalingsperiode (boven 20 jaar) in de toekomst zal dalen. De vergelijking van onzekerheid suggereert de volgende volgorde van belang van componenten (grootste naar minste): GCM > emissie scenario > (empirische) downscalingmethode > hydrologisch model modellering (keuze van kalibreringsperiode en equifinaliteit).

Om een veilige overstromingsverdediging in een veranderende omgeving te garanderen, moet de aanpassing aan de klimaatverandering in het ontwerp van rivier dijken in acht worden genomen. De grote onzekerheid in de prognoses van het toekomstige klimaat leidt echter tot uiteenlopende schattingen van de waarschijnlijkheid van toekomstige overstromingen. Hoe om te gaan met de onzekerheden en kans op overstroming en klimaatverandering in de toekomst, dit is een onvermijdelijke vraag in de aanpassingsproblematiek. In hoofdstuk 6 wordt onzekerheid, geïntroduceerd door klimaat prognoses, geïntegreerd in de 'verwachte voorspellende overstromingskans', en wordt de aversie van risico geïntroduceerd in de aanpassing van de rivier dijken. De onzekerheid van de gevolgen van klimaatverandering op de kans op overstromingen wordt weergegeven door de onzekerheid in de variabelen van het probabilistische model. Deze parameter onzekerheid wordt geschat op basis van de resultaten van de GCMs in de IPCC AR4. De parameter onzekerheid, geschat vanuit verschillende GCMs onder geselecteerde scenario's, is geïntegreerd in de verwachte voorspellende waarschijnlijkheid van overstroming, die vervolgens in de risicomijdende economische optimalisatie wordt gebruikt. Verschillende

optimale resultaten werden verkregen op basis van uiteenlopende waarden van de risicoaversie index. Het voorbeeld van een dijkring in China wordt bestudeerd als een case dat gebruik maakt van de voorgestelde aanpak. Uit resultaten blijkt dat door de onzekerheid van klimaatverandering het optimale veiligheidsniveau afneemt en de optimale dijkhoogte wordt verhoogd tot 8.23m (met een risico aversie index van 1.5) in een geleidelijk veranderend klimaat. Deze waarde kan zelfs hoger zijn indien het klimaat sneller verandert. Geïntegreerde aanpassingsmaatregels zijn dan meer noodzakelijk dan slechts het verhogen van een dijk om in de toekomst te reageren op de onzekere gevolgen. De voorgestelde aanpak stelt besluitvormers in staat om te gaan met de verandering van het klimaat en de bijbehorende onzekerheid door de risicoaversie niveau aan te passen.

Wang Lu

December 2014 in Delft

Content

Chapter 1 Introduction

1.1 Background

1.1.1 Uncertainties in assessing hydrological impacts of climate change

There have been unequivocal evidences of humane-induced climate change in the past century (Solomon 2007). Substantial changes of the climate during the coming decades and centuries will be influenced by the greenhouse gas emissions of the future world. Because of the deep uncertainty in the future climate status, it is not possible to give probabilistic predictions of the future climate. The generally used approach is to use scenarios to understand the uncertainty about human activities, the response of the climate system to human activities, the impacts of climate change, and the implications of mitigation and adaptation measures (Moss et al. 2010).

The future climate states corresponding to the assumptions of the future world are commonly simulated by multiple General Circulation Models (GCMs). The GCMs are mathematical models of the general circulation of a planetary atmosphere or ocean based on the physical laws. They attempt to explicitly simulate the atmospheric and oceanic processes that regulate the direction and magnitude of climate changes on global and at least large regional scales (Räisänen 2007). The projections of climate models corresponding to climate change scenarios provide fundamental information for impact assessments. Due

to the uncertainty of GCM simulations, such as radiative forcing, initial conditions, model formulation and model inadequacy, the uncertainty in climate change projections has to be considered in impact assessments. Typically, uncertainty in climate models can be investigated by using multiple model structures with different greenhouse gas scenarios, i.e., the so called "ensemble of opportunities". This approach is commonly realized through the multi-model ensembles such as the Fourth Assessment Report of the Intergovernmental Panel on Climate Change (IPCC AR4)/Phase 3 of the Coupled Model Intercomparison Project (CMIP3). An alternative approach is the perturbed physics ensembles, which perturbs the parameters representing various physical processes to evaluate uncertainty in GCM formulations and initial conditions (Murphy et al. 2004, Stainforth et al. 2005).

The mismatch of modelling scales is a problem which has to be resolved when using the outputs of climate models in assessing climate change impacts. The spatial resolution of GCMs is typically around 2° latitude and 3° longitude, and their outputs are currently not considered reliable at time scales shorter than 1 month (Prudhomme et al. 2002). However, climate change usually impacts the process at much finer spatial and temporal scale, such as the generation of river floods. Thus, there is a mismatch between the resolution of climate models and the local scale of impact modelling. Downscaling methods are commonly used in climate change impact assessments in order to bridge the gap between large-scale GCMs and local-scale impact models. Generally, dynamical and statistical downscaling are two distinct approaches to transfer large-scale GCM outputs to local-scale variables. Dynamical downscaling nests a regional climate model (RCM) into the GCM to simulate physical processes at a fine scale. Although RCMs preserve the physical coherence between atmospheric variables, they have disadvantages. For example,1) they are computationally intensive, 2) they are generally not available for varied scenario ensembles, 3) the model skill depends strongly on biases inherited from the driving GCM (Fowler et al. 2007). It is not practical for RCMs to provide multi-decade simulations with multiple GCMs and/or greenhouse gas scenarios (Maurer and Hidalgo 2008). These shortcomings complicate the use of RCMs in the impact-related research. Therefore, statistical downscaling has been widely used in impacts studies, especially in those which perform uncertainty assessment. Statistical downscaling methods have the advantages of relative ease of application and less expense of computation. They are flexible to provide climate information at any required resolution and, thus, can be used directly for climate change impact studies (Murphy 1999, Wilby et al. 2004, Fowler et al. 2007). Past research shows that the performance of statistical downscaling can be comparable to dynamical downscaling (Kidson and Thompson 1998, Mearns et al. 1999, Murphy 2000, Haylock et al. 2006). The downscaling uncertainty has been typically analysed by comparing various kinds of downscaling methods. The performances of downscaling methods depends partly on the climate model used, additional uncertainty could raise from the interactions of downscaling methods and GCMs.

To assess hydrological responses to climate change, hydrological models are useful tools to simulate the local hydrological processes corresponding to future climatic conditions.

Conceptual rainfall-runoff models have been widely used in the assessment of climate change impacts on water resources and river floods. Conceptual rainfall-runoff models use simple mathematical equations to describe the main hydrological processes. They attempt to incorporate realistic representations of the major non-linearities inherent in the rainfall-runoff relationships based on simplified forms of the physical laws. The general procedure of modelling hydrological responses under climate change is to force downscaled GCM simulations into rainfall-runoff models. The uncertainties that stem from model structures and parameters are inherent in hydrological modelling. These uncertainties have been investigated by various methodologies including state-space filtering, model averaging, and formal and informal Bayesian approaches (Beven and Binley 1992, Beven and Freer 2001, Montanari 2007, Vrugt et al. 2009), but relatively few climate change impact studies have drawn on these approaches (Surfleet and Tullos 2013). Previous impact-related studies have paid considerable attention on assessing the uncertainties associated with GHG emission scenarios and GCM structures, the choice of which has been considered as the main uncertainty in the impact analysis of future climate change. More and more studies stress the necessity and importance of routinely testing the performance of hydrological models and analysing the related uncertainty in the impact assessments (Wilby 2005, Bastola et al. 2011, Seiller et al. 2012). The uncertainty associated with model structures is commonly analysed by using model ensembles consisting of varied conceptual configurations (Jiang et al. 2007, Bae et al. 2011, Bastola et al. 2011, Chen et al. 2011, Najafi et al. 2011) or by comparing different spatial scales of configuration (Booij 2005, Das et al. 2008, Surfleet et al. 2012). It is not until recent years that parameter uncertainty is intensively investigated in the studies of hydrological impact under climate change (Bastola et al. 2011, Li et al. 2012, Brigode et al. 2013).

Considerable uncertainty arises from each component of the cascade in impact assessments as introduced above: GCM projections under future greenhouse gas emission scenarios, downscaling methods and hydrological modelling. Majority of the previous studies have been focused on the analysis of uncertainty from each component or the uncertainty envelope of the modelling framework without confidence intervals. There has been few attempts to address the propagation of the uncertainties through the cascaded models (Cameron et al. 1999, Surfleet and Tullos 2013) and to provide the probabilistic impact predictions based on climate projections (New et al. 2007). Estimating likelihood based on the performances of models in simulating historical observations or on the agreement of model results faces the risk of obtaining false probability in future predictions. Cautions should be taken when using probabilistic impact predictions because they remain conditional on the available data and resources (Dessai and Hulme 2004). The relative contributions from different sources of uncertainty could vary among basins with different hydro-climatic conditions. It is important to identify the dominating uncertainties, reduce the uncertainties caused by errors and explore the full uncertainty range. The uncertainty analysis is thus should be an integral part of any climate change impact assessment.

1.1.2 Adaptation to climate change under uncertainty

The extreme climatic and hydrological events could become more frequent in the future due to the change of climate. In particular, the intensification of the global water cycle due to the radiative effects of changes in atmospheric compositions could lead to the increase in flood risk. The frequency of the great floods with discharge exceeding 100-year level from the worldwide large basins has increased substantially during the twentieth century. A statistically significant positive trend was detected from both the streamflow measurements and the climate model projections, and the model suggested that the increasing trend will continue (Milly et al. 2002).

The change in flood risk suggests a need for adapting flood defenses to climate change. The IPCC defines adaptation as an ''adjustment in ecological, social, or economic systems in response to actual or expected climatic stimuli and their effects or impacts''(IPCC 2001). Adaptation strategies for river flood management can be implemented as "hard" and "soft" measures. Hard measures reply predominately on adapting human-built infrastructures, e.g. heightening and strengthening river dikes and reinforcing buildings that could be inundated. In contrast, soft measures utilize natural system or non-structure technologies, e.g., land-use planning and early warning system. Compared to soft adaptations, which are usually less expensive, flexible and at local level, hard measures require large investments and long-term planning at national level. Hard flood defenses effectively protect large areas from being flooded and will continue to play a key role in the future. Adapting hard flood defenses may exert large consequences over the social and environmental systems, studies should therefore be carried out to achieve appropriate solutions.

Adapting to climate change is a decision problem with uncertainty. How climate will change in the future is highly uncertain, and the impact of climate change on hydrological conditions is also uncertain due to the lack of knowledge of the environmental system. There have been many assessments on the hydrological responses to climate change. The wide range of the outputs from the hydrological models driven by GCM ensembles demonstrates the large uncertainty of the future predictions.

Large ensembles of climate models are increasingly available which could provide useful information for developing adaptation strategies to climate change. The majority of the previous studies employing ensembles of climate projections have focused on assessing climate change impacts and the associated uncertainties, the results of which have not been well incorporated in the adaptation decision making. Lopez et al. (2009) claimed that the climate model ensemble provides a better understanding of the possible ranges of future conditions and enables decision makers to easily compare the merits of different management options and the timing of adaptations. The utility of climate projections in making adaptation decisions to climate change uncertainties is still under development.

The adaptation decision could be made using the recently popular "bottom-up" approaches which emphasize on developing robust adaptation responses to a range of plausible future climatic conditions. For instance, Lempert and Groves (2010) employed the Robust Decision Making for supporting decisions in water management under climate change uncertainty. This approach use simulation models to assess the performance of adaptation plans over thousands of plausible futures; it identifies those futures where the plans fail to perform adequately and helps decision makers understand the vulnerabilities of their plans and assess the options for ameliorating these vulnerabilities. Similar idea was carried forward by Prudhomme et al. (2010) in assessing the design allowance for flood risk in the catchments in UK. Dessai and Hulme (2007) used a local sensitivity analysis to determine whether or not a decision to adapt to climate change is sensitive to uncertainty in the various elements of the modelling framework (e.g., emissions of greenhouse gases, climate sensitivity and global climate models).

The conventional "top-down" approaches have dominate the present impact-related studies to date. These approaches are scenario led and drive cascaded models as described in Section 1.1.1. Quantitative estimates of future impacts are provided by the impacts models conditional on the scenario used. Adaptations are expected to response to the anticipated impacts. The top-down approach could characterize climate change uncertainty and provide basis for reducing the uncertainty. However, the majority of previous studies did not keep on to utilize these information in the following adaptation studies. This may be because that the uncertainty envelope expands at each step in the cascaded models, and the range of outcomes offered to the decision-maker is bewildering (or worse, spans changes of opposite sign) (Prudhomme et al. 2010). How to cope with the uncertainty revealed by impact assessments in adaptation decision making is still a question to be answered.

1.1.3 Introduction of the study area

The study area selected here is the Huai River Basin, China (Figure 1.1). The Huai River Basin is located in eastern China between the Yellow River basin and Yangtze River basin, at the latitude from $30^{o}55'$N to $36^{o}36'$ N and the longitude from $111^{o}55'$E to $121^{o}25'$E. It covers the area from the Tongbai-Funiu Mountains in the west to the Yellow Sea in the east with a total area of about 270,000 km^2. The basin lies in the transition zone between a humid subtropical climate (in the south) and a semi-humid warm temperate climate (in the north).
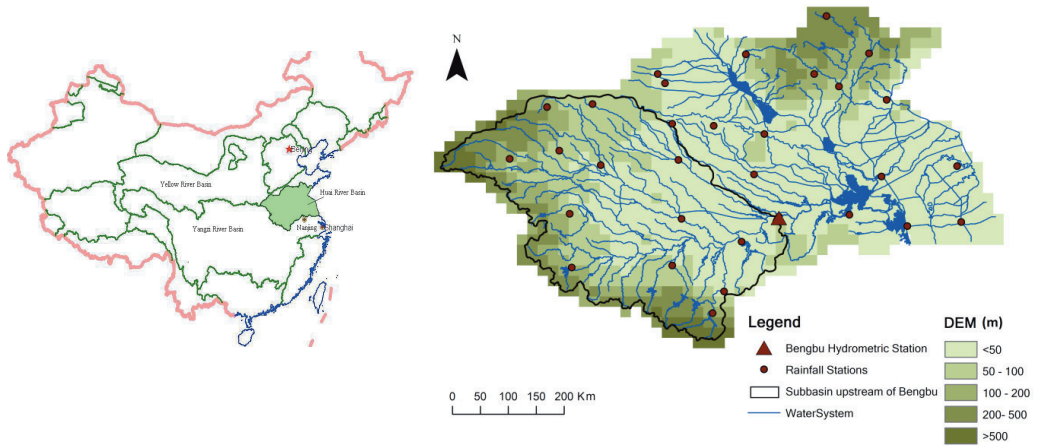
Figure 1.1 Map of the Huai River Basin (a) Location of the Huai River Basin and other river basins in China. (b) Map of the water system and elevation of the study area.

The January 0 ^{o}C isotherm and the 800 mm isohyet generally run along the main stream of the Huai River, which is regarded as the geographical divide of northern and southern China. The annual mean air temperature ranges from 11 ^{o}C to 16 ^{o}C. The maximum monthly mean temperature occurs in July with the multi-year mean of 25 ^{o}C, while the minimum monthly mean temperature occurs in January with the multi-year mean of 0 ^{o}C. Heavy rainfall mainly occurs in the summer from June to September, with large annual and seasonal variability (Figure 1.2). The Huai River Basin has had a long history of floods, and the change of climate is likely to significantly increase the flood vulnerability in this area.
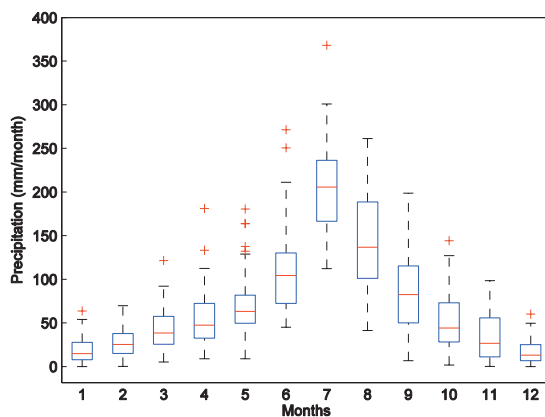
Figure 1.2 Boxplots of observed monthly precipitation over the Huai River Basin over a period of 30 years (1961-1990)

An increase in temperature has been observed in the past decades over the study area (see Figure 1.3). The Mann-Kendall trend test confirms the upward trend at a significance level of 0.01, and an abrupt change was detected in the year of 1997.

$$y = 0.0202x + 14.037$$
$$R^2 = 0.26263$$
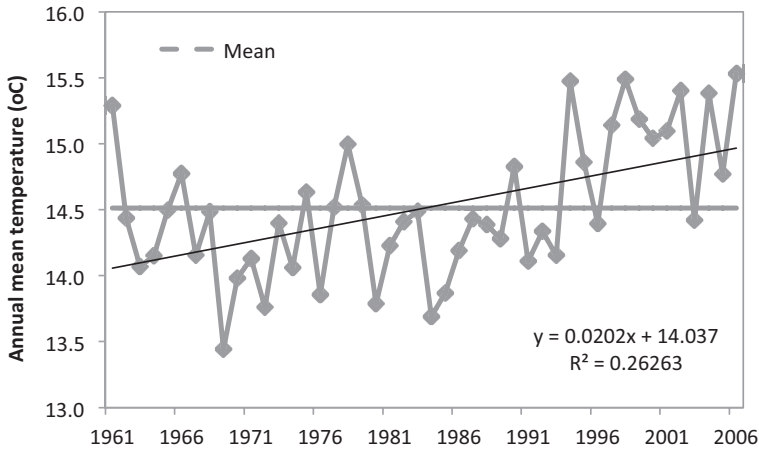
Figure 1.3 Historical record of the basin-mean annual temperature

The topography of the Huai River basin is mostly characterized by low plains with numerous lakes and depressions. In the west and southwest of the basin, there is mountain area along the basin boundaries. The Huai River has many tributaries, among which, 21 tributaries have a catchment area lager than 1000 km^2. The floods along the Huai River generally happen in July or August. The period between 1 May and 31 September is officially regarded as the Huai River flood season. The high discharges in the main stream usually last more than one month with several peaks. The high discharges are generally caused by the large-scale precipitation which leads to the intersection of the main stream discharge and the tributary discharges.

The Bengbu Hydrologic Station, with a catchment area of 122,000 km^2, is located along the main stream at the midstream of the Huai River (shown as the red triangle in Figure 1.1). The calculation of the total water flux is complicated by the complex irrigation canal network when the river flows pass the station into the low plains near Yellow Sea and Hongze Lake. Thus, the analysis of the streamflow at this station is crucial for understanding the runoff regime of the whole basin. The annual hydrographs of 1954, 1991, 2003 and 2007 in which the extreme floods occurred were shown in Figure 1.4. The shapes of these hydrographs could be one single peak or multiple peaks. In flood season, the hydrographs started to rise between May and June and the fell to the low level between October and November. The high flow usually lasted more than three months. The peak discharge could occur in July or August. The historical maximum peak discharge that occurred on 6th August in 1954 was 11500m^3/s.
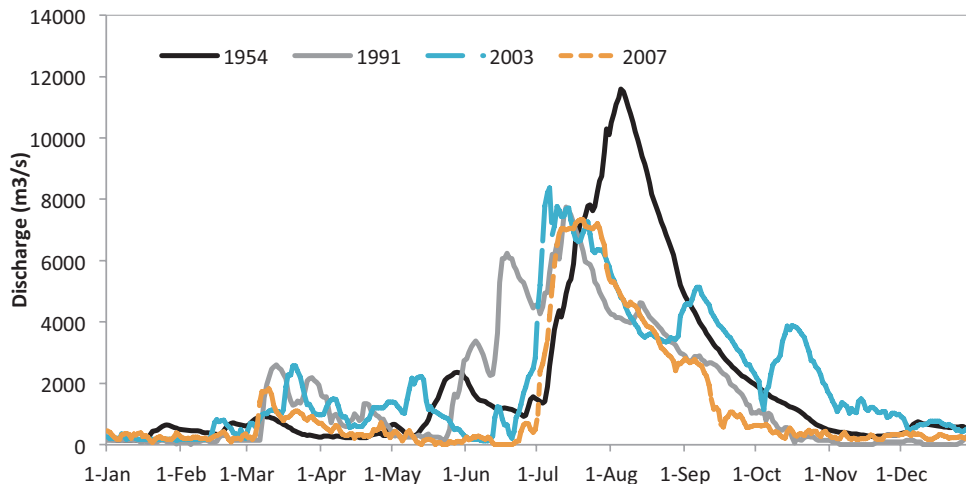
Figure 1.4 Annual hydrographs at the Bengbu station in the years of 1954, 1991, 2003 and 2007

The total water volume in summer at Bengbu station over the period of 1961-2006 is shown in Figure 1.5. The total water volume in summer was calculated as the area below the hydrograph and it can be seen as an index of extreme flood. The inter-annual variability of the summer water volume is large. Although the trend line has a positive slop, the Mann-Kendall trend test does not suggest a significant increase trend.

$$y = 0.2432x + 122.94$$
$$R^2 = 0.00136$$
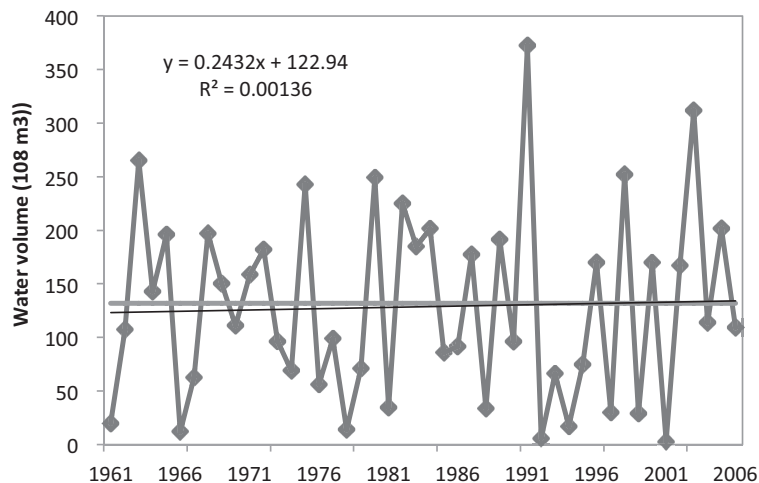
Figure 1.5 Historical records of total water volume in summer at the Bengbu station

In the Huai River basin, the rapid development of agriculture and industry began in the 1980s. Frequent droughts and floods, such as the heavy flood in 1991, have spurred new construction of water supply and management projects and the intense use of the existing

infrastructures including more than 5700 reservoirs and 5000 sluice gates (Yang et al. 2010). With the increase in the catchment area and the channel length, the effects of hydraulic structures on discharges decrease downstream (Quan et al. 2009). The contribution of the upstream hydraulic structures to decrease the peak discharge at Bengbu station is limited. Take for example the flood in 2003, the water volume stored in the reservoirs only absorbed 10% of the total water volume passed Bengbu station during the 30-day period with the maximum water volume (Wang and Zhang 2005). The effect of the sluices in the wet season is less significant than in the dry season (Hu 2012). The sluices are totally opened during floods. The dams and sluices upstream reduced 30% of the peak discharge at Bengbu in 1991 (Zhang et al. 2010).

In this thesis, the economic optimisation method for climate change adaptation is developed and tested on the case of Bengbu Old Dike Ring. Bengbu City, with an area of 601.5 km^2 and a population of 1.05 million (2009), is a very important city in regard to transportation, industry and business in Anhui Province, China. The GDP in 2009 was 53.2 billion RMB. The main stream of the Huai River flows through this city from the west to the east and divides it into two parts (231.53 km^2 in the north part and 369.97 km^2 in the south part). The urbanized area covers 105 km^2. The city is protected by several dike rings.

Figure 1.6 Satellite map of the Bengbu City and the Old Dike Ring

The risk assessment is carried out over the most urbanized area, which is surrounded by the reverse "U"-shaped Old dike ring on the south bank of the Huai River. The Old dike ring, with a length of 12.6 km, protects the lower land area of 49 km^2. The area is bounded by the Longzi River in the east, the Huai River in the North, the Xijia Ditch in the west and the higher located land in the south. This area, as the center of the Bengbu city, is directly threatened by floods from the main stream of the Huai River. In flood seasons, the discharges of the tributaries, the Longzi River and the Xijia Ditch, are obstructed due to the high water level in

the main stream. Consequently, floods from the main stream of the Huai River is the primary cause of flooding in the study area.

The Old dike ring is designed to prevent the south part of the city from being flooded by the Huai River. It runs along the south bank of the Huai River connecting to Cao Mountain in the east and Tiger Mountain in the southwest. The Old dike ring was built in 1951 and was strengthened to the present-day safety level in the 1990s, which was the greatest historical flood, in 1954, with a return period of 40 years. The strengthening, including paving the concrete revetment, removing the sluice and building a road on top, started in 1998 to reassure that the dike reaches the design safety level. The design crest level is the highest water level in 1954 with 2.5m of freeboard. The study area has not been flooded from the water from Huai River since the dike ring was constructed.

1.2 Problem outline

The objectives of this thesis are 1) to set up a modelling framework for assessing climate change impacts on future river floods; 2) to analyse the uncertainty stemming from each component in the modelling framework; 3) to explore the plausible uncertainty envelope of the future flood frequency; and 4) to develop a decision making method for decision makers to economically optimise the adaptation of flood defences to climate change

In order to clarify the objectives of this study as stated above, the following questions have to be answered. The chapter number, in which the corresponding question is answered, in shown in brackets.

- How will the climate of the Huai River Basin change in the future? What is the uncertainty associated with greenhouse gas emission scenarios and climate models? (Chapter 2)
- What is the influence of the uncertainty in empirical statistical downscaling methods? And how large is it compared with the uncertainties from emission scenarios and climate projections? Is there a most suitable empirical downscaling method for the purpose of downscaling extreme rainfall over the study area? (Chapter 3)
- What is the transferability of the calibrated hydrological model to a different climate? How much will hydrological modelling influence the projection of future streamflow? What is the relative contributions of hydrological model parameters? (Chapter 4)
- What is the plausible range of the projected future flood frequency suggested by the modelling framework? What is the major contributor to the total uncertainty? (Chapter 5)
- How can the uncertainty in the projections of future floods be taken into account in the risk-based design of river flood defences? What is the influence of different

decision-making strategies on the design of river flood defences under climate change? (Chapter 6)

1.3 Outline of this thesis

An introduction to commonly used future climate projections and the plausible range of climate change over the study area is given in Chapter 2. Empirical statistical downscaling methods and the associated uncertainties are discussed in Chapter 3. The parameter uncertainty of the hydrological model in the context of climate change is analysed in Chapter 4. An overall uncertainty assessment of the modelling framework is presented in Chapter 5. A risk-averse economical optimisation method for adapting flood defences to climate change is developed in Chapter 6. Conclusions and recommendations are presented in Chapter 7.

Chapter 2 Projections of climate change

Greenhouse gas emission scenarios and the commonly used projections of climate change are introduced in this chapter. The ability of climate models to reproduce the present-day climate over the study area are analysed, and the changes in future climate suggested by the multi-model ensemble are presented.

2.1 Introduction

The basis of impact assessments is the information about how the climate will change in the future, which is usually represented by projections of the future climate generated by climate models under the scenarios of the future world. The reason of using the term "projection" rather than "forecast" or "prediction", is that climate modelling experiments are dependent on assumptions concerning the future world (Räisänen 2007). The goal of generating scenarios is not to predict the future, but to better understand uncertainties in order to reach robust decisions under a wide range of possible futures (Moss et al. 2010).

The development of scenarios in climate change research usually starts with socio-economic scenarios, based on which emissions scenarios are produced. The developments in the creation and use of emission scenarios and climate projections in the past two decades were summarized by (Moss et al. 2010). There have been overviews of the methods for developing scenarios in climate change research (Alcamo et al. 1995, Nakicenovic et al. 2000, Carter et al. 2007). Specifically, emissions scenarios developed by the Intergovernmental Panel on Climate Change (IPCC) have been widely used in the impact assessment of climate change. The IPCC was established jointly by the World Meteorological Organization (WMO) and the United Nations Environment Programme (UNEP) to assess periodically the scientific, technical and socio-economic information on climate change. The IPCC has developed several sets of emissions scenarios in its reports and stimulated the development of climate modelling experiments in the research of climate change.

The projections of climate change used in this thesis are the data sets used in the preparation of The Fourth and Fifth Assessment Report of IPCC (AR4 and AR5). These data sets are climate models outputs developed by leading modeling centers around the world collected by Program for Climate Model Diagnosis and Intercomparison (PCMDI). The World Climate Research Programme's (WCRP's) Working Group on Couples Modeling (WGCM) organized this activity of data collection in part to enable projections of climate change accessible by climate change-related researchers. These collections of data are officially known as the "WCRP CMIP3 multi-model dataset" and the "WCRP CMIP5 multi-model dataset".

2.2 Emissions Scenarios

In climate change research, scenarios are used to represent assumptions of the future world including social-economic development, world population, land use and greenhouse gas emissions. Emissions scenarios are the descriptions of possible future emissions of greenhouse gas into the atmosphere. Emissions scenarios for climate change research are not forecasts or predictions, but are the reflection of expert judgments regarding plausible future emissions (Moss et al. 2010). They focus on long-term (decades to centuries) trends rather than "short-term" fluctuations.

The Intergovernmental Panel on Climate Change (IPCC) has developed several generations of emission scenarios including the 1990 IPCC Scenario A (SA90) (Houghton et al. 1992), the 1992 IPCC scenarios (IS92) (Leggett et al. 1992) and the Special Report on Emissions Scenarios (SRES) (Nakicenovic et al. 2000).

The SA90 scenario developed in 1990 included a 'business as usual' future and three policy scenarios. The IS92 family of emissions scenarios (Leggett et al. 1992) developed by IPCC in 1992 consists of different sets of assumptions about future population totals, economic development and land use change. The construction of this set of scenarios is not aimed at the application in impacts assessments, and the socio-economic and demographic

developments assumed in impact assessment may be not consistent with the assumptions of the worlds used to construct emissions scenarios (Arnell et al. 2004).

The following generation of emissions scenarios was published in the IPCC's Special Report on Emissions Scenarios (SRES) (Nakicenovic et al. 2000). The SRES scenarios were constructed in a fundamentally different way from the IS92 scenario set, which enables them to be more than just inputs of climate models. In order to provide consistent world futures with impact estimates, the SRES scenarios were projected to represent a diverse range of different development pathways for the world. Four storylines were defined to describe the possible evolvement of the world population, economies and political structure over the next few decades. Their main characteristics are introduced by Arnell et al. (2004). Greenhouse gas emissions scenarios were produced with integrated assessment models based on the four storylines. Six marker emissions scenarios were defined and driven into climate models to generate corresponding scenarios of climate change. In contrast with previous scenarios that were generated using only one or two models, the development of SRES scenarios involved many different modelling teams.

IPCC's SRES narrative storylines and associated socio-economic characterizations were specifically designed to be used in the assessment of future climate change. There have been many publications on impact assessments using the SERE scenarios, among which the most widely used scenarios are A2, A1B and B1, which represent high, median and low levels of greenhouse gas emissions, respectively. It is notable that the SRES storylines do not cover all possible future worlds and they do not encompass the full range of possible socio-economic futures (Arnell et al. 2004), but they provide the basis for, to some degree, a range of possible future impacts of climate change. SRES are the scenarios used in WCRP CMIP3 multi-model experiments.

A new set of emission scenarios named "representative concentration pathways" (RCP) was described by Moss et al. (2010) and is driven to the climate models participating the WCRP CMIP5 experiments. Unlike the SRES scenarios that did not include the intervention of mitigation policy, the RCP scenarios assume that policy actions will be taken to achieve certain emissions targets. Four RCPs (RCP 2.6, RCP 4.5, RCP6.0 and RCP 8.0) have been formulated based on a range of projections of future population growth, technological development, and societal responses. RCP2.6 is a mitigation scenario in the lower end; RCP4.5 is a scenario with a less aggressive mitigation policy. RCP6.0 and RCP8.5 are non-mitigation scenarios, and the emissions of RCP8.5 are comparable with those of A1FI of SRES.

A comprehensive overview of the CMIP5 experiment design and differences between the CMIP3 and CMIP5 experiments was summarized by Taylor et al. (2012). Compared to CMIP3, CMIP5 includes increased number of comprehensive models providing more complete set of output fields. The spatial resolutions of the CMIP5 models are generally finer than those of

the CIMP3 models, and more outputs at daily scale are available. The CMIP5 multi-model ensemble was found improved performances than the CMIP3 ensemble in simulating the observations in the twenties century (Lauer and Hamilton 2012, Li et al. 2012, Sperber et al. 2012). Bastola (2013) compared the temperature and precipitation projected from the climate models run with the SRES and RCP scenarios over 28 watersheds located within the Southwest United States. His results show that the CMIP3 models run with SRES resulted in greater spread of relative changes than the spread for the CMIP5 models run with RCP scenarios. These two sets of model ensembles suggested different seasonal changes in the future. For the resulted streamflow projections, the climate model uncertainty dominated the emission scenario uncertainty.

2.3 Climate scenarios

Climate scenarios are plausible representations of future climate conditions, among which the most important variables for impacts assessments are temperature and precipitation. They can be produced using a variety of approaches including: incremental techniques, spatial and temporal analogues, extrapolation, expert judgment and physical climate and Earth system models (Mearns et al. 1999, Moss et al. 2010). Climate modelling experiments have been widely used in climate change research to generate climate projections driven by emissions scenarios and other related conditions such as land use. The earliest model-based 'scenarios' in climate change research were to force a doubling or quadrupling of greenhouse gas into early climate models.

General Circulation Models (GCMs), are currently the best way to model the complex processes that occur at the earth system's level. They are the numerical representations of the earth natural system and have solid physical basis. They are useful tools to study the behaviour of the climate system and its response to human-induced perturbations such as increases in greenhouse gas concentrations. They divide the atmosphere and oceans into grid cells, and simulate interactions of the atmosphere, land surface, ocean and sea ice. Due to limitations in computing power, the atmospheric components in current GCMs typically have a horizontal resolution in the order of 250 km × 250 km.

Due to the lack of reliable observed data and the internal variability in both observed and simulated climate, there is no perfect model that agrees completely with observations. Lambert and Boer (2001) found that the biases in the individual model simulations are almost invariably larger than the biases in the multi-model mean fields. Together with the fact that projections of future climate change vary between different models, the multi-model ensembles are generally used to provide a quantitative estimate of uncertainty in future climate change. Räisänen (2007) discussed the reliability of climate models using the simulations covering a 20th century and a 21st century simulation based on the SRES A1B emission scenario from the IPCC AR4 climate models. He believed that climate models can provide useful information on the future climate based on the arguments of their physical-

based modeling built-up, their good simulations of several large-scale aspects of present-day climate and observed climate change, qualitative or semi-qualitative agreement between different models and consistent simulations with observation-based estimates of global climate sensitivity.

Multi-GCM ensembles have been commonly used in the analysis of climate change studies. The latest data set of climate change projections is the Fifth phase of the Coupled Model Intercomparison Project (CMIP5) archive which provided the data basis for the Fifth Assessment Report (AR5) of the IPCC. The CMIP5 data set is the collection of the outputs of state-of-the-art climate models driven by the RCP emission scenarios. The analysis in Chapter 2, 3, 4 and 5 is based on the selected GCM outputs from CMIP5 (see Table 2.1).

Table 2.1 The GCMs outputs used in this thesis

Country	Modeling Center	Model	Resolution (^{o}) (Lon × Lat)
Australia	CSIRO-BOM	ACCESS1.0	1.875×1.25
China	BCC	BCC-CSM1.1	2.8×2.8
Canada	CCCma	CanESM2	2.8×2.8
USA	NCAR	CCSM4	1.25×0.94
USA	NSF-DOE-NCAR	CESM1(CAM5)	1.25×0.94
France	CNRM-CERFACS	CNRM-CM5	1.4×1.4
Australia	CSIRO-QCCCE	CSIRO-Mk3.6.0	1.875×1.875
USA	NOAA GFDL	GFDL-CM3	2.5×2.0
Korea	NIMR/KMA	HadGEM2-AO	1.875×1.25
UK	MOHC	HadGEM2-ES	1.875×1.25
Russia	INM	INM-CM4	2.0×1.5
France	IPSL	IPSL-CM5A-MR	2.5×1.25
Japan	MIROC	MIROC5	1.4×1.4
Germany	MPI-M	MPI-ESM-MR	1.875×1.875
Japan	MRI	MRI-CGCM3	1.1×1.1
Norway	NCC	NorESM1-M	2.5×1.875

A comparison between the climatology of observation and that of GCM outputs in the baseline period (1961-1990) is presented in Figure 2.1 and Figure 2.2 for the Huai River Basin. The observed climatology was calculated as the arithmetic mean of the observations at the stations within the basin. The modelled climatology was calculated as the arithmetic mean of the values of the grid cells covering the basin. GCMs showed better ability in simulating temperature than precipitation. The intra-annual variation of temperature is well reproduced by the models. The curve of observed temperature is encompassed by the ensemble of model simulations, and it generally stays in the middle of the modelled envelope.

Varied results were produced by the GCMs when reproducing the historical precipitation. Some of the GCMs produced different intra-annual variation of monthly precipitation. Almost all the GCMs overestimated the precipitation in spring (March, April and May) and underestimated the precipitation in the flood season (July and August). Observed winter precipitation (December, January and February) stayed within the modelled envelope, although most of the models provided an overestimation.

The variability among the GCM outputs can be attributed to the differences in the physical-based modelling build-ups and the model resolutions. The backbone of climate models is formed by the fundamental laws of physics that describe the conservation of mass, energy and momentum. Parametrisation equations are also required to describe the processes at the sub-grid scale, such as the phase change of water and transfer of radiation. The modelling centres participating the ensemble run the models with different parametrization schemes. They differ both in their basic structures and in the numerical values used in their equations, which leads to the variability in the model outputs. It is notable that the model outputs from Korea Meteorological Administration/National Institute of Meteorological Research (NIMR/KMA) and Met Office Hadley Centre (MOHC) agree with each other in simulating precipitation (see Figure 2.2) as both of the two modelling centres run the HadGEM2 model. The model resolution is also a factor influencing the accuracy of the model outputs. The outputs of the models with large grid size (BCC-CSM1.1, CanESM2 and GFDL-CM3) do not agree with the observed inner-annual pattern of precipitation; while the models with finer resolutions are generally able to reproduce the maximal monthly precipitation in the flood season. However, fine resolution does not always lead to good model performance, e.g., MRI-CGCM3 dramatically underestimated the summer precipitation, which implies that the model build-up could have more contribution to the variability among the model outputs than the model resolution.
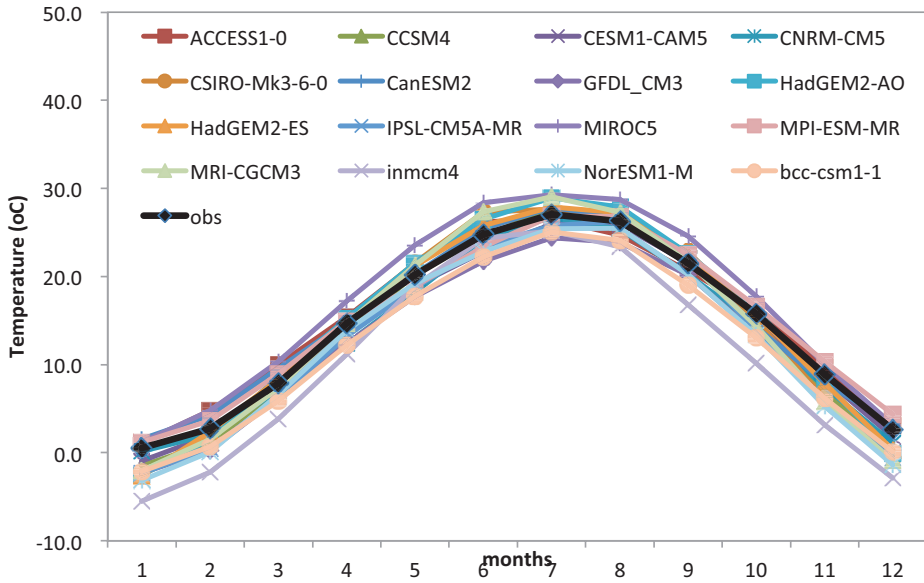
Figure 2.1 Climatology of observed and modelled temperature in the baseline period (1961-1990)
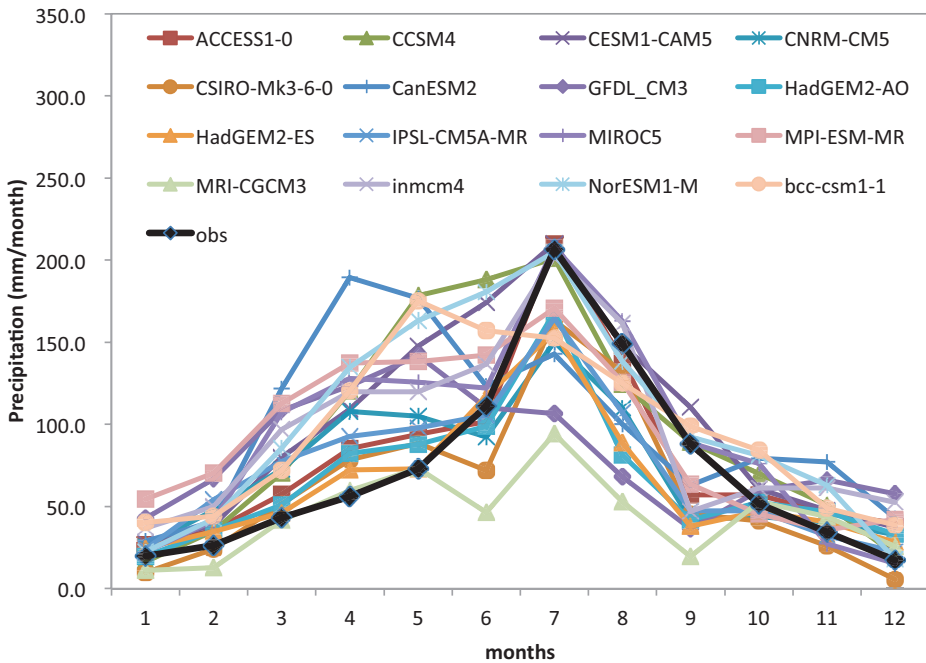
Figure 2.2 Climatology of observed and modelled precipitation in the baseline period (1961-1990)

2.4 Plausible change in climate over the Huai River Basin

First, the observation from an example gauge station (located in the center of the basin) was compared to the grid values provided by climate models in the baseline (1961-1990) and future period (2071-2100). The emission scenario at the high end (RCP8.5) was used. Secondly, the changes in mean and standard deviation of the basin-mean temperature and precipitation under scenario RCP8.5 are presented. The changes over time suggested by the ensemble of climate models under different emission scenarios are discussed at the end of this section.
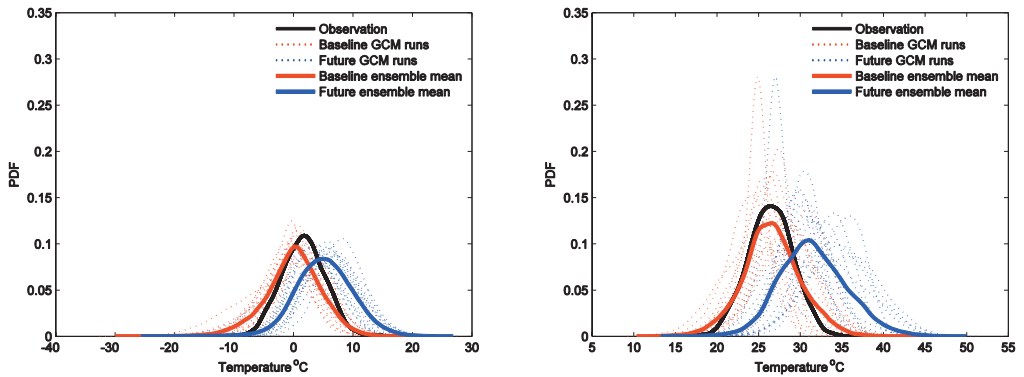
Figure 2.3 PDFs of daily temperature in winter (left) and summer (right) at Station 7 from raw GCMs under the scenario of RCP8.5 and observation
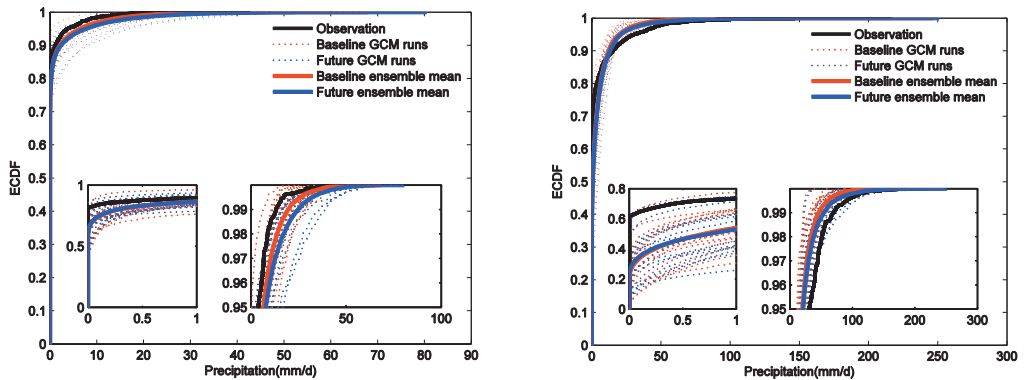
Figure 2.4 Empirical CDFs of daily precipitation in winter (left) and summer (right) at Station 7 from raw GCMs under the scenario of RCP8.5 and observation

The observed daily temperature at the example gauge station in winter (DJF) and summer (JJA) as well as the projections from the GCM ensemble for the baseline period (red curves) and the future period (blue curves) are shown in Figure 2.3. Each individual GCM run is indicated by the dotted curves; the thick solid curves indicate the ensembles mean (taking all

GCM sums as equal-weighted samples). The GCM ensemble generally has a cold bias in winter for the baseline period, while both cold and warm biases can be found in summer. The agreement among model projections is better in winter than in summer. All models project an increased mean temperature in both winter and summer for the future period.

Figure 2.4 shows the empirical CDFs of observed and projected daily precipitation at the selected station in winter and summer. The observed wet-day frequency, shown as the intercept on the y-axes in the magnified subfigure on the left, is overestimated by the GCM ensemble in both seasons. A wet bias in winter and a dry bias in summer at the high-end of the distribution is projected by most of the GCMs. A slight increase from the baseline to the future period is observed at the high end of the projected daily precipitation.

Table 2.2 Projected changes in daily temperature and precipitation intensity under the scenario of RCP8.5 (underlined numbers represent a decreasing trend, bold italic numbers with * represent maximum increasing trend among models, mm/wd means mm/wet day)

Models / Seasons	Change in Temperature				Change in Precipitation			
	Shift of Mean (^{o}C)		Ratio of S.D.		Shift of Mean (mm/wd)		Ratio of S.D.	
	Winter	Summer	Winter	Summer	Winter	Summer	Winter	Summer
ACCESS1.0	5.49	6.63	1.02	1.14	0.54	1.70	1.46	1.27
BCC-CSM1.1	4.52	5.22	*0.91*	1.18	0.53	0.42	1.22	1.20
CanESM2	4.71	5.67	*0.99*	1.06	0.24	1.49	1.16	1.57
CCSM4	3.92	4.48	*0.93*	1.09	0.54	*-0.07*	1.28	1.10
CESM1(CAM5)	4.82	4.87	1.00	1.03	0.66	1.01	1.38	1.31
CNRM-CM5	3.33	3.40	1.11	1.01	0.59	0.68	1.33	1.19
CSIRO-Mk3.6.0	5.40	6.32	*1.12**	1.16	1.06	0.46	*2.01**	1.13
GFDL-CM3	*6.76**	5.92	*0.99*	*0.95*	0.69	1.88	1.37	1.36
HadGEM2-AO	*6.76**	5.92	*0.81*	1.11	0.99	1.23	1.79	1.26
HadGEM2-ES	6.62	6.26	*0.89*	1.10	0.59	1.62	1.58	1.44
INM-CM4	3.35	2.30	*0.95*	*0.88*	*-0.75*	0.80	*0.94*	1.11
IPSL-CM5A-MR	6.59	*6.64**	1.04	*1.34**	0.31	*-0.08*	1.07	1.38
MIROC5	5.07	4.11	1.08	1.05	0.58	0.55	1.15	1.17
MPI-ESM-MR	5.27	4.33	1.04	1.04	*2.07**	1.74	1.27	1.27
MRI-CGCM3	4.15	2.89	*1.12**	1.02	0.55	*2.02**	1.25	*1.58**
NorESM1-M	4.89	4.97	*0.96*	1.10	0.22	*-0.28*	1.17	1.06
Ensemble mean	**5.10**	**4.99**	**1.01**	**1.13**	**0.59**	**0.86**	**1.26**	**1.25**

Detailed future changes in daily temperature and precipitation intensity projected by each GCM and the ensemble means are shown in Table 2.2. All models project an increased mean temperature in winter and summer; the shift ranges between 3.33-6.76 ^{o}C for winter and 2.30-6.64 ^{o}C for summer. The ratio of standard deviations between future and baseline periods is close to one, which indicates that the models do not project significant changes in the variance of daily temperature in the future. Compared to temperature, the standard

deviation of future precipitation intensity is projected to have a larger increase, up to twice of the baseline period in winter. However, the increase in the mean intensity is not as large as for temperature. Four out of 16 models even project a minor decrease in mean precipitation intensity.

The annual change of the areal mean temperature and precipitation over the sub-basin upstream of Bengbu is presented in Figure 2.5 and Figure 2.6. The change was calculated relative to the baseline period (1961-1990). The median of the ensemble under each scenario is indicated by solid curves.
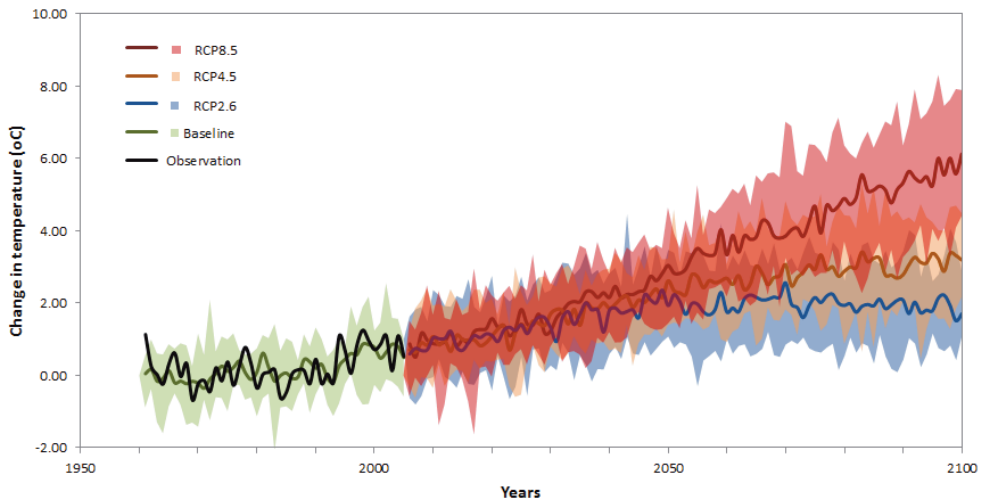

Figure 2.5 Change in temperature over time over the sub-basin upstream of Bengbu
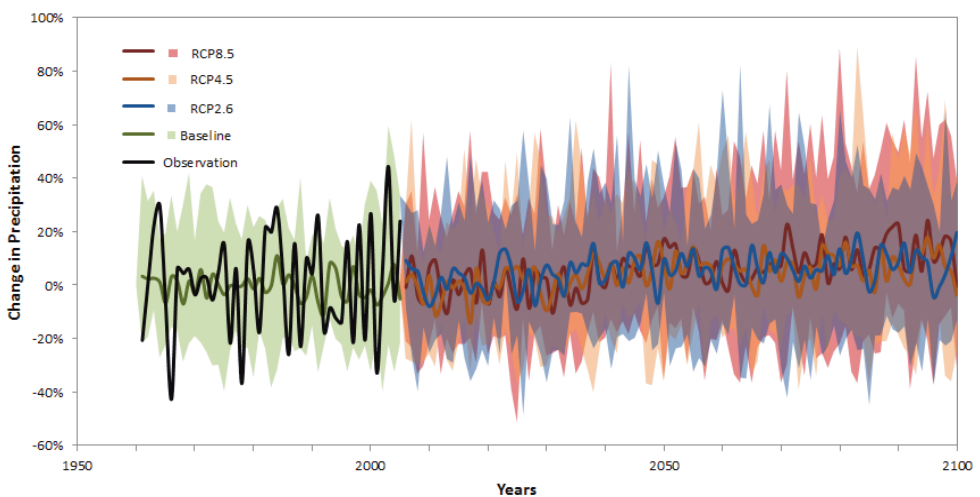

Figure 2.6 Change in precipitation over time over the sub-basin upstream of Bengbu

There is an obvious increase in temperature. The increasing trend has occurred in the 1990s of the 20th century. The observation generally falls in the envelope of the GCM ensemble in the baseline period, and the ensemble is able to reproduce the changing trend of the observation. The ensembles representing different emission scenarios suggest similar results at the beginning of the 21st century, while the ensembles gradually spread toward the end of this century. The high emission scenario resulted in the increase ranging from 4^oC to 8^oC in the year of 2100. Temperature under the low emission scenario does not increase after the year of 2050 due to the mitigation measures. In contrast, the median emission scenario continues to increase in the second half of this century, but the increasing range is not as large as the high emission scenario.

In terms of precipitation, the difference among emission scenarios is marginal. Both increases and decreases are suggested by the ensemble members. The future precipitation in a year is projected to increase by up to 80% compared to the baseline period. A slight increase in annual precipitation in the second half of the 21st century is suggested by the medians of the ensembles. The ensemble envelop becomes larger with time.

2.5 Discussion

In this chapter, a brief introduction of emission scenarios is provided as well as a preliminary analysis of climate models' simulative ability against the baseline observation and the future projections. Generally, climate models are more skilful in reproducing temperature than precipitation. Climate models tend to overestimate the wet-day frequency due to the average over a grid area. Wet-day frequency of climate model outputs needs to be adapted before being used in the impact assessments. The projections of temperature is greatly influenced by greenhouse gas emissions. The temperature over the study area is suggested to increase by 4^oC to 8^oC at the end of this century under the high emission scenario without mitigation measures. Varied projections of future precipitation were resulted from different climate models. The standard deviation of precipitation intensity is suggested to increase especially in summer, which may lead to extreme floods with large magnitude in the future.

Biases against the baseline observations remain in the outputs of climate models with varied model formulations and resolutions, especially in the simulated precipitation, which indicates that the model outputs have to be post-processed to deal with the biases before being used in climate change impact assessments. The results does not show a clear relationship between the model performance on reproducing the present-day climate and the model resolution. The higher-resolution models could lead to precipitation with higher spatial variability. However, previous studies show that higher resolution does not guarantee more skilful model performance or smaller uncertainty (Räisänen 2007, Masson and Knutti 2011). Masson and Knutti (2011) found that the resolution of models participating the CMIP3 ensemble is correlated with their performance in reproducing temperature but not

precipitation. More comprehensive representation of the subgrid-scale processes should be developed to reach a better model performance especially for precipitation.

The variability among the results of different GCMs implies the considerable uncertainty due to the lack of understanding of the climate system. The multi-model ensembles should thus be used to take account of this uncertainty. The use of the multi-model ensembles allow exploring the relationships between the prediction skill in the future and the modelling skill in reproducing the baseline observation. However, it might be misleading to rank the future climate change projections based on the discrepancy between the model simulations and the baseline observations. For example, a skilful turned model might produce the smallest discrepancy but have large but compensating process-based errors. Previous studies found that climatological errors and projected changes are weakly correlated (Knutti et al. 2006, 2010b)(Murphy et al. 2004, Masson and Knutti 2011). The uncertainty in multi-model ensembles cannot fully represent the true uncertainty in the real world. The true uncertainty could be larger than the ensemble uncertainty as it is argued that the actual uncertainty in the representation of subgrid scale processes is not covered by the differences between the parametrization schemes used in existing models (Allen and Ingram,2002; Palmer et al., 2005). On the other hand, multi-model ensembles could exaggerate the uncertainty when some models is less credible than others. Summing up, impact-related studies could use multi-GCM ensembles to take account of the uncertainty in future climate change projections, and the interpretation of this uncertainty should be used with cautions.

Chapter 3 Empirical statistical downscaling methods

The objective of this chapter is to assess the uncertainty in the empirical statistical methods for downscaling daily GCM outputs and to provide the basis for using these downscaling methods in climate change impact assessments at a local scale.

3.1 Introduction

Due to the bias against observations and the lack of sufficient spatial resolution, it is well acknowledged that outputs of Global Climate Models (GCMs) need to be post-processed (including bias correction and downscaling) prior to being used for climate change impact studies. Assessments of climate change impacts usually focus on the local scale, while GCMs are run at coarse spatial resolution and are inherently unable to resolve important sub-grid scale features. Thus, downscaling methods are developed to bridge this gap in order to obtain the weather and climate information at the local scale. The downscaling methods can be divided into dynamical downscaling and statistical downscaling. The computationally-intensive nature complicates the use of dynamical downscaling in providing multi-decade simulations with multiple GCMs and/or greenhouse gas scenario (Wilby et al. 2000, Maurer and Hidalgo 2008, Tabor and Williams 2010, Jarosch et al. 2012). In contrast, statistical

downscaling methods are computationally efficient and sufficiently flexible to be used directly for climate change impact studies (Xu 1999, Wilby et al. 2002, Wood 2002, Diaz-Nieto and Wilby 2005, Fowler et al. 2007). Numerous previous studies have shown that the performance of statistical downscaling can be comparable to dynamical downscaling (Kidson and Thompson 1998, Mearns et al. 1999, Murphy 2000, Haylock et al. 2006).

Among the various statistical downscaling methods, a group of methods known as "empirical downscaling methods" (Chen et al. 2013) or "empirical scaling methods" (Mpelasoka and Chiew 2009) aiming to reduce the bias in climate model outputs is becoming increasingly popular especially if the analysis requires multi-GCM projections. In this group of methods, statistical transformation functions are calibrated and then used to adjust observations or raw climate model outputs to generate future climate scenarios at local scale. In contrast to the use of large-scale atmospheric fields as predictors in "perfect prognosis" statistical downscaling, empirical statistical downscaling methods directly use the observed or modelled variables of interest as predictors, which enable downscaling over regions where large-scale atmospheric observations are not available. Moreover, the use of relatively simple statistical transformations makes these methods particularly attractive (Salathe 2005, Fowler et al. 2007, Leander and Buishand 2007, Chiew et al. 2009, Mpelasoka and Chiew 2009, Teutschbein and Seibert 2012, Chen et al. 2013).

Depending on their use of calibration strategies, empirical downscaling can be divided into bias correction based methods and change factor based methods (Ho et al. 2012). Both these strategies aim to cope with the bias in climate model outputs, albeit being based on different assumptions. The bias correction based methods assume that the discrepancies between observation and model simulations stay constant in time, while the change factor based methods assume that the change from the present day to the future in the observed climatology will be the same as the change in the modelled climatology suggested by climate models. These methods also differ in the statistical transformations which are performed to adjust different statistics of the predictors including mean, variance or probability distribution.

Previous studies show that different choices of calibration strategies can lead to substantially different outcomes which may be as large as the differences between emission scenarios (Ho et al. 2012). The performance of different statistical transformation methods may also differ substantially (Gudmundsson et al. 2012). Despite the increasing use of these methods, a detailed investigation of the range of possible combinations of calibration strategy and statistical transformation methods as well as associated uncertainties has not yet been undertaken.

This chapter has the following specific objectives: 1) to classify the existing empirical statistical downscaling methods and to compare the possible combinations of calibration strategy and statistical transformation, 2) to test the performance of calibration strategies

and statistical transformation methods on downscaling GCMs daily precipitation and temperature to station scale, 3) to assess the uncertainty associated with empirical statistical methods for the full range of calibration strategies and statistical transformation methods tested.

3.2 Empirical methods for statistical downscaling

To describe the two distinct calibration strategies of empirical statistical downscaling (change factor and bias correction), the observed climatic variable during the baseline period is denoted as X_O and its future projection as X_O'; the climate model simulations of this variable are given as X_M and X_M' for baseline and future periods, respectively. Then the bias correction based methods can be generally formulated as:

$$X_O' = T_{BC}(X_M'), \quad T_{BC} : calibrated\ on\ X_M\ and\ X_O \qquad\qquad 3\text{-}1$$

while the change factor based methods are generally formulated as:

$$X_O' = T_{CF}(X_O), \quad T_{CF} : calibrated\ on\ X_M\ and\ X_M' \qquad\qquad 3\text{-}2$$

where T_{BC} and T_{CF} are the statistical transformation functions for the bias correction based methods and the change factor based methods, respectively.

In each group, the downscaling methods are classified into five types based on the statistical transformations used. The different combinations of calibration strategies and statistical transformations lead to ten empirical statistical downscaling methods as shown in Table 3.1. The transformation methods with bias correction strategy are described in the following paragraph; the transformation methods with change factor strategy have the same forms with the bias correction based methods and only differ in the variables (Table 3.1). Herein, these 10 methods were used to downscale daily GCM temperature and precipitation to station scale. To account for the seasonality, transformation functions were calibrated with daily data grouped into four seasons.

- **Mean based (MB) method**: The simplest transformation is to match the mean of climate model simulations to that of observations and subsequently remove the mean bias in the climate model simulations. Additive and multiplicative correction factors were respectively applied to the modeled time series of temperature and precipitation.
- **Variance based (VB) method**: This is a more sophisticated method which corrects both the mean and variance of climate model simulations to match those of the observations. This is done by including the standard deviation in the transformation function.
- **Quantile mapping (QM) method**: In this method a quantile-based mapping (Panofsky and Brier 1958) is constructed from modelled probabilistic distribution to observed

probabilistic distribution. Specifically, a value of modeled variant, e.g. the *p*th percentile in the modeled distribution, is corrected as the value of the *p*th percentile in the observed distribution. The basic assumption of this method is that the distributions of the modelled variable from the baseline period to the future period remain similar. The probabilistic distribution of climatic variables can be described by theoretical or empirical CDFs. Here, the commonly used 99-percentile tables were employed (Boé et al. 2007, Deque 2007) due to the superior performance of empirical CDFs in the previous studies (Themeßl et al. 2011, Gudmundsson et al. 2012, Gutjahr and Heinemann 2013). The values in between the percentiles were obtained by linear interpolation, and the values exceeding the percentile tables were corrected using the correction factor at the highest (or lowest) percentile.

- **Quantile correcting (QC) method**: This method is also a quantile based correction. It allows incorporating the information of the change in modelled distributions from the baseline period to the future period, which is different with the basic assumption of the quantile mapping method that no evolvement occurs in the modelled distribution over time. At each quantile, the difference between the modelled and observed value during the baseline period is assumed to be stationary and then applied to the modelled distribution in the future period. If there is no change in the modelled distribution over time, the quantile correcting method will derive the same results as the quantile mapping method. It can also be considered as a variant of the mean based method that corrects model simulations at different quantiles instead of applying one single correcting factor throughout.

- **Transfer function (TF) method**: This method uses the same distribution-correction principle as the quantile mapping method, but applies the correction in a parametric way. Parametric functions are fitted to the quantile-quantile relationship between modeled and observed variables during the calibration period, which was then used to correct the future modeled values. Various transfer functions have been used in previous studies (Piani et al. 2010, Dosio and Paruolo 2011, Rojas et al. 2011). Here, power functions and linear functions were used to correct precipitation and temperature, respectively. However, for both precipitation and temperature, linear functions were used to correct extreme values (exceeding the 90th percentile or less than the 10th percentile for temperature, and exceeding the 90th percentile for precipitation).

Table 3.1 Empirical statistical downscaling methods

(Subscript 'O' represents observation, and 'M' represents modelled variable; with or without the apostrophe represents future and calibration period respectively; F and F^{-1} represent ECDF and reverse ECDF, respectively.)

Calibration strategy	Methods & Abbreviation	Transformation for precipitation	Transformation for temperature	Reference of existing methods
Bias-correction strategy	Mean based method M1: MB-BC	$X'_O = X'_M \cdot \dfrac{\mu_O}{\mu_M}$	$X'_O = X'_M + \mu_O - \mu_M$	Schmidli et al. (2006) ; Lenderink et al. (2007)
	Variance base method M2: VB-BC	$X'_O = \dfrac{(X'_M - \mu_M)}{\sigma_M} \cdot \sigma_O + \mu_O$	The same with precipitation	Bouwer and Aerts (2004); Ho et al. (2012); Hawkins et al. (2013);
	Quantile mapping M3: QM-BC	$X'_O = F_O^{-1}[F_M(X'_M)]$	The same with precipitation	(Wood 2002, Wood et al. 2004); Ines and Hansen (2006); Deque (2007); Themeßl et al. (2011);
	Quantile correcting M4: QC-BC	$X'_O = X'_M \cdot \dfrac{F_O^{-1}[F_{M'}(X'_M)]}{F_M^{-1}[F_{M'}(X'_M)]}$	$X'_O = X'_M + F_O^{-1}[F_{M'}(X'_M)] - F_M^{-1}[F_{M'}(X'_M)]$	Mpelasoka and Chiew (2009); Li et al. (2010); Hemer et al. (2012)
	Transfer function M5: TF-BC	$X'_O = a \cdot X'^{b}_M$	$X'_O = a \cdot X'_M + b$	(Piani et al. 2009, Piani et al. 2010); Zhang (2005)
Change-factor strategy	Mean based method M6: MB-CF	$X'_O = X_O \cdot \dfrac{\mu_{M'}}{\mu_M}$	$X'_O = X_O + \mu_{M'} - \mu_M$	Prudhomme et al. (2002); Fowler et al. (2007)
	Variance base method M7: VB-CF	$X'_O = \dfrac{(X_O - \mu_M)}{\sigma_M} \cdot \sigma_{M'} + \mu_{M'}$	The same with precipitation	Shabalova et al. (2003); Hawkins et al. (2013)
	Quantile mapping M8: QM-CF	$X'_O = F_{M'}^{-1}[F_M(X_O)]$	The same with precipitation	Räisänen and Räty (2012)
	Quantile correcting M9: QC-CF	$X'_O = X_O \cdot \dfrac{F_{M'}^{-1}[F_O(X_O)]}{F_M^{-1}[F_O(X_O)]}$	$X'_O = X_O + F_{M'}^{-1}[F_O(X_O)] - F_M^{-1}[F_O(X_O)]$	Mpelasoka and Chiew (2009)
	Transfer function M10: TF-CF	$X'_O = a \cdot X^{b}_O$	$X'_O = a \cdot X_O + b$	Räisänen and Räty (2012)

The above statistical transformations do not change the temporal sequence of the predictor. In the case of downscaling daily precipitation based on bias correction strategy, because precipitation events are intermittent, the biases in both the frequency and intensity of the modelled precipitation need to be considered. As GCMs tend to project the "drizzle-effect" and overestimate the wet-day frequency, a frequency adaptation step was applied to match the modelled wet-day frequency with observations (Ines and Hansen 2006, Schmidli et al. 2006). A modelled wet-day threshold was determined from the GCM daily precipitation series such that the threshold exceedance matches the wet-day frequency in the observed series. The calculation of the modelled wet-day threshold can be expressed as

$$WT_M = F_M^{-1}[F_O(WT_O)] \qquad\qquad 3\text{-}3$$

where the minimum observed rainfall amount WT_O for a day to be considered wet was 0.1 mm, which is the minimal value of the historical rainfall records; F and F^{-1} represent empirical cumulative distribution function (ECDF) and reversed ECDF. Then the bias-correction based downscaling can be expressed as

$$X_O' = \begin{cases} T_{BC}(X_M') & \text{for} \quad X_M' \geq WT_M \\ 0 & \text{for} \quad X_M' < WT_M \end{cases} \qquad\qquad 3\text{-}4$$

3.3 Validation in a model world

3.3.1 Inter-model cross validation

To compare the different methods described above, the inter-model cross validation method (Räisänen and Palmer 2001, Murphy et al. 2004, Räisänen and Räty 2012) was adopted in this study. This is a 'perfect sibling' framework, where data from a set of model simulations are calibrated and verified against an independent model simulation which is treated as the pseudo-observation of the climate (or 'true' climate).

As shown in Figure 3.1, the model cross validation is performed over a multi-GCM ensemble (e.g. with N GCMs). The projection of one GCM (model i) including baseline climate and future climate is selected as the pseudo-observation. The pseudo-observation is considered as a "true" climate; and the outputs of other N-1 GCMs (i.e., calibrating models) in the ensemble are considered the biased simulation of the climate in the pseudo-observation. The projection of the future climate corresponding to the pseudo-observation is derived from each calibrating model and then verified against the "true" future climate in the pseudo-observation. Repeating the process N times to enable all ensemble members to be treated as the pseudo-observations, statistics can be obtained to compare the performances of different downscaling methods.
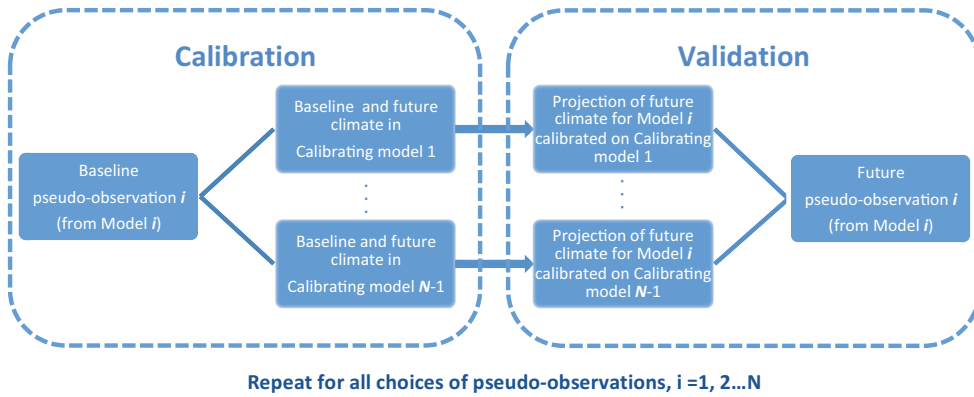
Figure 3.1 Sketch of inter-model cross validation

To mimic empirical statistical downscaling in the real-world, when a GCM is taken as a pseudo-observation, the gridded simulation was interpolated to station locations (30 stations) using bilinear interpolation. This way, the pseudo-observation at station scale corresponding to the selected GCM simulation is constructed. Statistical transformations were performed at each station to construct the downscaled Climate projections.

To assess the performance of the different downscaling methods, a factor of Mean Relative Error (MRE) was used to quantify the similarity of empirical CDFs between pseudo-observations and downscaled projections. MRE is calculated as

$$MRE_p = \langle \frac{\langle ABS(X'_p - X^O_p) \rangle_G}{\langle ABS(X^{Raw}_p - X^O_p) \rangle_G} \rangle_{SE,ST,O} \qquad \text{3-5}$$

Where X'_p and X^O_p are the pth percentiles of the downscaled and pseudo-observed distributions, respectively; X^{Raw}_p is the pth percentile of raw GCMs projection, $p = 0 \dots 100$; ABS denotes the absolute values; $\langle \cdot \rangle_G$ denotes taking average over all choice of calibrating GCMs (denoted as G); $\langle \cdot \rangle_{SE,ST,O}$ denotes taking average over all seasons (SE), stations (ST) and pseudo-observations (O).

MRE is essentially a ratio of the absolute error of downscaled projections to the absolute error of raw projections. When MRE is larger than 1, the downscaling method introduces more bias than the raw GCM; when MRE is equal to 1, the downscaling method performs the same as the raw GCM; when MRE approaches 0, the downscaling method projects the same distribution as the pseudo-observation.

CMIP5 (Coupled Model Intercomparison Project Phase 5) projections of daily precipitation and temperature from 16 GCMs (grid size ranging from 1.1^o to 2.8^o) were used in this study (see Table 2.1 in Chapter 2). The baseline (calibration) period was selected as 1961 to 1990 and the future period was selected as 2071 to 2100. All future GCM outputs were obtained

under a high greenhouse gas emission scenario (RCP8.5). The grid cells of the GCM with the largest resolution and the gauge stations are shown in Figure 3.2.
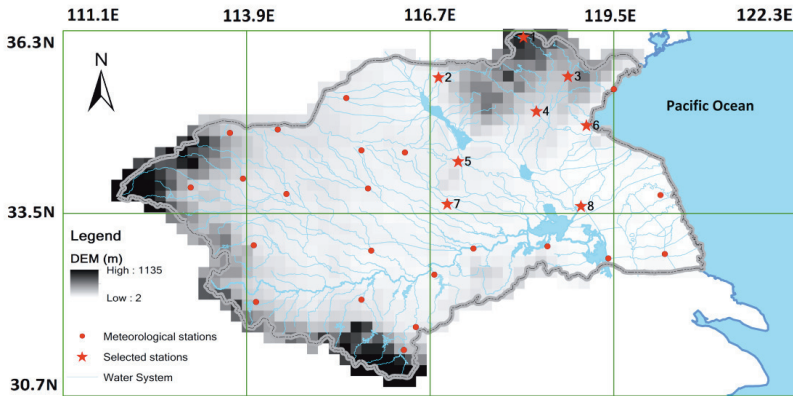

Figure 3.2 Stations and the grid cells of GCM BCC-CSM1.1 (2.8125°×2.8°) over the Huai River Basin

3.3.2 Results of inter-model cross validation

3.3.2.1 Temperature

Figure 3.3 (a) shows the MRE of temperature for all the methods under consideration. For comparison, the MRE of raw GCMs is also drawn as the horizontal line with a uniform value of one. The change factor based methods generally outperformed BC based methods especially at the upper part of the distribution, which is in agreement with Hawkins et al. (2013). Moreover, the spread between different transformation methods applied with the CF strategy is smaller than those applied with the BC strategy. As an exception, the quantile correcting methods with both calibration strategies show almost the same performance. The simplest mean based method with the change factor strategy has the best overall performance. With the bias correction strategy, the mean based transformation resulted in the smallest errors in the middle part of the distribution (30%-60% percentiles), but produced large errors at the lower and upper parts of the distribution owing to the uniform correction over the whole distribution. The transfer function method and variance based method with the change factor strategy have a similar performance around the middle part of the distribution (30%-70% percentiles) due to the use of similar transformation functions. At the extreme high and low tails of the distribution, TF methods have the largest MRE, which indicates that the use of linear transfer functions fitted to extrapolate the extreme values performed less well on projecting extremes.
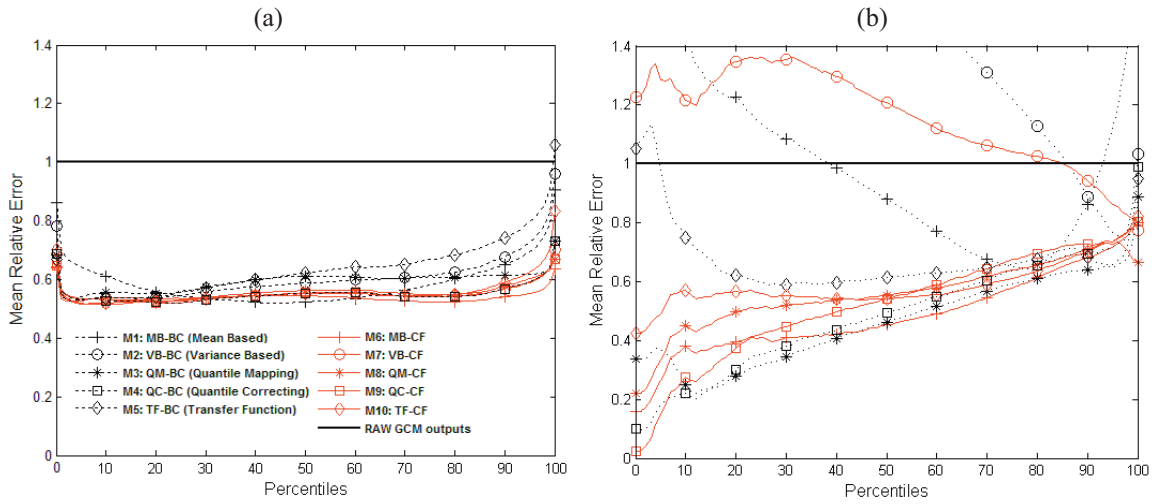
Figure 3.3 Performance ranking of empirical downscaling methods used for downscaling daily temperature (a) and daily precipitation intensity (b). BC and CF calibration strategies are indicated by black dashed lines and red solid lines, respectively.
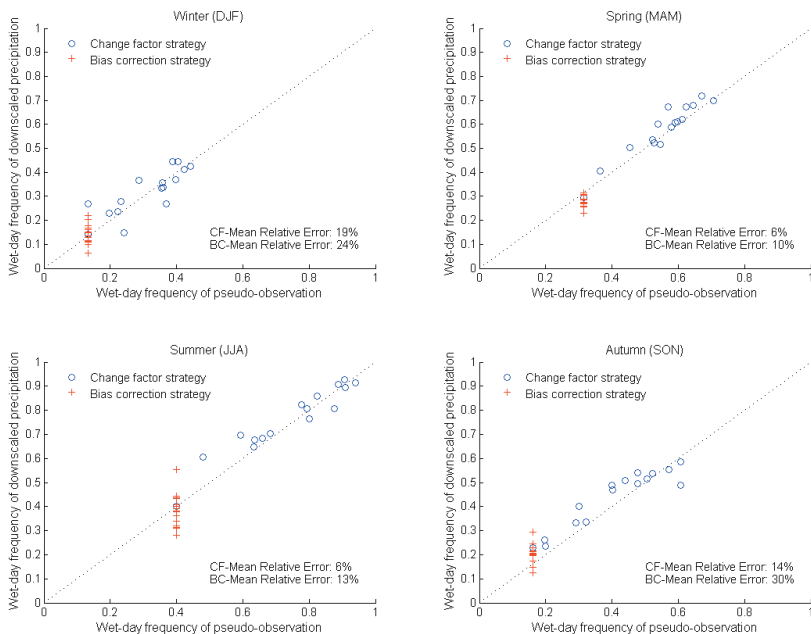
3.3.2.1 Precipitation

Precipitation intensity

The MRE of daily precipitation intensity for all the methods is shown in Figure 3.3 (b). In contrast to temperature, there is no overall better performing calibration strategy. The difference arising from the choice of transformation methods is larger than the difference arising from the choice of calibration strategies. The change factor based methods generally downscaled extreme values with lower MREs compared to the bias correction based methods, which is probably caused by the extrapolation uncertainty of the transformation methods. Because transformation functions with bias correction strategy were calibrated on GCM simulations of the baseline period, the transformation functions have to be extrapolated when the values of the future projection exceed the range of the baseline simulation. The performances of different downscaling methods vary obviously at the lower half of the distribution mainly owing to the choice of transformation methods. Similar to the results of temperature downscaling, with the change factor strategy the mean based method shows better performance than other more sophisticated methods. The non-parametric quantile mapping and quantile correcting methods with the bias correction strategy show relatively better overall performance, and they both outperform their counterparts with the change factor strategy. The variance based methods have the worst overall performance but show a decreasing error in the upper part of the distribution, which indicates they put more weight on adjusting the daily precipitation with high intensity. In the lower part of the distribution, the transfer function methods do not perform as well as other quantile-based methods.

Frequency of precipitation occurrence

Taking the example of one station (Station 7 in Figure 3.2), the occurrence frequency (the fraction of wet days) of downscaled precipitation and pseudo-observation in four seasons for the future period is compared in Figure 3.4. The comparison between calibration strategies is carried out by comparing two sets of "true-against-projection pairs" that respectively resulted from bias correction (BC) strategy and change factor (CF) strategy. The CF sample pairs are from 16 pseudo-observations against their corresponding projections downscaled from other models (blue circles). Since the frequency adaptation in BC strategy was only performed when the modelled wet-day frequency exceeds the wet-day frequency of a pseudo-observation, the BC samples are the pseudo-observation with the lowest baseline wet-day frequency against its projections downscaled from the other 15 models (red crosses). The mean relative error is used as the criterion to assess the performance of the two strategies. Generally, the BC strategy projects larger relative error than the CF strategy in every season at Station 7. The projections at other stations show similar results (not shown). Figure 3.4 indicates that the CF strategy generally underestimates the precipitation frequency. This can be explained by the increase in the precipitation frequency of the pseudo-observation from the calibration period to the future period. The lower relative error of the CF strategy compared to the BC strategy implies that the GCM-projected change in precipitation frequency from calibration period to the future period is smaller than the variability in projected precipitation frequency among different GCMs.

Figure 3.4 Comparison of the future precipitation frequency of pseudo-observation and downscaled precipitation using different calibration strategies

3.4 Downscaling for the future

The downscaling methods were also applied to obtain a downscaled future climate based on the information from historical observations. The 10 downscaling methods were used to downscale the outputs from the 16-GCM ensemble, which results in 160 combinations of downscaling methods and GCM outputs. This section investigates the uncertainty in the downscaled future local climate associated with the choice of different empirical downscaling methods (calibration strategies and transformation methods) and climate models.

3.4.1 Future climatology

Temperature

Since GCMs are not designed to simulate the actual temporal sequence of the climatic variable, the downscaled future mean climatology and the inter-annual variability of the monthly temperature were analyzed. The 30-year means and standard deviations of monthly mean temperature averaged over 30 stations from downscaled future GCM ensembles (2071-2100) and observations (1961-1990) are shown in Figure 3.5. The downscaled results of an individual GCM (HadGEM-ES) are also shown.

The downscaled GCM ensemble generally projected an increase in mean temperature. The agreement in the intra-annual variations among downscaled monthly means reflects the main feature of empirical statistical downscaling methods, i.e., they are designed to remove the bias in the statistics (at least the mean) of the GCM outputs. The uncertainty bound (the range encompassed by the maximum and minimum of the results downscaled from the 16 GCMs using the 5 statistical transformations) of the bias correction based methods (light grey area) is slightly larger than that of the change factor based methods (dark grey area).

In terms of the inter-annual variability, the bias correction based methods resulted in much larger uncertainty than the change factor based methods did due to the uses of different predictors. The varied results of the bias correction based methods reflect the large variability in the projected temporal structures among different GCMs. In contrast, the change factor based methods preserved the same temporal structure as observed daily time series. The mean-based change-factor (MB-CF) method (red crosses) resulted in exactly the same intra-annual variability as only the shift in mean was applied to the observed time series, and the differences between mean based method and other sophisticated methods were caused by adjusting other statistics of the observation.
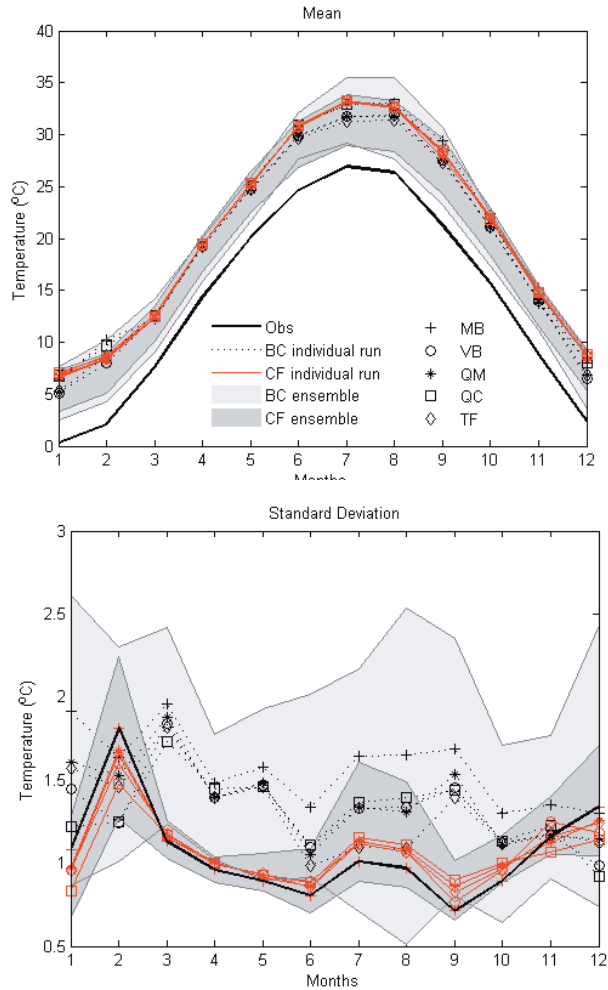
Figure 3.5 Interannual mean (top panel) and standard deviation (bottom panel) of monthly mean temperature from future projections (2071-2100) and observation (1961-1990). Grey areas indicate the ensemble of GCM outputs downscaled with bias correction (light grey) and change factor (dark grey) strategies. Lines with symbols are downscaled projections of model HadGEM-ES.

Precipitation

Because precipitation events are intermittent, the downscaled precipitation was assessed using three indicators: monthly total amount (mm/day), monthly mean intensity (mm/wet day) and monthly frequency (the proportion of the number of wet days within a month) (see Figure 3.6).
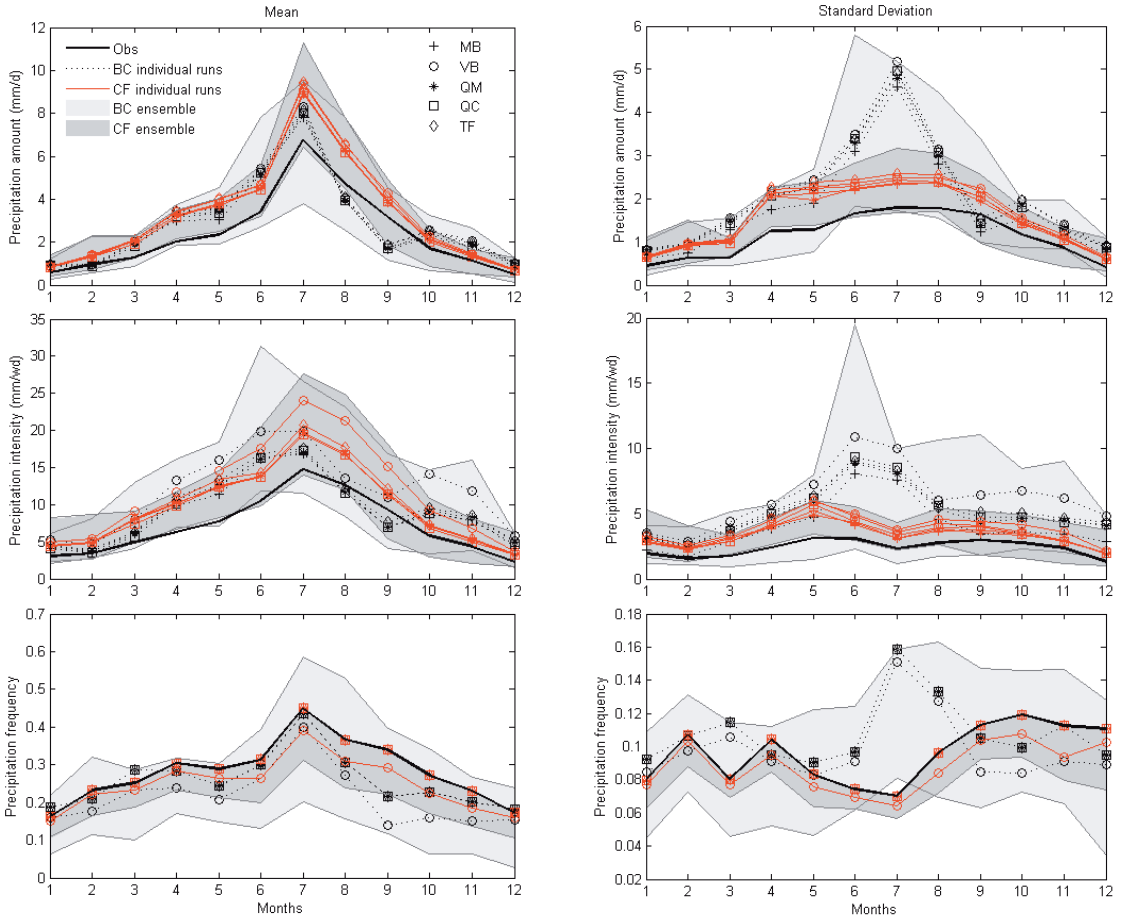
Figure 3.6 Interannual mean (left panel) and standard deviation (right panel) of monthly precipitation amount (top), intensity (middle) and wet-day frequency (bottom). Grey areas indicate the ensemble of GCM outputs downscaled with bias correction (light grey) and change factor (dark grey) strategies. Lines with symbols are downscaled projections of model HadGEM-ES.

Generally speaking, the two calibration strategies both projected increases in mean values and inter-annual variability of precipitation amount and intensity. However, similar with the results of temperature, the change factor based methods resulted in narrower uncertainty bounds than the bias correction based methods did. The choice of the calibration strategies has more significant influence on the inter-annual variability than on the mean values of the precipitation indicators.

By comparing the results from one GCM (black dotted and red solid lines), it can be seen that, for all precipitation indicators, the results from one calibration strategy with different transformation methods are very similar. The choice of calibration strategies leads to different annual patterns of the mean precipitation factors, which again reflects one of the features of empirical statistical downscaling methods in that they project the downscaled

time series with the same temporal structure of the predictor variable. In general the distribution-wise transformation methods projected larger inter-annual variability of precipitation amount and mean intensity than the mean based methods; however, the difference is marginal. This implies that scaling the mean of the distribution is capable of correcting most of the change in the inter-annual variation of the mean precipitation intensity; distribution-wise methods do not significantly improve the ability to project inter-annual variability of mean precipitation intensity.

The methods with the same calibration strategy produced the same downscaled wet-day frequency with the exception of the variance based method, which projected lower frequency compared to other methods. As the statistical transformations were performed over daily GCM output, the shift in mean and the scaling of standard deviation in the variance based methods may convert small values of wet days into negative values which would hence be converted as dry days. The same reason holds for the variance based method projecting higher monthly mean intensity than other transformation methods. However, there is no obvious deviation between the monthly amounts of the variance based method and other methods.

3.4.2 Comparison of different sources of uncertainty

To quantify the uncertainties associated with downscaling methods and GCMs, the "analysis of variance" method was used (Déqué et al. 2011, Räisänen and Räty 2012). The total variance of downscaled projections was divided into three parts of variation caused by GCMs, downscaling methods and the interactions between GCMs and downscaling methods (the GCM-method interactions), respectively. The variance caused by GCMs is represented by the variation of multi-method mean projections across GCMs, and the variance caused by downscaling methods is represented by the variation of multi-GCM mean projections across methods. The contribution of GCM-method interactions is explained as the method dependence of inter-GCM differences, or equivalently GCM dependence of inter-method differences. The percentages of variation components were calculated at each percentile, and the results were averaged over stations and months. The analysis of variance was respectively performed on downscaled projections at monthly and daily scales. The analysis was performed separately for the bias correction based methods, the change factor based methods and all downscaling methods.
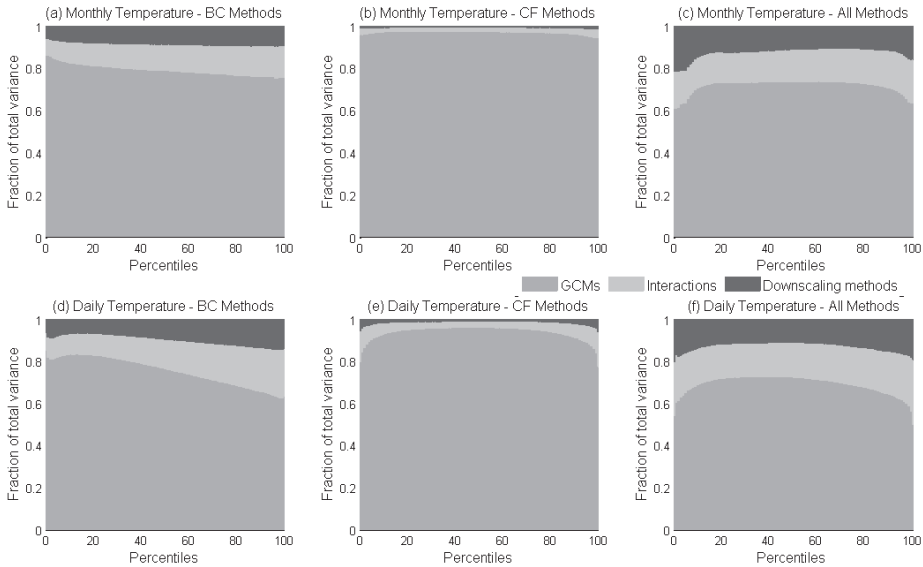
Figure 3.7 Fractions of temperature variance explained by GCM difference (dark grey), downscaling method differences (black) and the GCM-method interactions (light grey). Left, middle and right panels respectively show the results of BC methods, CF methods and all methods; top and bottom rows show the results at monthly and daily scale, respectively.

For temperature, the uncertainty associated with the choice of GCMs accounts for a large part of the total uncertainty (see Figure 3.7). The percentages of variance due to downscaling methods and the GCM-method interactions grow slightly from monthly scale to daily scale, and the growth is larger at the extreme high and low ends of the distribution. Bias correction strategy resulted in relatively more variance caused by downscaling methods and the GCM-method interactions than change factor strategy. The variance due to the bias correction based methods keeps increasing toward the higher end of the distribution due to the extrapolation uncertainty of transformation methods. Taking all the downscaling methods into account, the variance due to downscaling methods and GCM-method interactions respectively contribute 15% and 22% to the total variance of daily temperature averaged over the distribution.
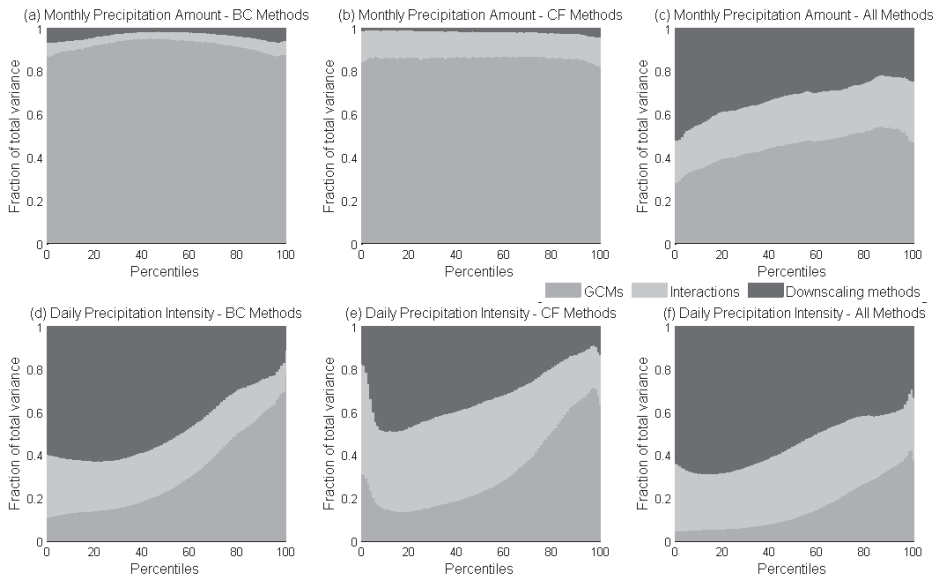
Figure 3.8 Fractions of precipitation variance explained by GCM difference (dark grey), downscaling method differences (black) and the GCM-method interactions (light grey). Left, middle and right panels respectively show the results of BC methods, CF methods and all methods; top and bottom rows show the results at monthly and daily scale, respectively.

Figure 3.8 shows the fractions of variance of downscaled precipitation due to GCMs, downscaling methods and the GCM-method interactions. The downscaling methods used are more influential on downscaled precipitation on a daily scale than a monthly scale. For downscaled monthly precipitation (the top row in Figure 3.8), downscaling methods have a minor contribution to the total variance in the case of single calibration strategy, and their contribution increases toward the tails of the distribution. However, the contribution of downscaling methods is comparable to the contribution of GCMs in the case of all downscaling methods, which indicates that the two calibration strategies lead to deviated results at monthly scale. For downscaled daily precipitation (the bottom row in Figure 3.7), the choice of downscaling methods and the GCM-method interactions dominate the total variance in the lower part of the distribution, but their impacts decrease at the higher end of the distribution. Comparing the two calibration strategies, the uncertainty related to transformation methods resulted in a smaller percentage of the total variance with the change factor strategy than with the bias correction strategy; however, the change factor based methods lead to more GCM-method interaction uncertainty than the bias correction based methods.
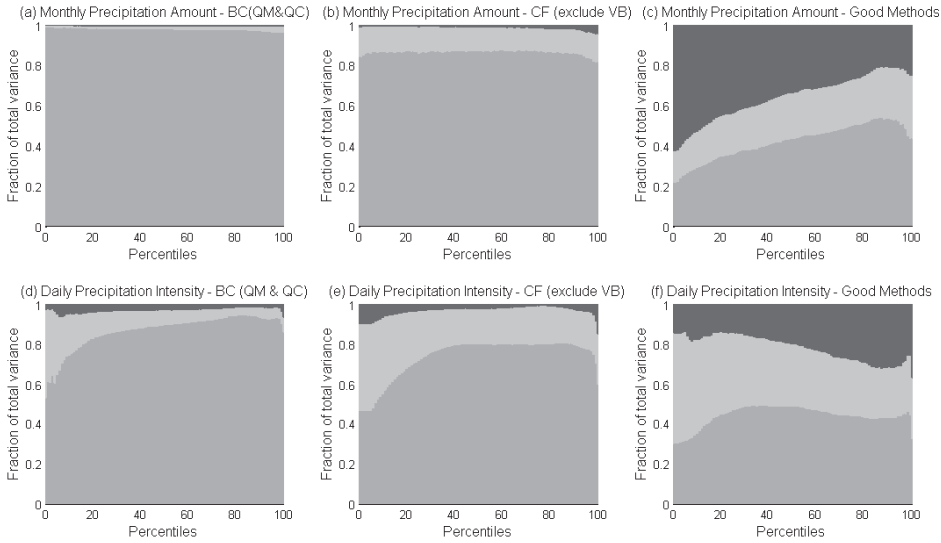
Figure 3.9 Similar with Figure 3.8 but excluding sub-optimal performing met. Left, middle and right panels respectively show the results of well-performing BC methods, well-performing CF methods and all well-performing methods.

As can be seen in the results of the inter-model cross validation (Figure 3.3b), the MB-BC, VB-BC, TF-BC and VB-CF methods lead to larger errors compared to other methods for downscaling precipitation. When making the decomposition of variance excluding these methods, the fraction of variance caused by downscaling methods decreases in the case of single calibration strategy (Figure 3.9). However, the contribution of all well-performing methods (excluding the sub-optimally performing methods) to the total variance of monthly precipitation amount (Figure 3.9c) is comparable to the contribution of all methods (Figure 3.8c). For downscaled daily precipitation intensity, the fraction of the variance caused by GCMs takes a large part of the total variance in the case of single calibration, while this fraction decreases toward the tails of the distribution. When taking into account all well-performing methods, the contribution of downscaling methods is about 20% of the total variance at the low end of the distribution, increasing to about 30% toward the high end of the distribution. Around 50% of the total variance at the low end of the distribution is due to the interactions between downscaling methods and GCMs. This fraction decreases to about 25% toward the high end of the distribution, where it is comparable with the contribution of downscaling methods.

3.4.3 Uncertainty in future changes at one station

The uncertainty in downscaled projections was also analysed with preference to one specific location. For Station 7, the changes in future downscaled temperature and precipitation intensity compared to the historical observations are shown in Figure 3.10. The change of

temperature was calculated as the shift at each percentile between the future projection and the baseline observation, and the change of precipitation intensity was calculated as the ratio at each percentile between the future projection and the baseline observation. The changes were averaged over seasons and GCMs.
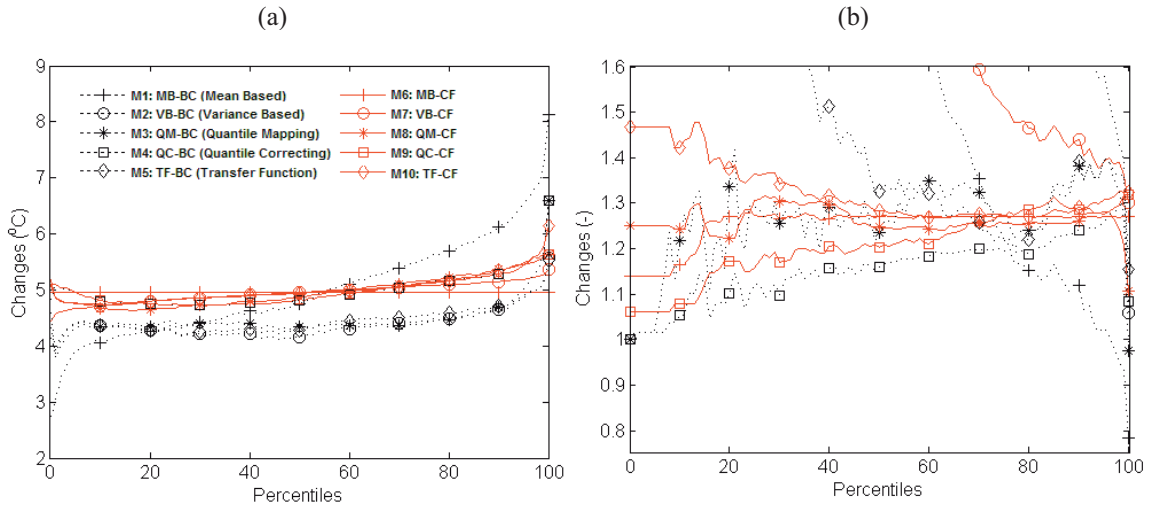
Figure 3.10 Changes at percentiles in downscaled future daily temperature (a) and daily precipitation intensity (b) at Station 7. BC and CF calibration strategies are indicated by black dashed lines and red solid lines, respectively.

The spread of different downscaling methods is generally in accordance with the results in the inter-model cross validation (Figure 3.3). For temperature, there is a deviation between the spread of the BC based methods and that of the CF based methods, and the former produced less warm future climate than the latter. The result of the MB-BC method intersects the results of other methods and deviates from them at the low and high ends of the distributions, which explains why the MB-BC method lead to small errors at the middle of the distribution and large errors at the lower and higher distribution in the inter-model cross validation (Figure 3.3a). The MB-CF method projected relatively greater changes at the low end and smaller changes at the high end compared to other methods applied with the CF strategy.

For precipitation, the spread of the projected changes is larger for low intensity than for higher intensity. The curves of the MB-BC, VB-BC and VB-CF methods obviously deviate from those of other methods. These observations are in accordance with the results in the inter-model cross validation. The TF-BC method lead to more deviated result from other methods compared to its performance in the virtual-world experiment, which is probably due to the larger difference between the observed and modelled wet-day frequencies. As expected, the MB-CF method resulted in a horizontal line for most part of the distribution. This line deviates toward smaller values at percentiles lower than 25% because the small values of

the projected precipitation intensity were rounded to zeros. The MB-CF, QM-CF, TF-CF, QM-BC and QC-BC methods projected comparative changes for high intensity precipitation.

3.4.4 Difference in temporal structure and spatial variability due to the choice of downscaling methods

The temporal structure and spatial variability of the downscaled future daily precipitation were shown in Figure 3.11 and Figure 3.12. The time series of daily precipitation at 8 stations within one grid of model BCC-CSM1.1 were selected (indicated as stars in Figure 3.2), and the summers in the years from 2071 to 2073 are taken as the example time segments. The downscaled climatic variables at different stations within a GCM grid inherit the same areal-mean GCM information from this grid cell. When downscaled by the change factor based methods, the stations within a GCM grid cell share the same relative change and the spatial variability stays the same with that of the observation. On the other hand, when downscaled by the bias correction based methods, the stations within a GCM grid follow the temporal structure of the GCM and the spatial variability on a specific day is thus lower compared to the observations. The methods applied with the same calibration strategy resulted in a similar temporal structure with the exception that the variance based methods lead to more dry days than other transformation methods.
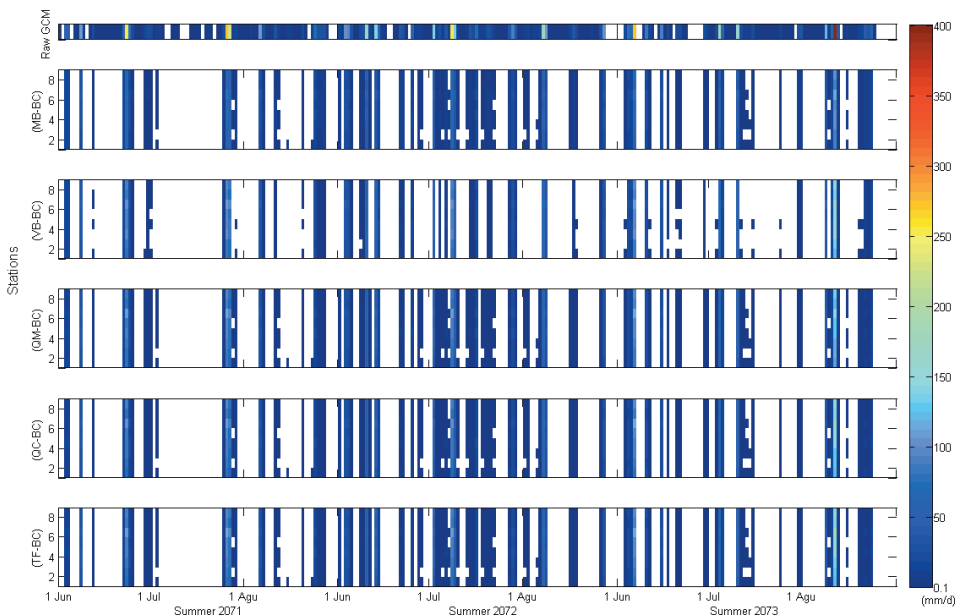
Figure 3.11 Time series for raw GCM (top) and downscaled daily precipitation using the BC based methods for selected seasons
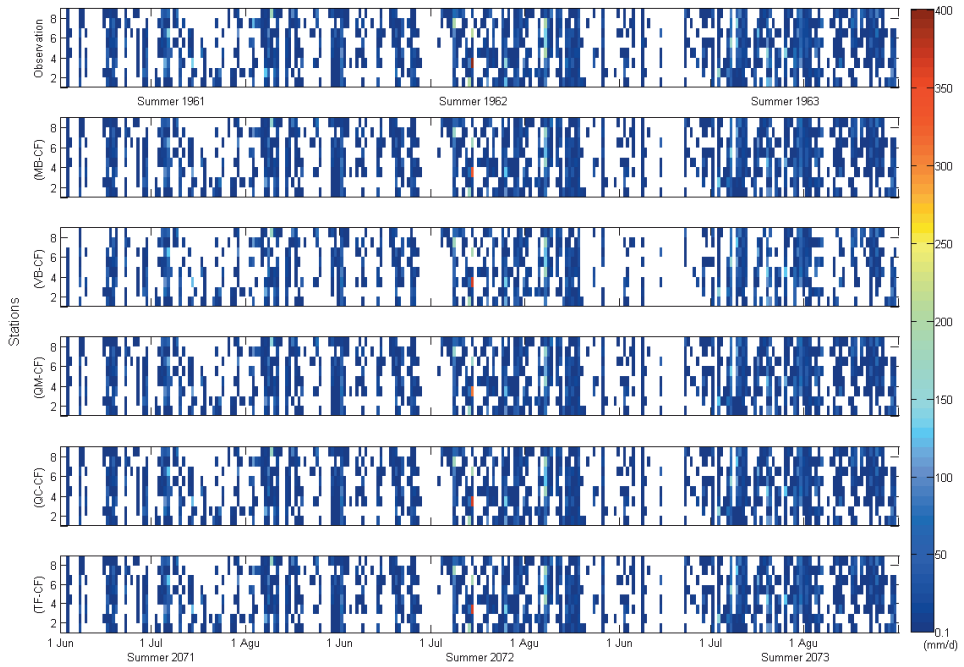
Figure 3.12 Time series for observed (top) and downscaled daily precipitation using the CF based methods for selected seasons

The empirical CDFs of the downscaled daily precipitation at Station 7 are shown in Figure 3.13a, and the empirical CDFs of the areal mean of the downscaled precipitation are shown in Figure 3.13b. The bias correction based methods resulted in smaller extreme values than the change factor methods at a specific station, which is caused by the extrapolation of the transformation functions for the future values exceeding the range of the baseline values. In contrast, the bias correction based methods resulted in greater areal-mean extreme values than the change factor based methods. This is due to the lack of spatial variability in the bias correction based methods, i.e., if the GCM projects a high value at a grid cell on a day, all the stations within the grid have high values on this day and the areal-mean value is thus exaggerated. For the same reason, bias correction based methods projected more dry days than the change factor based methods at the areal-mean scale.

The MB-BC method produced comparable areal-mean extreme values to the change factor based methods due to the former's underestimation of point extreme values. The MB-CF method resulted in comparable point and areal-mean values to those of other change factor based methods, which confirms our claim that with the change factor calibration strategy, simply adding (for temperature) or multiplying (for precipitation) the mean change factor is sufficient to represent the relative changes projected by GCMs. The variance based methods produced comparable sorted values with others but more dry days, which explains the large

deviation in the precipitation intensity. Thus, care should be taken when using the variance based methods when the length of dry spell is important.
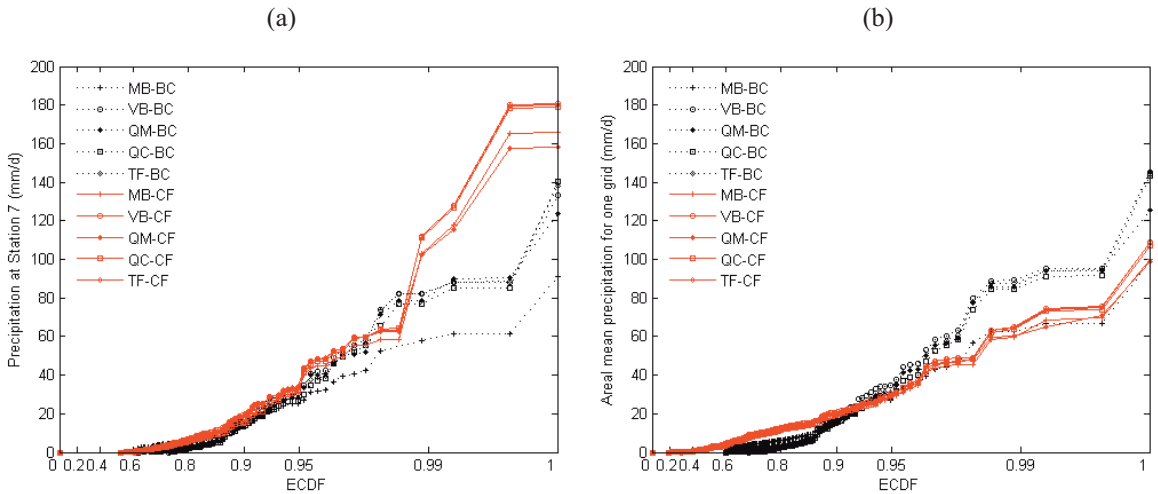
(a)   (b)

Figure 3.13 ECDFs of downscaled future daily precipitation at Station 7 (left) and areal mean at one GCM grid (right) for selected seasons

3.5 Discussion

Assessing the performances of calibration strategies and statistical transformation methods

For downscaling daily GCM temperature, the change factor based methods generally outperformed the bias correction based methods, which implies that the climate models provide more accurate simulations of relative change than absolute values. The different statistical transformation methods with change factor strategy showed similar performances, among which the simplest mean based method produced lower overall errors than other more sophisticated methods. These results can be explained by the property of the used pseudo-observations, i.e., GCMs tend to project a shift in mean temperature rather than a change in the higher-order statistics. In the bias correction based methods the probabilistic distributions of different GCM projections differ not only in the means but also in the scale and shape parameters of the distribution; thus, corrections of the higher-order statistics of the GCM outputs are required.

The obvious deviation in the performances of the two strategies at the higher part of the distribution is probably caused by the uncertainty associated with the extrapolation of the transformation functions. This is attributed to the use of a high-end greenhouse gas emission scenario (RCP85) which leads to the projected future temperature that significantly exceeds the maximum baseline temperature. If the projected increase in mean temperature is first removed from the future temperature time series before bias correction and later

added back to the corrected time series, the influence of the extrapolation uncertainty could be decreased. Quantile correcting method is the only member of the bias correction family that produced comparable performance with the change factor family, because no extrapolation is required in this method.

For downscaling daily GCM precipitation, there is no overall-better-performing calibration strategy. The difference arising from the choice of transformation methods is larger than the difference arising from the choice of calibration strategies with regard to the probabilistic distributions of daily intensity. The downscaled precipitation intensity was mainly influenced by the choice of statistical transformations at the lower part of the distribution. The bias correction strategy resulted in larger errors at the high extremes than the change factor strategy, which may be due to the unrealistic values projected by GCMs.

The comparative performances between mean based methods and distribution-wise methods with change factor strategy imply that the scaling of mean precipitation is sufficient to represent most of the relative change projected by GCMs. The advantage of using quantile-based methods is only apparent at the tails of the distribution. This mean-based change factor method has been widely used in the climate change impact assessments due to its ease of use. The variance based methods are not recommended to downscale daily precipitation as they focus on adjusting high precipitation intensity and thus may result in large biases in low intensity and wet-day frequency. The transfer function methods used in this study generally underperformed the quantile mapping methods especially at the low and high ends of the distribution. The parametric functions used here tend to fit well in the middle part of the distribution while sacrificing on accuracy at the ends of the distribution. In contrast, empirical quantile mapping methods are sufficiently flexible to describe the quantile-quantile relationships. However, when introducing more flexible parametric functions, the performance of the transfer function methods can be as good as the empirical quantile based methods. Examples can be seen in Gudmundsson et al. (2012)'s study. On the other hand, the use of empirical quantile mapping methods may be criticised to be less robust or constant in time since they have too many degrees of freedom (Piani et al. 2010). There has not been a consensus on the preference of parametric functions and empirical quantile mapping methods. Moreover, the suitability of parametric functions may also be dependent on the GCM outputs used.

The different results obtained for wet-day frequency from different calibration strategies are due to the distinctly different ways of projecting future precipitation series. The change factor based methods are designed to produce the downscaled future precipitation series preserving the same temporal sequence with that of the pseudo-observation. In contrast, the bias correction based methods use the modelled future precipitation series as predictor and apply the frequency adaptation to approximately match the modelled precipitation frequency to the pseudo-observations. The change factor strategy preserved the same wet-day frequency and tended to underestimate this in the future as most GCMs projected

increased future wet-day frequency. For the ensemble used here, the variation of wet-day frequency among GCMs projections was larger than the projected changes in each model. Thus, the bias correction strategy resulted in much more varied results than the change factor strategy. It should also be noted that the step of frequency adaptation in the bias correction based methods may also have an influence on the downscaled precipitation due to the risk of rejecting useful wet-day information.

The performances of change factor based methods in the virtual world were actually dependent on the degree of the similarity between the future changes projected by the calibrating GCM and the validating GCM. The relatively better performance of the MB-CF method in the virtual-world experiment only implies that the future changes projected by GCM members are more similar in mean than in higher-order statistics, and it does not guarantee that the MB-CF method will lead to more reliable results for the real-world future. This might be a drawback of using the inter-model cross validation. Moreover, the bilinear interpolation at the pseudo-station locations in the inter-model cross validation did not result in the variability and existence of extremes common in true station data. Thus, the uncertainty analysis on the downscaled precipitation based on a real station was carried out to confirm the results from the virtual world (shown in Section 3.4.3). These latter results generally confirmed the results from the virtual-world experiment. The uncertainty behavior in projecting future real-world climate was found similar to that in the inter-model cross validation.

Assessing the uncertainty of downscaling methods in downscaling future climate

The bias correction and change factor calibration strategies led to fundamentally different time structure and spatial variability in the downscaled climatic variables. This issue is more important in downscaling precipitation because precipitation event is intermittent and unevenly spatially distributed. When aggregating the downscaled point values to areal-mean values, the bias correction based methods were found to underestimate the wet-day frequency and exaggerate the extreme values. The results confirm the findings of Maraun (2013), who discussed the inflation problem when bias correction based methods are used to bridge the scale mismatch between observations and GCM outputs.

For the 16-GCM ensemble used in this paper, the uncertainty bound of inter-annual variability projected by the bias correction based methods is much larger than that projected by the change factor based methods. This is understandable as although the different GCMs project varied future temporal structures, they still tend to project similar relative changes. The difference in uncertainty bounds produced by the two calibration strategies stems from their underlying assumptions, i.e., assumption that GCMs project realistic absolute values and temporal structures (BC methods) or that they only project reliable relative changes (CF methods).

The choice of GCMs has been acknowledged as one of the main uncertainty sources in climate change impact assessments. Compared to the GCMs, the downscaling methods adopted played a relatively less influential role in the downscaled temperature. When downscaling precipitation, however, the uncertainty associated with the choice of downscaling methods is comparable to the GCM uncertainty, which is in agreement with previous studies (Chen et al. 2013). Moreover, downscaling methods played a dominant role on downscaling the low precipitation intensity owing to the frequent occurrence of wet days with small precipitation amounts. The influence of GCMs increased when the temporal step of downscaled variable was aggregated from daily to monthly scale. For monthly precipitation, the large increase of downscaling-method variance from the single-strategy case to the all-method case indicates that the choice of calibration strategies is the main source of downscaling methods uncertainty.

The bias correction based methods resulted in relatively more percentages of total variance than the change factor based methods at each percentile of the probabilistic distributions of downscaled variables. In other words, the choice of transformation methods is more influential when with bias correction strategy. This implies that the bias-corrected GCM outputs vary with the different transformation methods, while the relative changes projected by GCMs can be described by different transformation methods in better agreement. The interaction uncertainty between GCMs and the change factor based methods is larger than that between GCMs and the bias correction based methods, which indicates that the difference due to the choice of transformation methods is more dependent on the employed GCMs when implementing change factor strategy.

When excluding the sub-optimally performing transformation methods, the results of the monthly precipitation were similar to the results including all methods (comparing Figure 3.8 and 3.9). However, the results of the daily precipitation intensity were quite different. This indicates that a large proportion of the downscaling method induced variance in precipitation intensity was mainly due to the sub-optimally performing transformation methods. The choice of GCMs became the dominant source of uncertainty in the case of the single calibration strategy. The influence of downscaling methods increased when the differences due to the calibration strategy were taken into account, which reiterates that more uncertainty is introduced by the calibration strategies than the statistical transformation methods.

Chapter 4 Hydrological modelling in the context of climate change

This chapter assesses the uncertainty associated with the hydrological modelling, with particular reference to parameter calibration, when assessing the hydrological impacts of climate change on river flows.

4.1 Introduction

The focus of previous impact-related research that considered parameter uncertainty has been toward addressing the equifinality effect (Beven and Freer 2001), i.e., different sets of parameters lead to equally good model performances. There has not been a consensus on the role of the uncertainty arising from parameter equifinality. Wilby and Harris (2006) proposed a probabilistic framework for combining information from multiple emission scenarios, GCM structures, statistical downscaling methods, and hydrologic model parameters and structures over the River Thames. Their results indicate that uncertainty in hydrological model parameterization has greater influence on high flows than low flows. In contrast, New et al. (2007) found that low flows of River Thames are most sensitive to parameter uncertainty using the same hydrological model as Wilby and Harris (2006)'s study but different GCM projections. Tian et al. (2013) assessed the uncertainty in high and low

flows due to model structures and parameters over two rainfall-dominated basins in China. Their results show that the parameter uncertainty of the high flows becomes larger as the discharge increases, and the influence of parameter uncertainty differs with different model structures. Similar results were found in the study of Bastola et al. (2011), who investigated the role of hydrological modelling uncertainties in climate change impact assessment of four Irish catchments. Moreover, they also demonstrated that prediction uncertainties from model parameterization varied among catchments and grew wider in time when moving from the period of 2050s to the period of 2070s. Jung et al. (2012) investigated the parameter uncertainty by sampling the behavioural model parameters (determined according to a statistical performance measure) and obtained the result that hydrological parameter uncertainty has more effect on snow-dominated regions than a rain-dominated basin. The aforementioned studies highlight the importance of conducting uncertainty analysis on the equifinality effect of model parameters on a case by case basis.

Besides the uncertainty associated with the equifinality of parameter sets, an additional uncertainty emerges when applying calibrated hydrological models under the future condition which differs from the condition in the calibration period. Merz et al. (2011) claimed that "care needs to be taken when using calibrated parameters for projecting into the future due to the potential large errors caused by a transient climate". The implicit assumption of using hydrological models is that the models calibrated based on historical records are still valid for other periods outside of the calibration period. Whether this assumption still holds in the future under a changed climate is a critical question that has not been well answered. There have been a few studies aimed at validating this assumption over different catchment sets and models (Wilby 2005, Vaze et al. 2010, Merz et al. 2011, Coron et al. 2012, Li et al. 2012). Most of the previous findings observed increased model errors when the climatic conditions between calibration and validation periods are different. In these studies, differential split-sample tests (Klemeš 1986) have been used to evaluate the transferability of calibrated hydrological models to a differing climatic condition.

Since the issue of identifying and understanding the transferability of hydrological model parameters to a contrasted climate has not been well resolved, significant uncertainty could emerge from the choice of the calibration periods that represent specific climatic characteristics. Unfortunately, the assessment of this uncertainty is usually ignored in the impact analysis. Brigode et al. (2013) investigated parameter uncertainty of two rainfall runoff models in the context of climate change impact assessment over 89 catchments in northern and central France. They found that the dependence of the parameter sets on the climate characteristics of the calibration periods had a significant contribution to the variability in projected future streamflow. Wilby (2005) found that for a simple water balance model the uncertainty in projected river flow changes due to choice of training periods was comparable to the uncertainty due to future greenhouse gas emission scenarios, although the uncertainty due to the choice of training periods is smaller for a more complex water balance model. The previous findings prove the need of routinely

carrying out the uncertainty assessment of hydrological modeling in the context of climate change impact studies.

This chapter assesses the uncertainties associated with the parameter calibration of a conceptual rainfall-runoff model when assessing the impacts of climate change on river flow in the sub-basin upstream of the Bengbu City (see Figure 1.1). The scope of this chapter includes 1) testing the transferability of hydrological model parameters among differing climatic conditions; 2) assessing the relative magnitude of uncertainties in projected future river flow arising from the choice of calibration periods and the equifinality effect. The results will provide a basis for the hydrological impact assessment of climate change.

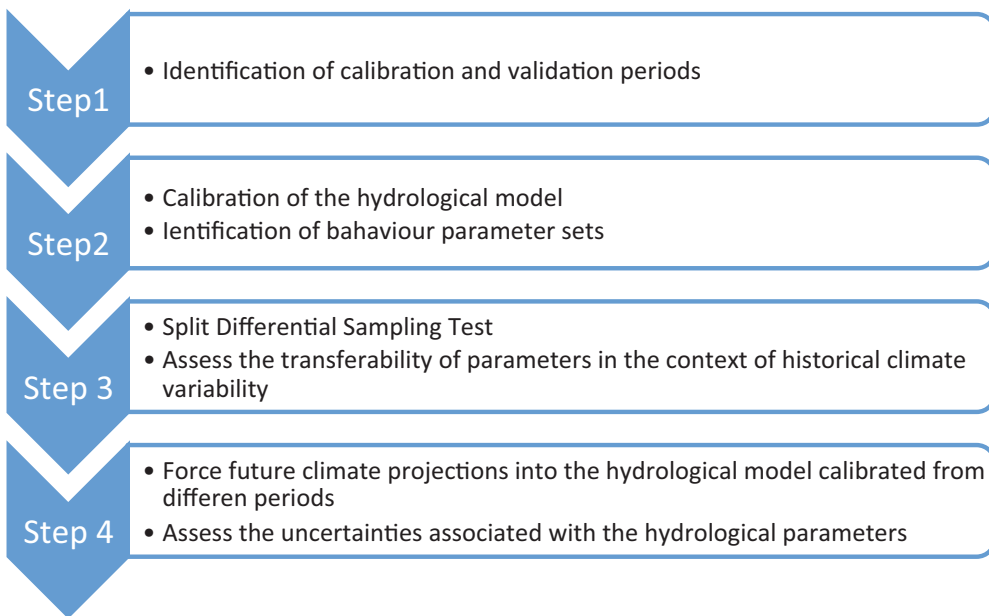The four-step methodology in this chapter is shown as below:

Step1
- Identification of calibration and validation periods

Step2
- Calibration of the hydrological model
- Ientification of bahaviour parameter sets

Step 3
- Split Differential Sampling Test
- Assess the transferability of parameters in the context of historical climate variability

Step 4
- Force future climate projections into the hydrological model calibrated from differen periods
- Assess the uncertainties associated with the hydrological parameters

Figure 4.1 Illustration of the methodology in Chapter 4

4.2 Differential split-sample test

For the hydrological modelling under climate change, hydrological models are commonly required to perform under a changed climate condition for the future projections. The "differential split-sample test" (Klemeš 1986) is able to test whether the hydrological models calibrated under the present-day climate can be used to project reliable river flow under a contrasting climate in the future. In this test hydrological models are calibrated and validated under contrasting climatic conditions. Historical records are divided into sub-periods to represent different climatic conditions.
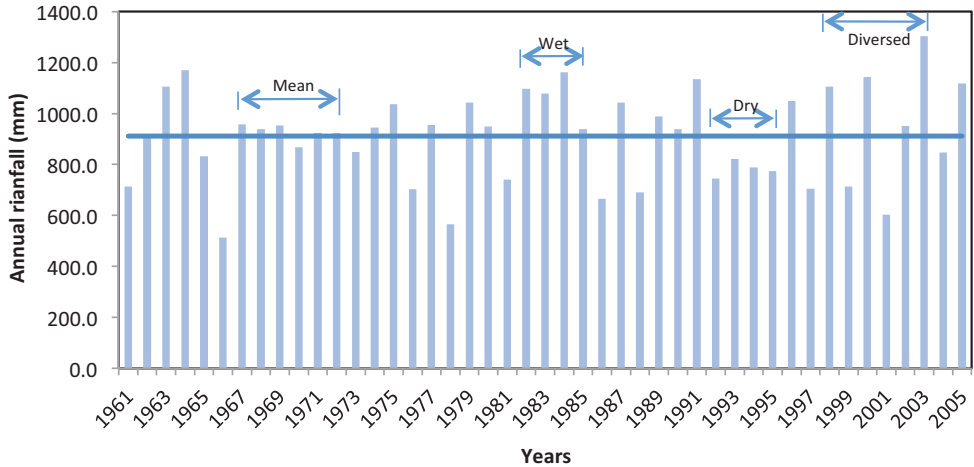
Figure 4.2 Annual area-mean rainfall of the sub-basin upstream of Bengbu with the selected calibration periods

The basin-mean annual rainfall series was used to determine the periods with various climatic conditions. The segment from 1992 to 1995 with consecutive annual rainfall less than the multi-year mean was selected as "dry" period. The segment from 1982 to 1985 with consecutive annual rainfall greater than the multi-year mean was selected as "wet" period. The segment from 1967 to 1972 was considered as "mean" period because the consecutive annual rainfall is within ±5% of the multi-year mean, while the segment from 1998 to 2003 was considered as "diverse" period because the consecutive annual rainfall has the highest variance. The hydrological model was calibrated on each of the four periods and validated on the remaining periods in turn. A 1-year warm-up period was considered for each calibration.

Table 4.1 Statistics of the full records and the sub-periods

	Full period	Dry	Mean	Wet	Diverse
Periods	1961-2005	1992-1995	1967-1972	1982-1985	1998-2003
Annual cumulative rainfall (mm/yr)	911.0	782.2	927.6	1068.6	969.6
Annual mean temperature ($^\circ$C)	15.0	15.4	14.5	14.5	15.6

For comparison, the whole historical period was also divided into three calibration periods with equal length: 1961-1975, 1976-1990 and 1991-2005. Each of the 15-year period is considered to contain sufficient information for model calibration, and the difference between the periods is considered as historical climatic variability. The parameters calibrated from the three periods were used to generate the future flow series under climate change.

A relatively short length of data (4 or 6 years) was used to calibrate the hydrological model, and the calibrated parameters were transferred to the validation periods with different

lengths from that of the calibration period. The influence of the length of the calibration period on the objective function was not considered in this study. Theoretically, a better calibration should be achieved by a longer set of data. However, model performance over the 4-year period was close to the model performance over the 15-year period. For example, the behavioural parameters calibrated from the period of 1998-2003 resulted in the NSE values ranging between 0.9-0.92, and the behavioural parameters calibrated from the period of 1991-2005 resulted in the NSE values ranging between 0.89-0.92. The previous studies also show the evidence that model performance is not dependent on the length of calibration data (Sorooshian and Gupta 1983, Yew Gan et al. 1997). Moreover, the analysis here is focused on comparing the changes in model performance between the validation results and the calibration results in each period. Thus, the influence of different lengths of calibration periods was ignored.

4.3 Xinanjiang Hydrological model

The Xinanjiang Model is a conceptual rainfall runoff model developed by Zhao (1992) in 1973. Its main feature is the concept of runoff formation on repletion of storage, which means that runoff is not produced until the soil moisture content of the aeration zone reaches field capacity, and thereafter runoff equals the rainfall excess without further loss. The generated runoff was originally separated into two components (surface water and groundwater) using Horton's concept. The model was updated by introducing interflow as an additional component in 1980. The three-runoff-component Xinanjiang Model has been successfully and widely used over humid and semi-humid regions in China.
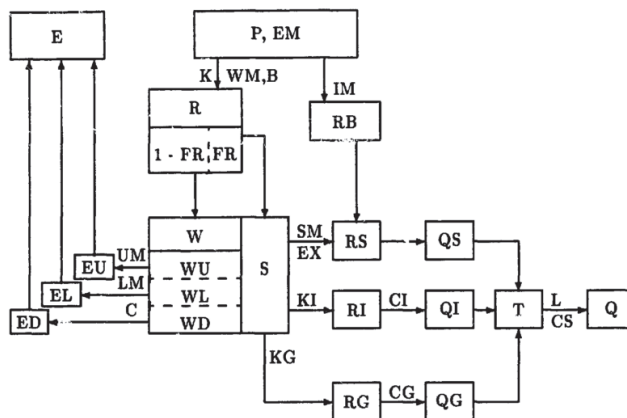

Figure 4.3 Flow chart of the Xinanjiang model (Zhao 1992)

The symbols outside the blocks are the parameters, and their definitions are given in Table 4.2. The symbols inside the blocks are the inputs, outputs and state variables, and the definitions are given below. E is the actual evapotranspiration from the whole basin; and EU, EL and ED are the actual evapotranspiration from the upper, lower and deep layers, respectively. P is the areal mean rainfall. EM is the measured pan evaporation. IM is the fraction of the impervious area. R is the generated runoff with three components: RS (surface runoff), RI (interflow), and RG (groundwater flow). FR is the variable runoff producing area. W is the areal mean tension water storage with the components WU, WL, and WD in the

upper, lower, and deep components, respectively. S is the areal mean free water storage. T is the total sub-basin inflow to the channel network. Q is the discharge from a sub-basin consists of the components QS, QI, and QG which representing surface runoff, interflow, and groundwater, respectively.

In the traditional Xinanjiang model, the outflow hydrograph is simulated for each sub-basin and then routed along the channels to the main basin outlet. The flow chart is shown in Figure 4.3. The inputs to the model are the measured areal mean rainfall depth (P) and the measured pan evaporation (EM) on each sub-basin. The outputs are the discharge from each sub-basin (Q), the sum of which is the outlet discharge from the whole basin, and the actual evapotranspiration from the whole basin (E), which is the sum of the evapotranspiration from the upper layer (EU), the lower layer (EL), and the deep layer (ED). The symbols for the state variables are shown inside the blocks of Figure 4.3, and parameters are shown outside the corresponding blocks, and their definitions are given in Table 4.2. The model structure consists of four parts: evapotranspiration calculation, runoff generation, separation of runoff components and flow routing.

Table 4.2 Parameters of Xinanjiang model and their ranges in calibration

	Structures	Notations	Definition	Sensitivity	Range/Value
I	Evapotranspiration calculation	*K*	*Ratio of potential evapotranspiration to pan evaporation*	*sensitive*	*0-2.5*
		UM	Tension water storage capacity of the upper layer (mm)	Relatively not sensitive	20
		LM	Tension water storage capacity of the lower layer (mm)	Relatively not sensitive	100
		C	*Evaporation coefficient of the deep layer, which depends on the proportion of the basin area covered by vegetation with deep roots*	*Relatively not sensitive*	*0-0.3*
II	Runoff generation	WM	Areal mean tension water storage capacity (equal to the sum of UM LM, DM) (mm)	Relatively not sensitive	200
		B	Exponent parameter with a single parabolic curve, which represents the non-uniformity of the spatial distribution of the soil moisture storage capacity over the sub-basin	Relatively not sensitive	0.65
		IM	The percentage of the impervious area of the sub-basin	Relatively not sensitive	0.02
III	Separation of runoff components	*SM*	*Areal mean free water capacity of the surface soil layer, which represents the maximum possible deficit of free water storage (mm)*	*sensitive*	*0-80*
		EX	Exponent of the free water capacity curve influencing the development of the saturated area	Relatively not sensitive	1.5
		KG	*Outflow coefficient of the free water storage to groundwater*	*sensitive*	*0.01-1*
		KI	*Outflow coefficient of the free water storage to interflow*	*sensitive*	*0.01-1*
IV	Runoff concentration and flow routing	*CI*	*Recession constant of the interflow storage*	*sensitive*	*0.1-1*
		CG	*Recession constant of the groundwater storage*	*sensitive*	*0.8-1*
		CS	*Recession constant in the Lag and Route method for water routing through the channel system within each sub-basin*	*sensitive*	*0.1-1*
		L	Lag parameter in the Lag and Route method	sensitive	2

Evapotranspiration calculation: Evapotranspiration is calculated through a three-layer soil-moisture model.

Until the storage of the upper layer (WU) is exhausted, the evapotranspiration of the upper layer (EU) is equal to the potential evapotranspiration which is proportional to the pan evaporation with the proportional parameter *K*. On exhaustion of the upper layer (capacity UM), any remaining potential evapotranspiration is applied to the lower layer, but the efficiency is modified by multiplying the ratio of the actual storage (WL) to the capacity storage (LM) of the lower layer. When the storage of the lower layer is reduced to a proportion C (the evaporation coefficient of the deep layer) of LM, the evapotranspiration in the deep layer (ED) occurs.

Since the future pan evapotranspiration cannot be measured, the Blaney-Criddle method (Blaney and Criddle 1950) was used to estimate the potential evapotranspiration:

$$PET = kp(0.46T + 8.13) \qquad\qquad 4\text{-}1$$

where, *PET* is daily potential evapotranspiration, *T* is daily mean temperature in $^{\circ}$C, *p* is the percentage of the daytime hours for each day out of total daytime hours of the year, and *k* is a monthly consumptive use coefficient, depending on vegetation type, location and season. This method has been commonly used to calculate the reference crop evaporation. According to (Blaney and Criddle 1950) for the growing season (May to October) k varies from 0.5 for orange tree to 1.2 for dense natural vegetation. In this study, the monthly consumptive use coefficient *k* is integrated into the evapotranspiration coefficient *K* in the Xinanjiang Hydrological model and is determined through the model calibration.

Runoff generation:

The Xinanjiang Model considers a non-uniform spatial distribution of soil moisture deficit and storage capacity in the catchment. The key hypothesis of the model is that the runoff at a point only occurs when the tension water capacity at that point is reached. A tension water capacity curve was introduced to represent a non-uniform distribution of the tension water capacity throughout the sub-basin. The relationship between the proportion of the area producing runoff and the tension water capacity at a point can be described as:

$$\frac{dR}{dP} = \frac{f}{F} = 1 - \left(1 - \frac{WM'}{WM}\right)^B \qquad W < WM$$
$$\frac{dR}{dP} = 1 \qquad W \geq WM \qquad\qquad 4\text{-}2$$

where *WM'* is the tension water capacity at a point, *WM* is the areal mean tension water capacity, *B* is an exponent parameter, *R* is runoff, *P* is rainfall, *F* is the total area of a sub-basin, and *f* represents the pervious area of *F. f/F represents the proportion of the pervious area of the basin whose tension water capacity is less than or equal to WM'*.

Separation of runoff components: The concepts of free water storage (S) is used to separate the generated runoff (R) into three components: surface runoff (RS), interflow (RI) and groundwater (RG). The free water storage capacity at a point is assumed to be distributed between zero and a point maximum value in a parabolic manner over the portion of the area which is currently producing runoff. The parabola is described by the parameters of areal mean free water storage capacity (SM) and the exponent of the free water capacity curve (EX). The component of surface runoff (RS) is determined by this parabola. The remainder of the runoff becomes an addition, ΔS, to the free water storage S, which in turn contributes RI laterally to inflow and RG vertically to groundwater. RI and RG are proportional to the free water storage with the proportional parameter *KI* and *KG*, respectively.

Runoff concentration and flow routing:

The surface runoff directly enters the channel system. The interflow component and the groundwater component are routed through linear reservoirs representing interflow and groundwater storage, respectively. The linear reservoirs are dependent on the recession constants of the interflow storage (CI) and the groundwater storage (CG), respectively. The sum of the three flow components is the total inflow to the channel network. The total inflow to the channel network is routed to the basin outlet using "Lag and Route" method with parameters L and CS.

Due to the data availability of the historical records and the future climate projections, the lumped version of the Xinanjiang Model is used in this study, i.e., the basin-mean daily rainfall and temperature data were used as the model inputs and the output is the simulated daily discharge at the basin outlet (Bengbu). According to the sensitivity of the model performance to the parameters, the parameters that were calibrated and analysed are emphasized by the bold and italic symbols in Table 4.2, and the ranges of values from which the calibration takes are also shown. The values of the less sensitive parameters are assigned according to the recommendations of the previous applications and a preliminary sensitivity analysis.

Model calibration and performance criteria

The Huai River is regulated by hydraulic structures (e.g., reservoir and sluices). To exclude the influence of human interventions, the hydrological model was run at daily step but calibrated at monthly step with the consideration that the influence of hydraulic structures on monthly water volume is not significant. The objective functions were calculated for monthly mean discharge series. Two objective functions were selected: the Nash-Sutcliff Efficiency (NSE) and the percentage volume error (PVE).

NSE is a common measure of goodness-of-fit to evaluate hydrological model performance. NSE primarily focuses on the peaks and high flows of the hydrograph (Krause et al. 2005),

but it is also influenced by extreme low flow events and, thus, can be a good individual calibration target in highly variable flow regimes (Price et al. 2012). NSE is defined as

$$NSE = 1 - \frac{\sum_{i=1}^{N}(M_i-O_i)^2}{\sum_{i=1}^{N}(O_i-\bar{O})^2}$$ 4-3

where O_i and M_i are the observed and modelled monthly mean discharge at the month i, respectively; $\bar{O}$ is the observed mean monthly mean discharge, and N is the number of months. The higher the NSE is, the better performance the model produces. Monthly fits of the models can be considered 'very good' when NSE for these individual fits is greater than 0.75, 'good' when NSE is between 0.65 and 0.75, and 'satisfactory' when NSE is between 0.5 and 0.65 (Moriasi et al. 2007).

PVE is used to assess the water balance over the calibration period. It provided information on the agreement between observed and modelled total discharge, which is defined as

$$PVE = \frac{\left|\sum_{i=1}^{N}(M_i-O_i)\right|}{\sum_{i=1}^{N}O_i} \times 100\%$$ 4-4

where O_i and M_i are the observed and modelled monthly flow at the month i, respectively; and N is the number of months. Monthly fits of the models can be considered 'very good' when the absolute value of the volume error for these individual fits is less than 10%, 'good' when the error is between 10% and 15%, and 'satisfactory' when the error is between 15% and 25% (Moriasi et al. 2007). Here, PVE is used as a constraint, i.e., the behavioural parameter sets should result in the value of PVE less than 10%.

The Monte Carlo simulation is commonly used to explore the behaviour parameter space of hydrological models (Wilby and Harris 2006, New et al. 2007, Jung et al. 2012). Here, the Monte Carlo simulation was employed to address the effect of parameter equifinality, i.e., the phenomenon that different parameter sets lead to equally good model performance. For each calibration period, the Monte Carlo simulation was undertaken with 1 000 000 runs for the Xinanjiang model; each run randomly generated parameter values drawn from plausible ranges (see Table 4.2). Each parameter set was used to generate daily flow at Bengbu given observed daily rainfall and temperature. The 1000 best parameter sets for each calibration period were selected as "behaviour" parameter sets according to the goodness-of-fit measures defined above. Then, the hydrological model were run with the behaviour parameter sets to simulate daily flow at Bengbu during the validation periods for the differential split-sample test as well as during future period under changed climate.

To assess the ability of the hydrological model simulating historical discharges, the annual discharge (m³/s) and annual maximum 30-day mean discharge (AM 30d discharge) (m³/s) were analysed when transferring the parameters to the different validation periods. The relative bias of the multi-year mean was used as performance criterion to give information about the errors of the model simulations against the observations, which is given as

$$Bias = \frac{\bar{M} - \bar{O}}{\bar{O}} \times 100\%$$ 4-5

where $\bar{M}$ and $\bar{O}$ are the modelled and observed multi-year mean values of the flow character.

The annual maximum 30-day mean discharge was selected as flood index with the underlying assumption that the water withdrawing from the river in wet years can be ignored and the dams and sluices in the upstream don't have significant influence on the outlet at the downstream. The effect of land use change was not taken into account in the calibration, and it is assumed that the land use in the basin stays unchanged in the future.

4.4 Future climate information and performance criteria

The daily precipitation and temperature projected by four GCMs from the CMIP5 were selected to provide the future climate information (See Table 4.3). All GCM projections were obtained under a high greenhouse gas emission scenario (RCP 8.5). The gridded projections were downscaled to the station scale using the mean-based change-factor downscaling method (the so-called delta change method) (Prudhomme et al. 2002, Fowler et al. 2007) and then aggregated to provide areal mean input for the hydrological model. Following the common practice, the period from 1961 to 1990 was selected as baseline period and the period from 2071 to 2100 was selected as the future period. The selected GCMs project the future climate that is wetter than the climate of the baseline period with the increase ranging from 9.8% to 43.5%.

Table 4.3 Statistics of climate projections

	GCM1	GCM2	GCM3	GCM4
Model name	CCSM4	BCC-CSM1.1	MPI-ESM-MR	HadGEM2-ES
Country-Modelling Center	USA-NCAR	China-BBC	Germany-MPI-M	UK-MOHC
Resolution ($^\circ$ lon x lat)	1.25×0.94	2.8×2.8	1.875×1.875	1.875×1.25
Annual rainfall (mm/yr) and the relative change against the baseline observation (%)	994 (+9.8)	1017 (+12.3)	1142.9 (+26.1)	1300.3 (+43.5)
Annual mean temperature ($^\circ$C) and the change ($^\circ$C) against the baseline observation	19.2 (4.4)	19.6 (+4.8)	19.6 (+4.8)	20.8 (+6.0)

To assess the uncertainty in the projected future river flow, the relative changes in the projected future annual mean discharge and AM 30d discharge against the observations in the baseline period were calculated. The relative magnitudes of the uncertainties from different sources were assessed using the analysis of variance. The projected relative changes were grouped by the choice of the calibration periods, and the total sum of squares of the relative changes was partitioned into two components: the sum of the squares of the differences of group means from the grand mean (representing the uncertainty stemming from the choice of the calibration periods) and the mean of the sum of the squares of the differences of the projected relative changes from their group mean (representing the uncertainty stemming from the equifinal parameter sets).

$$SS_{tot} = SS_{cali} + SS_{equi} \qquad\qquad 4\text{-}6$$

$$SS_{cali} = \sum_{i=1}^{c} n_i (\bar{\Delta}_i - \bar{\Delta})^2 \qquad\qquad 4\text{-}7$$

$$SS_{equi} = \sum_{i=1}^{c} \sum_{j=1}^{n_i} (\Delta_{ij} - \bar{\Delta}_i)^2 \qquad\qquad 4\text{-}8$$

where SS_{tot} is the total sum of squares, SS_{cali} is the sum of squares resulted from the choice of the calibration periods, SS_{equi} is the sum of squares resulted from equifinal parameter sets, Δ_{ij} is the projected relative change using the parameter set j calibrated from the calibration period i, $\bar{\Delta}_i$ is the group mean of the results from the calibration period i, $\bar{\Delta}$ is the grand mean, n_i is the number of the samples in group i and c is the number of the groups.

The relative magnitudes of the uncertainties from the choice of the calibration periods and the equifinal parameter sets were calculated as the percentages of the corresponding sum of squares over the total sum of squares.

4.5 Parameter transferability under historical climate variability

4.5.1 Calibration and validation of the parameters over different periods – comparison of NSE

The scatter plots of the parameter values against the NSE values resulted from the four calibration period are shown in Figure 4.4. The hydrological model has a poor performance over the dry period with NSE less than 0.6, which is around the performance rating of satisfactory. The model return NSE up to 0.83 in the mean period and higher than 0.9 in the wet and diverse periods. The identification of the parameters which control water balance (K and C) is greater than other parameters. The evaporation coefficient C showed greatest identifiability in the dry period and poor identifiability in the wet period. The identifiability of other parameters did not show difference among the calibration periods. NSE values varies little across a wide range of the parameter KG, CS and other water routing parameters (CI and CG, not shown), which highlights the non-uniqueness of the optimal parameter sets, i.e., different combinations of the parameter values lead to equally good model performances.

The parameter identification does not vary much with the difference in the climatic specificity of the calibration periods. The identification of the parameters related to the water balance is good, while the parameters related to the water routing has a poor identification. The poor identification of the parameters related to water routing is due to the monthly objective functions used to calibrate the model. Moreover, the study area is a large river basin containing many tributaries, while the inputs and parameters of the hydrological model are areal means over the whole basin area. The only observation of discharge at the basin outlet cannot guarantee the calibration of the accurate parameters related to water routing. The influence of the hydraulic structures may also attributes to this issue.
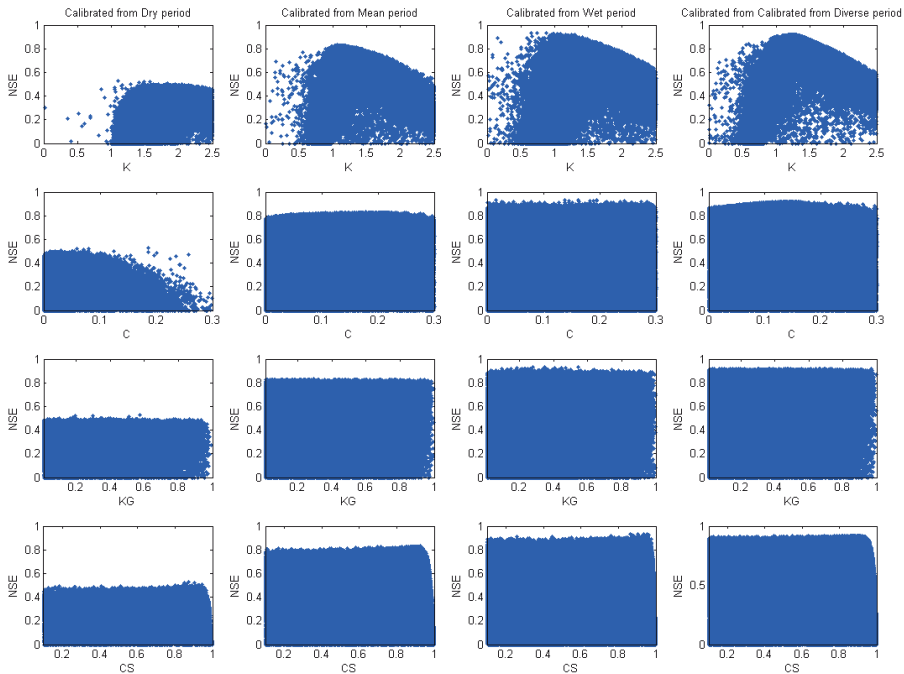
Figure 4.4 Identifiability of the Xinanjiang model parameters calibrated from the dry, wet, mean and diverse sub-periods

The transferability of model parameters between calibration periods is tested using Differential Split-Sample Test. The parameter sets determined form each calibration period were validated on the remaining three sub-periods, respectively. 1000 best performed parameter sets were selected from each calibration period to take account of the equifinality effect. The boxplots of model performances on each validation period are shown in Figure 4.5. For comparison, the model performances during the calibration for each sub-period are also shown in the figure.

For each validation period, the parameters from the diverse period provided the best overall model performance, while the parameters from the dry period resulted in the largest spread of model performances. There is a general decrease of model performance on each sub-period when using the parameters calibrated from other periods. The decrease is the most obvious on the dry period, where most of the parameters calibrated from other sub-periods lead to very poor model performances. When validated on the mean period, the parameters from the wet period and the diverse period resulted in higher values of NSE than those from the dry period. When validated on the wet period, the parameters from the other sub-periods led to comparable averaged model performance, but the parameters from the dry and mean periods resulted in larger spread of model performances than the parameters from the diverse period. There is also a large spread in the results of the parameters from

the dry period when validated on the diverse period. The parameters from the mean and wet periods have similar average performances when validated on the diverse period, although the spread of the results from the wet-period parameters is larger.
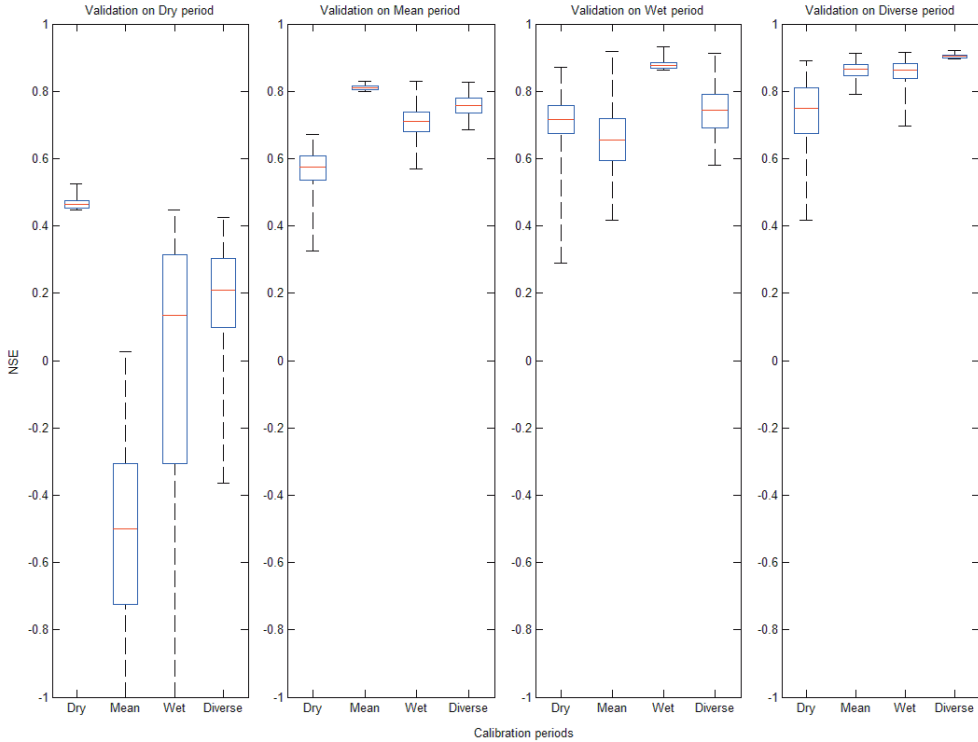
Figure 4.5 Model performances on sub-periods with the parameters calibrated from different calibration periods

The above results show that parameters calibrated from the diverse period provide relative more robust model performance compared with those calibrated from other periods. Although the model performance during the calibration is poor, some of the parameters calibrated from the dry period can result in good model performances when transferred to a wetter period. The transferability of the parameters from a wet period to a dry period is poorer than that from a dry period to a wet period.

It is notable that the hydrological model used here had much poorer performance on the dry period compared to other periods. This could be related to the issues of data quality and the simulative ability of the hydrological model. In the dry period, the sluices at the river were operated more often to preserve water for the nearby water withdrawing, which may influence the water balance in the model calibration. Moreover, there are both high-flow information and low-flow information in the wet periods due to the seasonality, while the dry period contained less high-discharge event, which makes it difficult to obtain accurate

parameters. On the other hand, the Xinanjiang Model is designed for simulating the rainfall-runoff process in the humid or semi-humid basin, and the runoff is generated when the soil moisture content of the aeration zone reaches field capacity. In the continuous dry period the antecedent soil moisture is at a low level. The runoff may be generated when the rainfall intensity exceeds the infiltration rate before the soil moisture storage is reached. Moreover, the spatial variability of rainfall cannot be represented by the areal-mean input, which is also likely to have more impact on the dry period than the wet period.

The transferability of parameters was also carried out among the 15-year calibration periods (see Figure 4.6). Similar with the previous analysis, the spread of NSE increases when the parameters were transferred to other periods. The simulative ability of the parameters transferred to other periods is acceptable as all the NSE were greater than 0.65, which again indicates that the calibration period containing various information leads to robust model simulation.
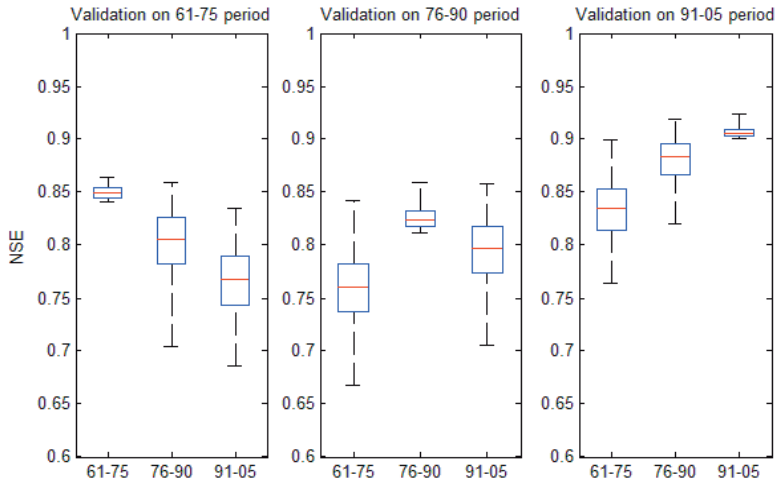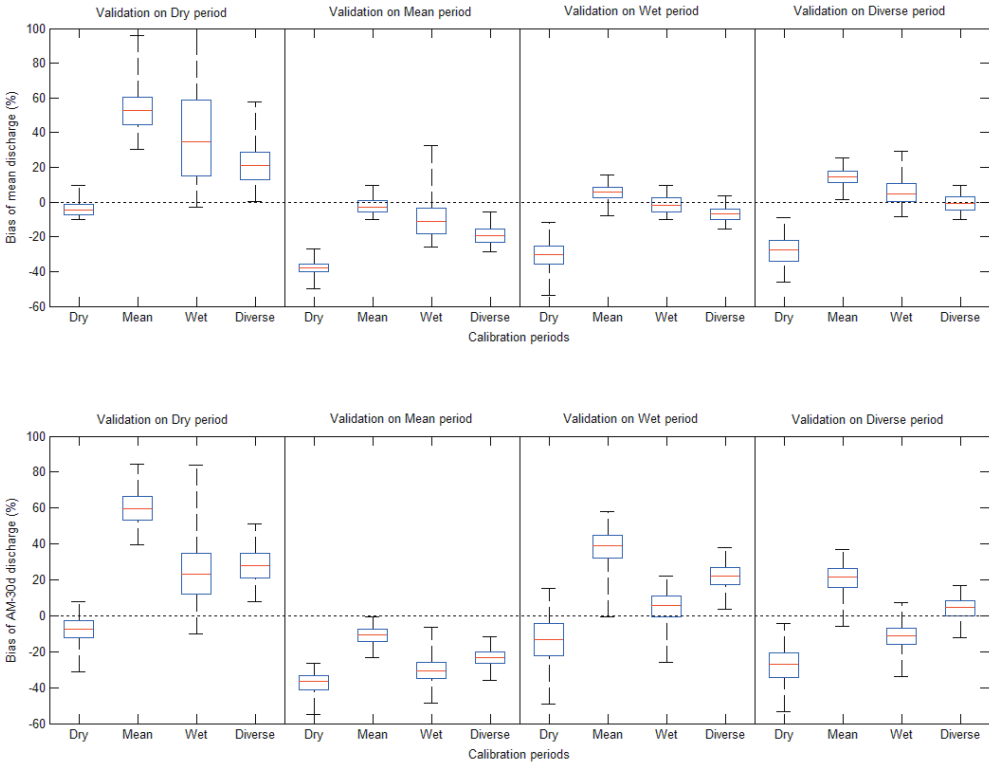

Figure 4.6 Model performances on three-split sub-periods with the parameters calibrated from different calibration periods

## 4.5.2 Model simulations over different periods – comparison of bias

Figure 4.7 Spread of the biases in the simulated flow characters (annual mean discharge at the top and AM 30d discharge on the bottom) on the validation periods using the parameters calibrated from different calibration periods

The spread of the biases in simulated annual mean discharge and AM 30d discharge when transferring the parameters to the different periods is show in Figure 4.7. The calibration bias, i.e., the simulation bias for a period which uses the parameters calibrated from that period, is also shown in the figures for the sake of comparison. When transferring the parameters calibrated from the dry period to wetter periods, the hydrological model tended to underestimate the mean discharge and the AM 30d discharge. The model performance is worse on the mean period (with the absolute value of the biases greater than 20%) than on the wet and diverse periods. When the parameters calibrated from the mean period were transferred to the other periods, the model tended to overestimate the flow characters. When transferred to the wetter periods, the parameters generated reasonable mean discharge (with the absolute value of the biases less than 0.2), but most of them resulted in large biases in the AM 30d discharge. Most of the parameters calibrated from the wet period generated reasonable simulations when transferred to the diverse period, vice versa. Both of

the parameter sets from the wet and diverse periods tended to generate wet biases in the dry period and dry biases in the mean period, as shown in the results of mean discharge.

The results show that when transferring the parameters calibrated from wetter periods to the dry period, considerable wet biases were generated in the discharge. Conversely, when transferring the parameters calibrated from the dry period to wetter periods, dry biases were generated. However, contrary results are observed for the transferring among the mean and wetter periods. The parameters calibrated from the mean and diverse periods are able to generate reasonable simulations of mean discharge in the wet period, but they tend to overestimate the extreme. There is a relatively good transferability between the parameters calibrated from the wet period and the diverse period.
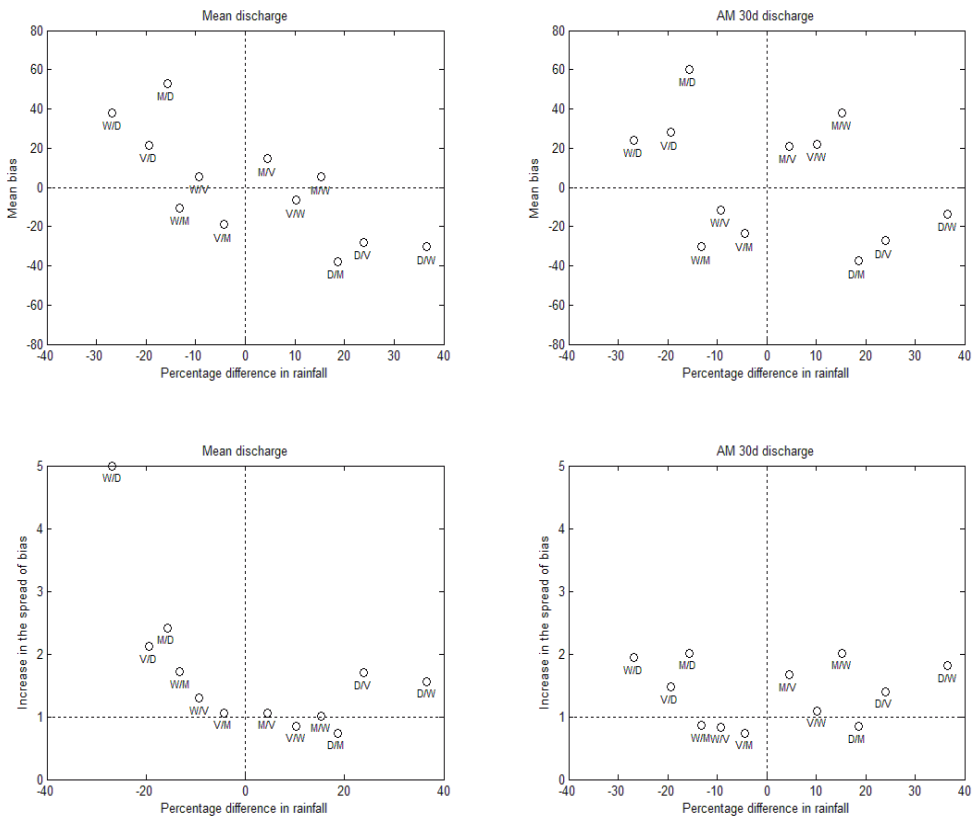
Figure 4.8 Statistics of simulation biases against percentage differences in rainfall between the validation and calibration periods. The sub-figures at the top show the mean simulation bias for mean discharge (left) and the AM 30d discharge (right); the sub-figures at the bottom show the increase in the spread of simulation biases for mean discharge (left) and the AM 30d discharge (right). The labels below the dots show the pairs of calibration/validation periods.

The dependence of simulation bias on the difference in annual rainfall between the validation and calibration periods is shown in Figure 4.8. The positive values on the x-axis

represent the simulation results where the rainfall in the validation period is greater than the calibration period and vice versa. The top row shows the scatter plot of the mean bias resulted from the equifinal parameter sets against the percentage difference in annual rainfall between the validation and calibration periods. The mean bias greater than zero represents an overestimation, and the mean bias less than zero represents an underestimation. The bottom row shows the increase in the spread of bias, which is calculated as the ratio between the standard deviation of bias resulted from equifinal parameter sets on the validation period and the standard deviation of bias resulted from equifinal parameter sets on the calibration period. The ratio greater than one representing an increase in the spread of the results due to equifinality, and the ratio less than one representing a decrease in the spread of the results due to equifinality. The statistics for annual mean discharge is shown in the left panel, and the statistics for AM 30d discharge is shown in the right panel.

For the simulations of annual mean discharge, the absolute value of bias increases when the difference between the rainfall in the validation and calibration periods gets larger. Moreover, the increase of bias is generally greater when the parameters calibrated from a wet period are transferred to a drier period compared to the other way around. Similarly, the spread of bias resulted from equifinal parameter sets also generally increases with the difference between the rainfall in the validation and calibration periods, and the increase is greater when the parameters calibrated from a wet period are transferred to a drier period than the other way around. The results indicate that the calibrated parameters have a relatively better transferability in simulating annual discharge when being transferred to a wetter period compared to when being transferred to a drier period. The model performance decreases with the increase in the rainfall difference from the in the calibration period.

For the simulation of extreme discharge, the scatter of the bias is large. The results of the parameters calibrated or validated over the dry period show a different trend compared to the results of transferring between other periods, i.e., the absolute values of bias decreases when the difference in rainfall between the validation and calibration periods increases. For transferring the parameters between the mean, wet and diverse periods, the overestimations occur when the parameters are validated on a wetter period, and the underestimations occur when the parameters are validated on a drier period. A general increase in the spread of bias is found when transferring the calibrated parameters to a different period; the exceptions lies in the calibration/validation pairs of wet/mean, wet/diverse, diverse /mean and dry/mean, which indicates less spread in the results due to equifinal parameter sets. The increase in the spread of bias due to equifinality is up to twice of the spread in calibration. In contrast with the result of the mean discharge, the influence of equifinality on the extreme discharge does not differ much whenever the parameters were calibrated to a drier period or a wetter period.

4.6 Uncertainty in projecting future river flow
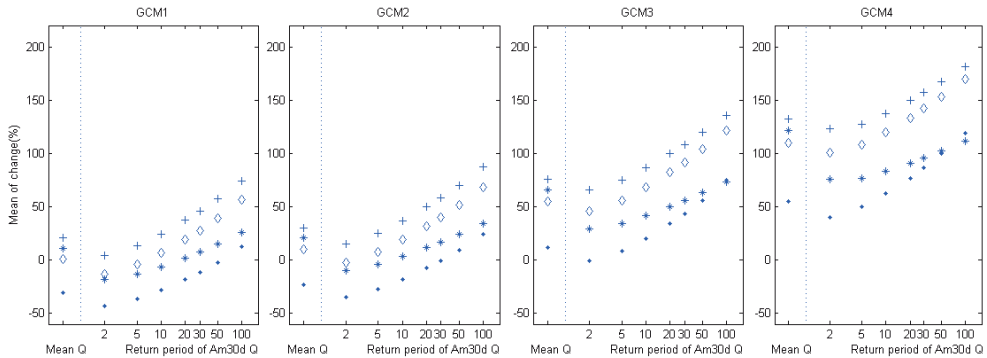
Figure 4.9 Projected changees in mean discharge and AM 30d discharge resulted from the five GCMs using the parameters calibrated from different periods. (Dot, cross, start and diamond represent the results of using the parameters calibrated from the dry, mean, wet and diverse periods, respectively).

Since the uncertainty caused by transferring the model to a different climate is investigated here, the future relative change was calculated against the observation in the baseline period with the underlying assumption that the simulation biases from different calibration periods are at the same magnitude in the baseline period. Figure 4.9 shows the projected changes in the future river flow. For each GCM, mean values of the projected changes in the extreme discharge resulted from the equifinal parameter sets calibrated from each calibration period are plotted against return periods. Mean values of the projected change in the multi-year mean annual discharge is also shown at the left of each subfigure for the sake of conciseness. According to the projected annual rainfall, the GCM1 to GCM4 represent the future climate that is 9.8%, 12.3%, 26.1% and 43.5% wetter compared to the climate in the baseline period, respectively.

The employed GCM is a dominant influence for the future changes in the multi-year mean annual discharge. The increase in the projected discharge is not proportional to the increase of annual rainfall. The projected changes in mean discharge resulted from the parameters calibrated on the wet, mean and diverse periods are close to each other (with the difference less than 25%).The hydrological model calibrated over the dry period generated much lower mean annual discharge compared to the model calibrated over the wetter periods, which is in line with the model performances in the Differential Split-Sample Test.

For the results of extreme flow, greater change is observed at the high-return period extreme discharge compared to the low-return-period extreme discharge. The spread of the changes between different calibration periods gets larger when the projected annual rainfall increases especially for the change in the low-return-period extreme discharge, which implies that the difference due to the choice of the calibration periods increase when the future climate gets wetter. The hydrological model calibrated from the mean and diverse periods resulted in higher extreme discharge compared to the dry and wet periods. Although

GCM1 and GCM2 projected slightly increase in the annual rainfall, the hydrological model calibrated over the mean and diverse periods projected the increase of more than 50% in the high-return-period extreme discharge.
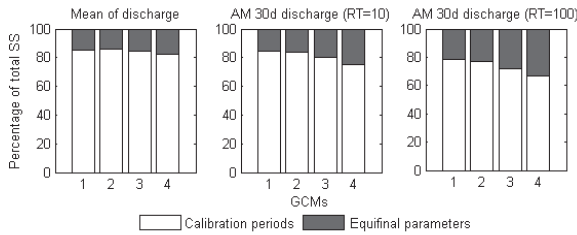
Figure 4.10 Percentages of total sum of squares resulted from the difference in the choice of differing calibration periods and the equifinal parameter sets

To compare the relative magnitudes of the uncertainties, the total uncertainty in the flow characters resulted from each GCM projection is partitioned into two parts: the uncertainty stemming from the climatic specificity of the calibration periods and the uncertainty stemming from equifinality. The magnitude of the uncertainty is represented by the proportion of the sum of squares. Figure 4.10 shows the percentage of total sum of squares resulted from the two sources of uncertainty. The results of mean annual discharge suggested by the four GCMs are shown in the left, and the results of 10-year-return-period and 100-year-return-period of the extreme discharge is shown in the middle and right, respectively.

The uncertainty stemming from the climatic specificity of the calibration periods is larger than the uncertainty due to equifinality. For the mean annual discharge and low-return-period extreme discharge, the percentage of the sum of squares caused by the climatic specificity of the calibration periods takes around 80% of the total sum of squares. The influence of equifinal parameter sets gets larger in the high-return-period extreme discharge in a wetter future climate (up to 34%).
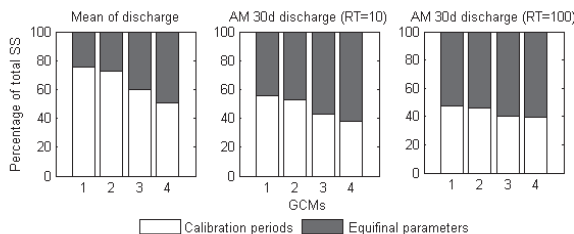
Figure 4.11 Percentage of total sum of squares resulted from the difference in the choice of long-length calibration periods and the equifinal parameter sets

The selected calibration periods above represent only the segments of the whole historical record with contrasted climatic specificities. In the common practice, the longer length of data is used to provide as much as possible information for the calibration. It is considered that robust parameters will be calibrated provided by the sufficient information contained in the calibration period. Even using the longest available data, the selected periods only represent part of the historical climate, additional uncertainty may be introduced by the screening of different historical periods to the future flow projections. To analyse this, the 45-year historical record was divided into three 15-year continuous sub-periods. 1000 behavioural parameters were calibrated from each of the sub-periods to account for equifinality.

The uncertainty due to the choice of the calibration periods takes the majority of the total uncertainty in the projected mean annual discharge, but the percentage decreases when the future climate is projected to be wetter. For the low-return-period extreme discharge, the uncertainty due to equifinal parameter sets takes around 40% of the total sum of squares in a climate that is close to the historical condition (GCM1 and GCM2), while this uncertainty takes more than half of the total sum of squares in a wetter climate. For the extreme discharge with high return periods, the uncertainty due to equifinal parameter sets accounts slightly more than the uncertainty due to the choice of calibration periods.

4.7 Discussion

Transferability of parameters

The Differential Split-Sampling Test allows testing the transferability of hydrological model parameters to a different period in the context of historical climate variability. The examinations of model errors reveal that the parameters calibrated from climatic-specified periods are not equally transferrable. Better transferability of the parameters calibrated from a dry period to a wet period was observed than the other way around. The parameters calibrated from the diverse period showed the highest transferability to other periods. This is understandable as the diverse period contains both high-flow and low-flow, which enables all the parameters well calibrated. Dry biases in the simulated mean discharge were observed when transferring the parameters calibrated from a dry period to a wet period; conversely, wet biases were observed when transferring the parameters calibrated from a dry period to a wet period. The bias increased with the increase of the difference in rainfall between the calibration and validation periods. Similar results have found in previous studies (Yew Gan et al. 1997, Vaze et al. 2010, Li et al. 2012).

It is notable that the parameters calibrated from the mean period generated overestimated mean discharge when validated on the wet period. This exception is attributable to the rough simulation of potential evapotranspiration used in this study, where potential evapotranspiration (PET) is proportional to daily mean temperature. The mean period had the same simulation of mean PET compared to the wet period since the mean temperature

were the same in the two periods. Less water supply leads to less actual evapotranspiration given the same PET. The value of evaporation coefficient K calibrated from the mean period was thus smaller than the value calibrated from the wet period. Overestimation of mean discharge was generated when transferring K from the mean period to the wet period. The same reason explains the higher values of future discharge suggested by the parameters calibrated from the mean period. Introducing more climatic variables may improve the estimation of PET. It is also suggested that the influence of temperature should be considered when determining the climatically contrasting periods (an example can be seen in the study of Seiller et al. (2012)).

There is not a straightforward influence of parameter transferring on AM 30d discharge. Underestimation was observed when transferring the parameters calibrated from the dry period to a wetter period, and overestimation was observed when the parameters were transferred to the dry period. However, the opposite results were found when transferring parameters among the mean, wet and diverse periods. The slow routed interflow and groundwater takes a larger portion in a wet period than in a dry period. The SM parameter, which determines the proportion of surface flow, may over-partitioned part of interflow and groundwater to surface flow when transferred to a period that was wetter than the calibration period. Due to the fast routing of surface flow, the AM 30d discharge was thus overestimated. This can also be seen the future projections. The opposite results of the transferring the parameters 'to' or 'from' the dry period was probably caused by the high sensitivity of the parameters related to water balance, i.e., the parameter K led to the overestimation in actual evaporation and thus lower runoff.

Uncertainty comparison

Comparing the two sources of uncertainty, the choice of calibration periods introduced more uncertainty than the equifinal parameter sets in the future mean discharge. This can be attributed to the high sensitivity of the parameters controlling water balance to the choice of calibration periods. The water routing parameters, which are the main contributions to the equifinal effect, did not have obvious influence the multi-year mean discharge. Thus, the future mean hydrological condition was largely influenced by the choice of calibration periods. In term of high discharge, the contrasting climatic conditions of the selected calibration periods dominated the total uncertainty compared to the equifinal parameters. This uncertainty decreases when the calibration periods were not climatically contrasted, but it still contributed more than 30% of the total parameter uncertainty.

More variability was caused by the equifinal parameter sets in the high-return-period high discharge than in the low-return-period high discharge. When the calibration period contained enough information of climate variability, the uncertainty arising from the equifinality effect and that from the choice of calibration periods are comparable for extreme floods.

Performance of the hydrological model calibrated from the dry period

Part of the parameters calibrated from the dry period cannot provided satisfied performance (NSE values less than 0.6) when being transferred to other periods. In a future climate that does not differ much from the historical condition (results of GCM1 and GCM2), the model calibrated over the dry period generally projected lower discharge than the model calibrated over the wet period. In contrast, in the future climate that is much wetter than the historical period, the model calibrated over the dry period projected greater extreme discharge at higher return period than the model calibrated over the wet period did. The above observations may be explained by the response of a model to an extreme forcing. For example, the soil moisture content may be saturated under an extremely wet climate and a large part of the rainfall will be generated as runoff. The hydrological model calibrated from a dry period may produce less reliable results when forced by the rainfall that is much greater than that of the calibration period. Thus, care should be taken when driving the hydrological model by the future climate that is much wetter than the historical climate used to calibrate the model.

Impacts of land use change

In addition to climate change, land use changes can also influence the hydrograph. The forest cover plays an effective role in intercepting the precipitation and allows evaporation to take place directly into the atmosphere; thus, the amount of water available for overland flow is reduced. The decayed tree roots create hollows which act as a temporary storage reservoir to contain runoff and reduce the velocity of the flow. The large increase in forest cover could counteract the impact of climate change, i.e., decrease the frequency and magnitude of floods (Reynard et al. 2001). On the other hand, urban land processes the opposite hydrological properties of forest land. The extension of urbanisation increases the proportion of impermeable areas in the basin, which reduces the infiltration capacity and speeds up the response time of the basin to rainfall.

Effects of land use change are not taken into account in this study. In the Huai River basin, the extreme flood events are generally caused by long-lasting rainfall events which induces soil saturation, and therefore the change in the soil storage capacity due to land use change affects the surface discharge to a smaller extent. The index of flood event used here, i.e., the AM 30d discharge, is a factor related to the total water volume at monthly scale; it is less influenced by the change in the timing of flood peaks. Previous researches show that the effects of land use change on hydrological processes are mainly shown in the magnitude of low flows and the timing of flood peaks at the basin outlet(Bultot et al. 1990, Brath et al. 2002, Naef et al. 2002). Streamflow at the outlet of large basins proved rather insensitive to land use changes due to the relatively small proportion of affected area over the entire basin (Hurkmans et al. 2009). The peak flows with high return period are less sensitive to land use change than those with low return period (Hollis 1975, Brath et al. 2006). Considering the

properties of flood events in the study area and the previous findings, selecting the AM 30d discharge as an index of flood events avoids the distortion in the results due to the effect of land use change.

Due to the complex of the combined effects of climate change and land use change, it is important to separate and quantify the effect of each factor on river flows. Reynard et al. (2001) found that changing the land use can have a similar scale of impact to that due to climate change if an extreme large increase in urbanisation was assumed, while the "best guess" land use changes show little impact on flood response. Shi et al. (2012) compared the effects of climate change and land use change on the hydrological processes in the upstream of the Huai River. They found that climate variability played a dominant role in this basin and the effects of climate variability were offset by the effects of land use change which may explain the unapparent change in stream-flow. It would be interesting to investigate whether climate change effects are different under a different land use condition in the future work.

Chapter 5 Overall uncertainty in the impacts assessment

In this chapter, an overall uncertainty assessment of the modelling framework used to assess climate change impacts on river floods is carried out. The uncertainty associated with each component of the framework (introduced in Chapter 2, 3 and 4) is analysed and compared. The projected future flood frequency as well as the uncertainty envelope is presented.

5.1 Introduction

It is generally acknowledged that the climate is changing due to the enhanced greenhouse effect. The associated change in temperature and precipitation will impact the frequency and magnitude of floods in the future (Monirul Qader Mirza 2002, Das et al. 2011). Since the future climate is considered to be non-stationary, the traditional frequency analysis based on historical records cannot answer the question how flood frequency will change under future climatic condition. Thus, the GCM projections under multiple greenhouse gas emission scenarios have been commonly used in impact assessments. The future climate projections are firstly downscaled to the local scale and then driven into the hydrological model to provide continuous time series of river discharge. Future flood frequency is subsequently derived based on the time series of discharge.

There are examples of studies that use the process-based modelling framework translating climate model projections into river flow in order to assess flood risk under the future climatic conditions. Bell et al. (2007 a,b) developed a grid-based flow routing and runoff-production model for use with the output of a regional climate model (RCM), and the approach was used to assess the changing flood risk in catchments across the UK. They found that changes in flood frequency at higher return periods are generally less robust than at lower return periods. Raff et al. (2009) used statistical methods to downscale selected GCM outputs under multiple emission scenarios, and the downscaled climate projections were driven into a conceptual hydrological model to estimate flood frequency over the American river basins. Similar modelling configuration was also used in Leander et al. (2007, 2008)'s study over the Rhine River. Most of the previous studies assessing climate change impacts on flood risk use single downscaling method or single hydrological model setting. The uncertainties stemming from components of the model cascade need to be quantified and compared.

To date, the GCM structure has been recognised as the largest contributor to the uncertainty associated with the impact assessments (Kingston et al. 2011, Xu et al. 2011). The studies comparing the relative magnitudes among the uncertainties arising from other components have not reached a conclusion and may differ among basins with different climatological and hydrological conditions. Jung et al. (2011) showed that the uncertainty associated with urban flooding analysis is highly affected by the GCM structure in the shorter term flood frequency change, while the uncertainty is dominated by natural variability in the longer term flood frequency change. Kay et al. (2009) conducted an uncertainty assessment of flood frequency analysis in England and compared the uncertainties associated with the GCM structure, the GCM initial condition and the downscaling method. Their results indicated that uncertainties due to GCM initial conditions and RCM structure are more significant if the results from an extreme GCM simulation are excluded. Wilby and Harris (2006) developed a framework to explore the uncertainty in future low flows for the River Thames. The results suggest the following order of component significance (greatest to least): GCM > (empirical) downscaling method > hydrological model structure > hydrological model parameters > emission scenario. However, Maurer (2007) investigated climate change impacts on water resources using the climate projected by 11 GCMs under two emissions scenarios; and they found that future emissions scenarios play a significant role in the degree of impacts to water resources in California. Considerable uncertainty also occurs in the hydrological modelling. Jiang et al. (2007) employed six monthly water balance models to assess hydrologic model structural uncertainty. They showed that the selection of hydrologic models results in different hydrologic climate change impacts. Najafi et al. (2011)'s results showed that hydrologic model selection is more critical in the dry season than in the wet season in rainfall-dominated regions. Wilby (2005) and Cameron et al. (1999) found that uncertainty in projected river flow changes due to choice of training periods was comparable to the uncertainty due to future greenhouse gas emission scenarios. Finger et al.

(2012) carried out the uncertainty analysis of climate change impacts on future water availability based on multi future RCM climate projections, hydrological model parameters, and projected glacier extents. The analysis revealed that the fraction of uncertainty contributed by the components differs with seasons and future time horizons. Jung et al. (2012) claimed that major uncertainty sources might vary depending on the locations of the basins with differing hydro-climatology; and the degree of matches between the GCM or RCM simulations and conditions in each region and/or season will also influence the uncertainty analysis. Thus, the uncertainty analysis on modelling components is recommended to be taken routinely in the climate change impact assessments.

In this chapter, the climate change impact on flood quantiles is analysed using the process-based modelling framework consisting of multiple greenhouse gas emission scenarios, GCM structures, downscaling methods and hydrological model settings (including the choice of calibration periods and the equifinality effect of parameter sets) (Figure 5.1). The uncertainty assessment was carried out by comparing the uncertainty contribution from each component.
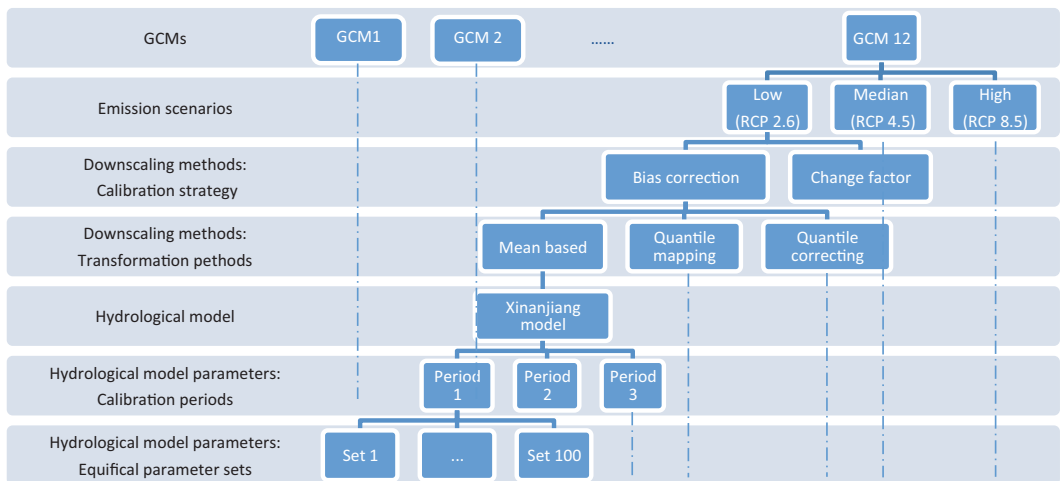
Figure 5.1 A modelling framework of the impact assessment

5.2 Sources of uncertainty

5.2.1 Emission scenarios and GCMs

The daily precipitation and temperature projected by 12 GCMs from the Coupled Model Intercomparison Project Phase 5 (CMIP5) were selected to provide the future climate change information (See Table 5.1). The GCM projections were obtained under three scenarios representing low (RCP2.6), median (RCP4.5) and high (RCP8.5) greenhouse gas emission. The grid size of these GCMs ranges from 1.1^{o} to 2.8^{o}. The baseline period is selected as the period from 1961 to 1990, and the future period is the period from 2071 to 2100.

The changes of future precipitation and temperature in summer (June, July and August) relative to the model simulations in the baseline period are also shown in Table 5.1. All GCMs projected increasing mean summer temperature. Higher greenhouse gas emission leads to higher temperature. The GCM ensemble projected the increase in mean summer temperature up to 3 ^{o}C under the scenario of RCP2.6, while the increase ranges from 2.9 ^{o}C to 7 ^{o}C under the scenario of RCP8.5. The GCM ensemble provided the divided projections in precipitation. Both increase and decrease in mean summer precipitation were projected by the ensemble members. Most of the members projected an increasing standard deviation indicating an increasing occurrence of low and extreme precipitation events. More extreme precipitation events are projected in the high emission scenario.

Table 5.1 Statistics of climate projections

		GCM information			Change in Precipitation						Increase in Temperature (^{o}C)		
					RCP2.6	RCP4.5	RCP8.5	RCP2.6	RCP4.5	RCP8.5	RCP2.6	RCP4.5	RCP8.5
GCMs	Country	Modeling Center	Model	Resolution (°)	mean	mean	mean	std	std	std	mean	mean	mean
1	China	BCC	BCC-CSM1.1	2.8×2.8	-2%	-4%	-3%	1	1	1	1.9	2.9	5.3
2	Canada	CCCma	CanESM2	2.8×2.8	27%	23%	35%	1.2	1.3	1.8	1.8	3.2	5.8
3	USA	NCAR	CCSM4	1.25×0.94	-4%	-4%	-7%	1.5	1.5	1.7	1.2	2.4	4.6
4	France	CNRM-CERFACS	CNRM-CM5	1.4×1.4	-2%	5%	18%	1	1.2	1.3	1.9	2.7	3.4
5	Australia	CSIRO-QCCCE	CSIRO-Mk3.6.0	1.875×1.875	-1%	-18%	-17%	1.2	0.9	1	2.6	4.5	6.7
6	USA	NOAA GFDL	GFDL-CM3	2.5×2.0	33%	40%	59%	0.9	1.3	1.1	3	4.1	6
7	UK	MOHC	HadGEM2-ES	1.875×1.25	7%	18%	27%	1.2	1.2	1.6	2.7	3.5	6.3
8	France	IPSL	IPSL-CM5A-MR	2.5×1.25	-4%	-10%	-11%	0.9	1	1.3	1.8	3.5	7
9	Japan	MIROC	MIROC5	1.4×1.4	-1%	2%	4%	1.2	1.1	1.3	1.8	2.4	3.8
10	Germany	MPI-M	MPI-ESM-MR	1.875×1.875	-3%	-6%	-7%	1.6	1.6	2	1.7	2.8	4.4
11	Japan	MRI	MRI-CGCM3	1.1×1.1	14%	40%	40%	1.1	1.4	1.2	1	1.5	2.9
12	Norway	NCC	NorESM1-M	2.5×1.875	1%	4%	-8%	1.2	1.7	1.4	1.7	2.6	4.9

5.2.2 Downscaling methods

The above future climate projections were downscaled to station scale by six variants of empirical downscaling methods. In this group of methods, statistical transformation functions were calibrated and then used to adjust observations or raw climate model outputs to generate future Climate projections at local scale. Two calibration strategies were employed, i.e., the bias correction strategy and the change factor strategy; three transformation methods were used, i.e., mean based method, quantile mapping method, and quantile correcting method. To avoid unrealistic areal mean extremes in precipitation discussed in Chapter 3, the bias correction based methods were carried out based on each

gird cell, i.e. each grid value of GCM outputs was transformed based on the areal mean precipitation or temperature at stations within this grid.

We denote an observed climatic variable during the baseline period as X_O and its future projection as X'_O; the climate model simulations of this variable are given as X_M and X'_M for the baseline and future periods, respectively. The downscaling methods can be expressed by the following equations:

1) Mean based method implementing the bias correction calibration strategy (MB-BC)

$$X'_O = X'_M \cdot \frac{\mu_O}{\mu_M} \quad \text{for precipitation} \qquad\qquad 5\text{-}1$$

$$X'_O = X'_M + \mu_O - \mu_M \quad \text{for temperature} \qquad\qquad 5\text{-}2$$

where μ_O and μ_M are the means of the observation and the modeled values in the baseline period, respectively. This method was also named as Local Intensity Scaling method by Schmidli et al. (2006). This method ensures that modeled and observed climatic variables have the same mean climatology. To handle the drizzle effect, the precipitation frequency was corrected using a wet-day threshold, which was determined from the model daily precipitation series such that the threshold exceedance matches the wet-day frequency in the observed series.

2) Quantile mapping method implementing the bias correction calibration strategy (QM-BC)

$$X'_O = F_O^{-1}[F_M(X'_M)] \qquad\qquad 5\text{-}3$$

where F and F^{-1} are empirical cumulative function (ECDF) and reverse ECDF, respectively. The commonly used 99-percentile tables were employed (Boé et al. 2007, Deque 2007) due to the superior performance of empirical CDFs in the previous studies (Themeßl et al. 2011, Gudmundsson et al. 2012, Gutjahr and Heinemann 2013).

3) Quantile correcting method implementing the bias correction strategy (QC-BC)

$$X'_O = X'_M \cdot \frac{F_O^{-1}[F_{M'}(X'_M)]}{F_M^{-1}[F_{M'}(X'_M)]} \quad \text{for precipitation} \qquad\qquad 5\text{-}4$$

$$X'_O = X'_M + F_O^{-1}[F_{M'}(X'_M)] - F_M^{-1}[F_{M'}(X'_M)] \quad \text{for temperature} \qquad\qquad 5\text{-}5$$

Li et al. (2010) termed this method a "equidistant CDF matching method" and they used a theoretical distribution to fit the monthly observed and modelled data. Mpelasoka and Chiew (2009) termed this method a "daily translation method" when using it to correct daily modelled rainfall. It can be considered a variant of mean-scaling method that correcting model simulation at the different ranks or percentiles instead of applying one uniform correcting factor.

4) Mean based method implementing the change factor calibration strategy (MB-CF)

$$X_O' = X_O \cdot \frac{\mu_{M'}}{\mu_M} \quad \text{for precipitation} \tag{5-6}$$

$$X_O' = X_O + \mu_{M'} - \mu_M \quad \text{for temperature} \tag{5-7}$$

This method is usually named as "perturbation method"(Prudhomme et al. 2002) or "delta change method" (Fowler et al. 2007). This method applies GCM-scale projections in the form of change factors to the baseline observations; and the change factors represent the climate change signal which is defined as climatological means between the future climate projection and the baseline simulation (Themeßl et al. 2011).

5) Quantile mapping method implementing the change factor calibration strategy (QM-CF)

$$X_O' = F_{M'}^{-1}[F_M(X_O)] \tag{5-8}$$

This methods can be considered as a variant of the delta change method which applies different change factors to the observation at different ranks or percentiles instead of uniform change factors.

6) Quantile correcting method implementing the change factor strategy (QC-CF)

$$X_O' = X_O \cdot \frac{F_{M'}^{-1}[F_O(X_O)]}{F_M^{-1}[F_O(X_O)]} \quad \text{for temperature} \tag{5-9}$$

$$X_O' = X_O + F_{M'}^{-1}[F_O(X_O)] - F_M^{-1}[F_O(X_O)] \quad \text{for precipitation} \tag{5-10}$$

In QC-CF method, the changes at each quantiles of modeled distribution from the calibration period to the future period are directly applied to adjust the corresponding quantiles of the historical observations.

5.2.3 Hydrological modelling

The lumped Xinanjiang Model was used to transform the climate condition to the hydrological condition. The model was run at daily scale, and the basin-mean daily rainfall and temperature data were used as model inputs. The objective functions were calculated for monthly mean discharge series in order to decrease the influence of hydraulic structures on the calibration. Two objective functions were selected as objective functions: the Nash-Sutcliff Efficiency (NSE) and the Percentage Volume Error (PVE).

Choice of calibration periods

To analyse the uncertainty stemming from the choice of calibration periods, the historical period was divided into three sub-periods with equal length: 1961-1975, 1976-1990 and 1991-2005. Each of the sub-period contains sufficient hydrological information, including dry

years and wet years, to calibrate the hydrological model. The hydrological model was calibrated on three calibration periods, respectively.

Equifinality effect

To analyse the influence of equifinality (Beven and Freer 2001), a set of behavioural parameters rather than an optimal set of parameter were used to project the future discharges. The equal weighted Monte Carlo algorithm was employed to calibrate the hydrological model. For each calibration period, 100 parameter sets for each calibration period were selected as behaviour parameter sets according to the goodness-of-fit measures defined above.

Table 5.2 Simulative ability of the hydrological model

Periods	1961-1975	1976-1990	1991-2005
NSE	0.859-0.865	0.839-0.859	0.913-0.924
PVE	0.5%-9%	0.2%-9.9%	0.1%-9.7%

The simulative ability of the hydrological model using the behavioural parameter sets over three calibration periods is shown in Table 5.2. The values of NSE are above 0.8 indicating a good simulative ability. The parameters calibrated on the periods of 1991-2005 produced higher values of NSE. This is because the NSE puts more weight on high discharge than low discharge, and there are more high-discharge events in this period than other periods. The index of PVE was used as a limit objective function, thus all the behavioural parameters lead to PVE values smaller than 10%.
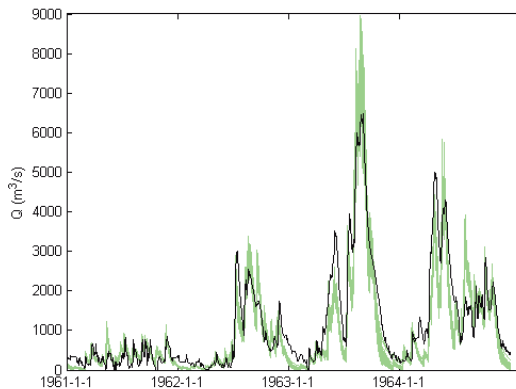
Figure 5.2 Observed hydrograph (black line) and the modelled hydrograph ensembles (shaded area)

The example of observed hydrograph and modelled hydrograph ensemble are shown in Figure 5.2. The modelled ensemble generally has a good agreement with the observation. Underestimation is observed for low flow, and overestimation is found for high flow. The simulative ability of the hydrological model is mainly limited by the lumped configuration.

The basin-mean input is not able to represent the spatial variability of rainfall, and the model parameters were calibrated as basin-mean level. Thus, the model has difficulties in simulating low and high flows.

5.3 Comparison of different sources of uncertainty

The uncertainty sources of emission scenarios, GCM structures, downscaling methods and hydrological model parameters are analysed and compared in this section. The results were grouped into five uncertainty sources. The sample size of each group is presented in Table 5.3. Each sample is weighted equally in the following analysis.

Table 5.3 Sample size of the group for each source of uncertainty

	Source	Group Size	Combination of Each group	Sample Size of
1	Choice of period for calibrating hydrological model (CP)	3	12(GCM)*3(ES)*6(DM)*100(EP)	21600
2	Equifinal parameter sets (EP)	100	12(GCM)*3(ES)*6(DM)*3(CP)	648
3	Downscaling method (DM)	6	12(GCM)*3(ES)*3(CP)*100(EP)	10800
4	Emission scenario (ES)	3	12(GCM)*6(DM)*3(CP)*100(EP)	21600
4	GCM	12	3(ES)*6(DM)*3(CP)*100(EP)	5400

The high water level at the outlet of the basin in flood season usually lasts more than one month due to the heavy rainfall over the large river basin. Thus, the annual maximum 30-day mean discharge (AM 30d discharge) was selected as the index of the flood event. The General Extreme Value (GEV) distribution was used to fit the observed and modelled AM 30d discharge.

Additional biases could arise from the modelling framework, e.g., the mismatch between the downscaled variable and the observation in the baseline period, the errors in the hydrological modelling and the fitting of the probabilistic distributions. These biases were propagated and eventually caused the discrepancy between the flood frequency curves derived from the simulations and the observation. To avoid these systematic biases, the relative change in the flood frequency is analysed here by assuming that the systematic biases stay constant from the baseline period to the future period and can be cancelled out. The relative change in a future flood frequency was calculated at each flood quantile against the corresponding baseline flood frequency resulted from the same model chain setting. The flood quantiles with return period of 2, 5, 20, 20 and 50 year were selected to be analysed. The mean changes of flood quantiles due to different sources of uncertainty are compared in Figure 5.3. The empirical cumulative density functions (ECDFs) of the changes at the quantiles with the return period of 5 year and 20 years are shown in Figure 5.4.
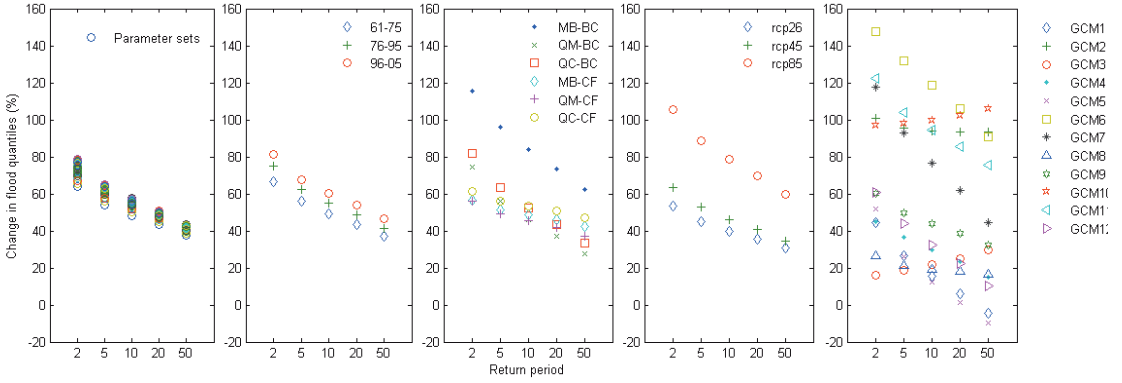
Figure 5.3 Changes in flood quantiles resulting from different uncertainty sources(from left to right: equifinal parameters, calibration periods, downscaling methods, emission scenarios and GCM structures)
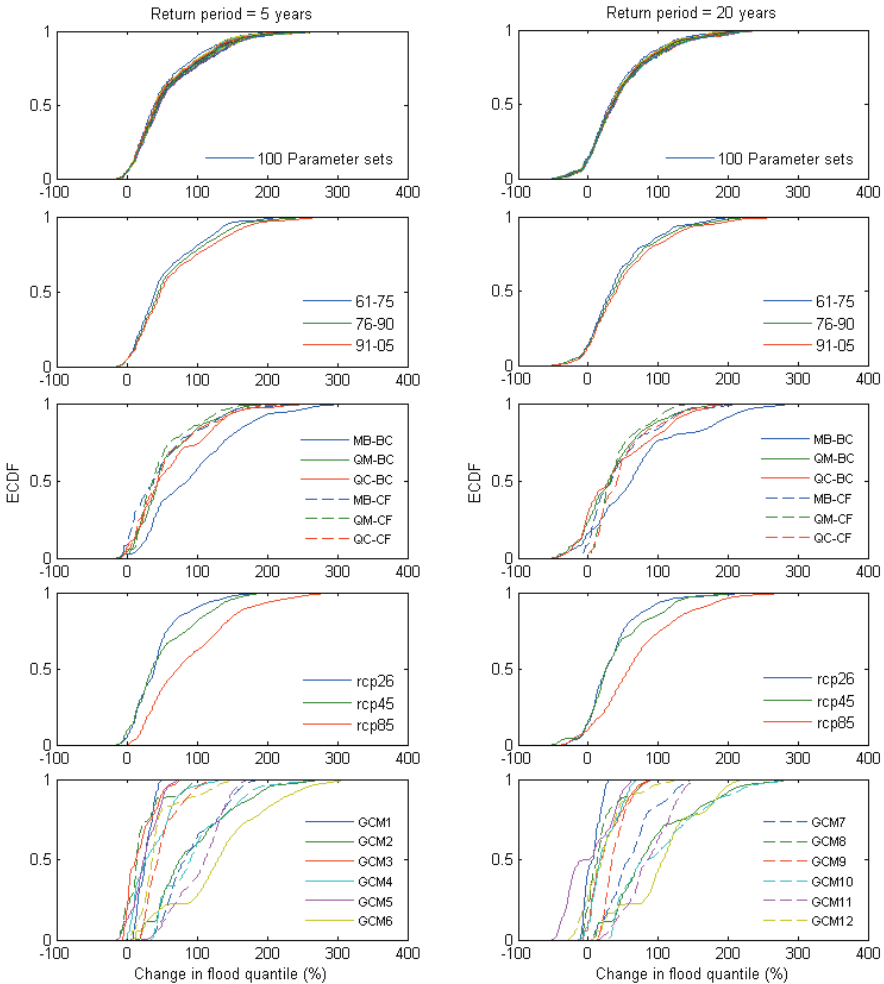
Figure 5.4 ECDFs of change in flood quantiles due to different sources of uncertainty (from top to bottom: equifinal parameter sets, calibration periods, downscaling methods, emission scenarios and GCM structures)

5.3.1 Uncertainty due to emission scenarios

Generally, a higher emission scenario leads to greater increase in flood quantiles. The scenario RCP2.6 has the least relative increase (around 40%) at each flood quantile (see the diamonds in the 4th sub-figure of Figure 5.3). The scenario RCP4.5 led to slightly larger flood magnitude than the scenario RCP2.6, while the scenario RCP8.5 led to much larger flood magnitude than the other scenarios. For both the quantiles with the return periods of 5 years and 20 years (see the 4th row in Figure 5.4), about 50% of the future projections under scenario RCP4.5 resulted in similar changes with those under RCP4.5, but the rest of the projections under RCP4.5 resulted in greater increase than those under RCP2.6. About 15% likelihood of a decreasing change is observed under each scenarios at the high-return-period quantile (20 years). The likelihood of decreasing low-return-period quantile (5 years) is less than 10% under the scenarios of RCP2.6 and RCP4.5, and the likelihood of decreasing low-return-period quantile is zero for the scenario of RCP8.5.

5.3.2 Uncertainty due to GCMs

Although many of the GCMs projected a decrease in mean summer precipitation, the GCM ensemble generally suggested an increase in flood quantiles (see the 5th sub-figure in Figure 5.3). There is large variation among the projections resulting from different GCM structures. The change at the 5-year-return-period quantile ranges from 16% to 148%, while the change at the 50-year-return period quantile ranges from -10% to 106%. The ordering of the effects of the GCMs differs among quantiles. The results can be divided into two groups: the GCMs projecting an increase in mean precipitation (GCM2, GCM6, GCM7 and GCM11) resulted in greater increase in flood quantiles compared with other GCMs projecting a decrease in mean precipitation. Most of the GCMs projected greater relative increases at low quantiles than high quantiles, while two exceptions are GCM3 and GCM10 which projected obvious increase in standard deviation of precipitation (see Table 5.1). It can be seen from Figure 5.3 that larger likelihood of a decreasing projection is found at the 20-year-return-period quantile than at the 5-year-return-period quantile.

GCM3 and GCM10 projected a smaller increase at low flood quantiles and a greater increase at high flood quantiles, which is a reverse ordering compared to the results from other GCMs. This may be explained by the increase of standard deviation projected by the two GCMs. GCM3 and GCM10 both projected decreasing mean precipitation but increasing standard deviation which is up to twice of the standard deviation in the baseline period. A large amount of precipitation with a high return period could be projected by these GCMs, which leads to an increase at the high flood quantiles.

5.3.3 Uncertainty due to downscaling methods

The range of the changes due to the choice of downscaling methods is comparable with those due to emission scenarios. A large part of the downscaling uncertainty is contributed

by the MB-BC method. As discussed in Chapter 3, only adjusting the mean values is not sufficient to correct the biases in GCM outputs, which explains the obvious deviation of the MB-BC method from other downscaling methods. Other downscaling methods suggested comparable results among each other. For the 20-year-return-period quantile, the bias correction based methods suggested up to 30% likelihood of the decreasing projection, which is higher than their counterparts based on the change factor calibration strategy. For the quantiles with low return periods, the bias correction based methods suggested greater increases than the change factor based methods.

The main difference between the bias correction based methods and the change factor based methods lies in the temporal structure and spatial distribution of the downscaled variables. The precipitation and temperature downscaled by the bias correction based methods have the same temporal series with the raw GCM outputs, while those downscaled by the change factor based methods maintain the temporal series of the observation. The difference in temporal structure does not have obvious influence on downscaled temperature, while downscaled daily precipitation can be significantly influenced by the choice of calibration strategies due to the intermittent property and the large variation in amount. For instance, some GCMs project continuous rainfall with wet spell longer than the historical level. Even the precipitation intensity is not projected to increase, extreme flood could be generated due to the saturated antecedent soil moisture condition and the large total rainfall amount.

5.3.4 Uncertainty due to hydrological modelling

The magnitude of the uncertainties due to the choice of the calibration periods and the equifinality effect are comparable. The size of the uncertainty range resulting from the different calibration periods is around 20%, and it decreases towards the higher quantiles. A similar phenomenon is also observed for the uncertainty range resulted from the equifinal parameter sets: the uncertainty range at the 2-year-return-period quantile is 20%, while it is less than 10% at the 50-year-return-period quantile. The ordering of the changes resulting from three calibration periods is the same at different quantiles, i.e., the parameter sets calibrated from the period of 1996-2005 always resulted in greater increase than the parameters calibrated from other period. This is probably caused by the difference of information contained in the three calibration periods. The high discharges in the period of 1996-2005 is greater than those in the other periods. Since the NSE objective function is biased towards high flow, the hydrological model tends to generate more runoff in order to simulate the high discharge.

5.4 Future hydrologic impact

For each scenario, the 90% one-sided upper and lower bounds of the projected future flood frequency ensemble as well as the mean of the frequency ensemble are shown in Figure 5.5. The future flood frequency was obtained by applying the relative changes to the present-day

flood frequency at each quantile. The 90% upper and lower bounds were respectively determined by the 90th and 10th percentiles of the ensemble of future flood frequency that is resulted from the combinations of all the participating GCMs, downscaling methods and hydrological parameter sets.

It can be seen that the uncertainty envelope, indicated by the width of the 90% bounds, gets wider with the increase in greenhouse gas emissions. By comparing the present-day flood frequency to the mean of the ensemble taking all samples, the flood event with a 10-year return period in the baseline period turns to be a 2-year-return-period event under the scenarios of RCP2.6 and RCP4.5. The change is more drastic under the scenario of RCP8.5, where the 2-year-return-period event in the future is as large as the magnitude of the flood event with the return period of 50 years in the baseline period. The ensemble suggests an absolute increase in the flood quantiles with a low return period, while a small fraction of the ensemble suggest a decrease in the flood quantiles with a high return period.

It can be seen from Table 5.1 that a great increase in mean summer precipitation is suggested by four GCMs (GCM2, GCM6, GCM7 and GCM11), while other GCMs generally suggest a decrease in mean summer precipitation. Thus, a constrained ensemble was taken by excluding the samples from the four GCMs which significantly enlarge the uncertainty envelope. The constrained ensemble consisting of the rest of the GCMs is considered to suggest conservable increase in future precipitation. The samples resulting from the MB-BC method were also excluded in the constrained uncertainty analysis as this method is not recommended in impact assessments according to the previous analysis. It appears that the uncertainty envelope of the constrained ensemble is half of that of the ensemble taking all the samples. Most of the ensemble members still suggest an increase in flood quantiles, although they project a decrease in mean summer precipitation. It can be concluded that GCM projections are in a good agreement in suggesting an increase in flood magnitude, and that the increase is not only caused by the increase in mean future precipitation but also by the increase in the variation of future precipitation.
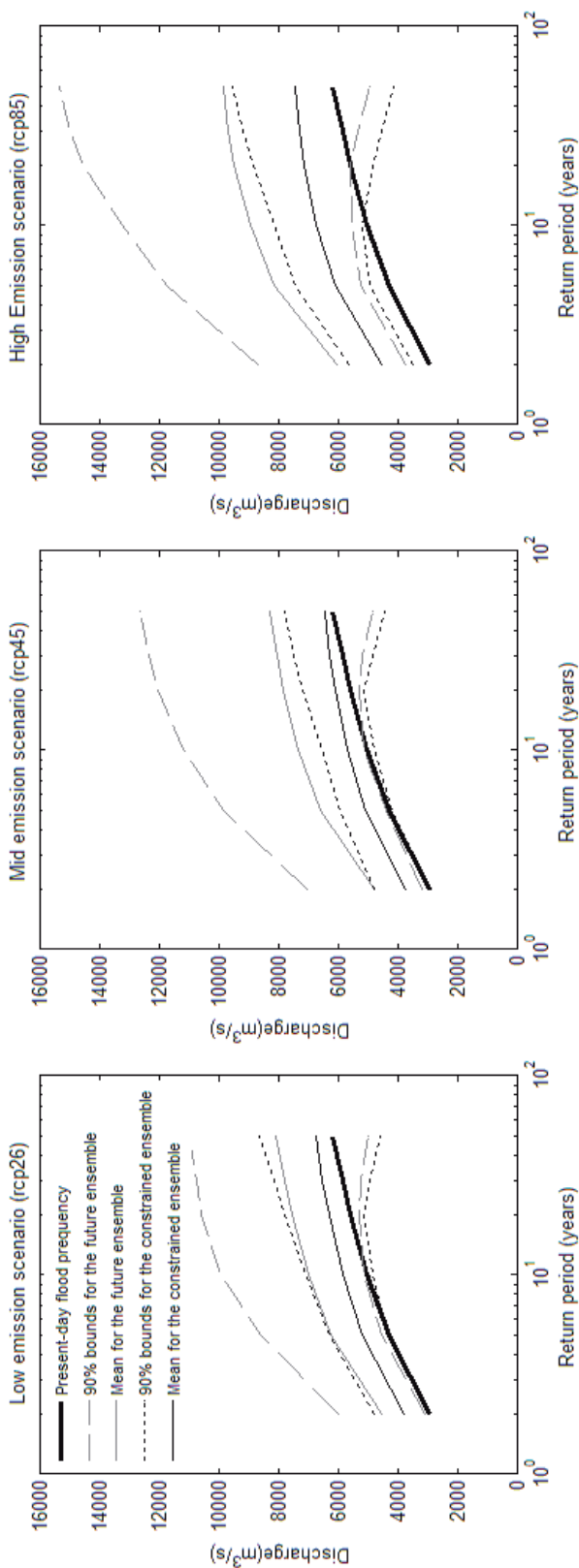
Figure 5.5 Projected future flood frequency in the future period of 2071-2100

5.5 Discussion

This chapter analysed different sources of uncertainty in climate change impact studies, with particular reference to the impact of climate change on flood frequencies in the sub-basin upstream of Bengbu in the Huai River Basin. Uncertainties stemming from greenhouse gas emission scenarios, GCM structures, downscaling methods and hydrological parameters were analysed and compared.

The choice of GCM structures is the dominant contributor to the total uncertainty. The GCM ensemble suggested a large uncertainty envelope of the future flood frequency. Much of the uncertainty was contributed by the GCMs projecting an increase in future precipitation. Most of the GCMs project a slightly decrease in mean summer precipitation; however, they suggested an increase in flood quantiles. The variation in precipitation intensity is projected to increase in the future, and flood events are thus expected to be more severe in the future. Twelve GCMs participating CMIP5 were selected due to data availability. If more GCMs are included, the uncertainty from GCM structures will not necessarily increase the range of uncertainty, but would lead to more robust conclusions.

The impact of greenhouse gas emissions is not as large as that of the choice of GCM structures, but it still contributes a large portion to the total uncertainty. The flood quantiles are expected to increase under all the scenarios. The scenario of RCP4.5 leads to a slightly greater increase in the flood quantiles compared with the scenario of RCP2.6, while the scenario of RCP8.5 leads to a much greater increase in flood quantiles than the other scenarios. This can be explained by the configuration of the emission scenarios: the RCP2.6 is a mitigation scenario in the lower end, and RCP4.5 is an intermediate scenario with less aggressive mitigation policy, whereas RCP8.5 is a non-mitigation scenario. The range of emission scenarios used is not the full CMIP5 range (the intermediate scenario without mitigation, RCP6.0, was not included due to the limited number of GCMs providing projections under it), but the high- and low- end of the emission scenarios were included which enables us to explore the plausible envelope of the emission uncertainty.

The choice of downscaling methods also contributes considerably to the uncertainty in the impact assessment. The downscaling methods used here differ in the calibration strategies and the transformation methods. The choice of calibration strategies has more influence than the choice of transformation methods. The methods based on the change factor strategy have good agreement with each other. The MB-BC method has been found to provide biased precipitation intensity, which leads to deviated results from other methods. When being propagated through hydrological modelling, this method led to more than 50% wet bias in the projections of extreme discharge. This method is thus not recommended in the impact assessments. All the downscaling methods used here produce deterministic downscaled time series. Dynamical downscaling methods and more sophisticated statistical downscaling methods (e.g., stochastic weather generator) were not used in the analysis due

to the consideration of time consumption. The uncertainty due to downscaling methods could be larger if more methods are considered, but this uncertainty is not expected to be as large as the GCM uncertainty according to the results of the previous studies (Chen et al. 2011, Chen et al. 2011).

The uncertainty from hydrological modelling is represented by the parameter uncertainty due to the choice of calibration periods and the equifinality effect. The uncertainty of the hydrological model is less than other sources of uncertainty. The uncertainty due to the model structure is not analysed here. Since the calibration of model parameters is aimed to compensate for the error in model structure, it is considered that the parameter uncertainty could to some degree encompass the structure uncertainty. Previous studies show that the high flow can be significantly influenced by the hydrological parameterisation (Wilby 2005, Finger et al. 2012).

All the samples of future discharge projections were analysed with equal weights in this study. The uncertainty analysis could also be done in a probabilistic way. For instance, Wilby and Harris (2006) weighted GCMs according to an index of reliability for downscaled effective rainfall when assessing uncertainties in climate change impacts on river low flow. The hydrological model structures and parameters can also be weighted according to their performance in simulating historical observations (Bastola et al. 2011, Najafi et al. 2011). Applying weights to the samples based on the performances in the historical periods enables us to provide the confidence intervals of the projection. However, the question whether the errors of models is stationary under future climate condition has not been well answered.

Overall, the considered ensemble suggests an increase in future flood magnitude with a large uncertainty envelope. Even when only the conservative GCMs are selected, considerable uncertainty remains. Further work will be needed to develop practical guidance for decision makers to cope with this uncertainty.

Chapter 6 Risk-averse economic optimization of adapting river dikes to climate change

In this chapter, a risk-averse economic optimisation method is proposed to adapt river dikes to climate change. The case study indicates the feasibility of coping with the uncertainty of climate change adaptation-decision makings by adopting a risk-averse attitude.

6.1 Introduction

There has been a growing concern on the adaptation to the impacts of climate change due to the recent overwhelming consensus on global warming. Since the occurrence of floods is highly susceptible to climatic conditions, much attention should be paid to the uncertainty of climate change in flood management.

Since Van Dantzig (1956) applied the method of economic optimization to flood prevention, the risk-based design has become a useful tool in the design of flood defences in the Netherlands. The climatic condition is usually assumed as unchanged when the economic optimization method is used. However, climate change can influence the probability of

future floods and hence flood risk; furthermore, the projections of future climate are very uncertain. In other words, climate change introduces uncertainty by having an uncertain effect on flood frequencies. In the usual application of risk-based design, the uncertainty of costs (the sum of investment and risk) is not considered because only the expectation of total costs is optimized (i.e., minimized). In order to integrate the uncertainty related to costs, the usual method can be extended by including a risk-aversion cost function (Vrijling et al. 1995): the sum of the expectation of total cost and the product of the risk aversion index and the standard deviation of the total cost. This risk-aversion cost function was initially proposed as a simple measure of social risk based on loss of life; it can also be used in economic decision making (Jonkman et al. 2003). However, only a few applications of this risk-aversion function consider the economic optimization for the design of dikes (Slijkhuis et al. 1997, Van Gelder and Vrijling 1998, Kuijper and Kallen 2010, Kuijper and Kallen 2012).

There has been an abundance of researches on the influence of climate change on river streamflow (Middelkoop et al. 2001, Milly et al. 2002, Xu et al. 2005, Leander et al. 2008, Kundzewicz et al. 2010, Das et al. 2011, Yang et al. 2012). Global Climate Models (GCMs) have been widely used in climate change research to generate plausible future climatic conditions driven by greenhouse gas emissions scenarios and other related conditions such as land use. Due to the uncertainty in GCM simulations, such as model formulation and model inadequacy, the uncertainty in climate change projections needs to be considered. The previous studies show that there is large uncertainty in the projected future climate from existing GCMs (Prudhomme et al. 2002, Kay et al. 2009, Bastola et al. 2011). Thus, projections from multi-GCM ensembles are generally used in the climate change impact related studies to help understand the uncertainty of future climate change. However, most of the previous studies focus on analysing the uncertainty in climate change impacts on hydrological regimes, and the approach of including this uncertainty in the design of flood defences has not been well developed.

In order to fill this gap, this chapter attempts to include the uncertainty in climate change impacts on flood probability in the risk-based design of river dikes. The result will also show how much the optimal dike height is influenced by this kind of uncertainty. To achieve this, the outputs from GCMs and a hydrological model were used to provide the projections of future river stage (water level). An applicable method was proposed to project the probabilistic models of the river stage in the future. The uncertainty related to climate change and its impact on flood frequency was represented by the uncertainty of the parameters of the probabilistic model. The risk-averse cost function was minimized to obtain the optimal dike height.

6.2   *Risk-averse economic optimization in the design of dikes*

The economic optimization of dike heightening was originally proposed by Van Danzig (1956). The total cost consists of flood risk and the investment cost of construction. Flood

risk is calculated as the product of annual flood probability and potential damage; and the cost of an investment is determined by the initial costs and the variable cost. The total cost can be written as

$$C = I_0 + I_1 \cdot X + p \cdot S \cdot \sum_{i=1}^{n} \left(\frac{1}{r+1} \right)^i$$

6-1

where I_0 is the initial investment, I_1 is the variable investment, X is the height which the dike is raised by, p is the annual flood probability, S is damage, and r is the discount rate. The discount horizon is n years.

In this function, I_0, I_1, S and r are treated as constants based on economic data from the study area. p, the probability of a flood per year, is calculated by an exponential function given the dike height

$$p(X) = e^{-\frac{h_0 + X - A}{B}}$$

6-2

where h_0 is the current dike crest height, A is the location parameter, and B is the scale parameter. This function was developed by Wemelsfelder (1939) to predict the probability of a storm surge level using the long-time series of observations from tidal gauges.

The total cost can be seen as a function of increased dike height X. The optimal dike height is determined by the value of X that minimizes the total cost

$$\frac{dC}{dX} = I_1 + \frac{S}{B \cdot r} \cdot e^{-\frac{h_0 + X - A}{B}} = 0$$

6-3

where the discount horizon is infinite. No uncertainty of the cost components is considered. Vrijling (1995) proposed a linear function as a simple risk-averse measure of the societal risk. It was originally applied to the loss of life. Slijkhuis et al. (1997) used this risk-aversion function in the economic optimization of the design of sea dikes and wrote the function as

$$Min[\mu(C) + k \cdot \sigma(C)]$$

6-4

where $\mu(C)$ is the expectation of total cost, $\sigma(C)$ is the standard deviation of total cost, and k is the index of risk aversion. The index of risk aversion reflects the risk-averse attitude of the decision maker. A larger index implies the decision maker has a more risk-averse attitude. Typically suggested value ranges from 0 to 3.

6.3 Including the uncertainty of climate change in the economic optimization

In the economic optimization, it is commonly assumed that an inundation occurs when the water level exceeds the height of the dike, which means only the failure mechanism of overtopping or overflowing is considered. Thus, the flood probability is assumed to be equal to the exceedance probability of water level at the dike crest. The exponential function mentioned above (Equation 6-2) is the standard way of determining design water levels for sea dikes, while annual maximum series of river discharge in China are commonly described by the Pearson type III distribution, the Log-Pearson type III distribution, the Weibull distribution, the Gumbel distribution and the Generalized Extreme Value (GEV) distribution. Considering its flexibility of the distribution function and the good distribution fitting in the study area (Xia et al. 2012), the GEV probabilistic distribution is used here:

$$p = 1 - e^{-\left[1 + C\left(\frac{H-A}{B}\right)\right]^{-\frac{1}{C}}}$$

6-5

where, p can be considered an exponential function of the shift parameter A, the scale parameter B and the shape parameter C at a given river stage (water level) H.

The occurrence of a flood per year can be treated as a Bernoulli trial Y with occurrence probability p. In a stationary environment, p is considered constant for a certain dike height. However, changes in climate introduce uncertainty to the probability of floods, because climate change is highly uncertain and a changing climate has significant effects on flood probability. Expressed mathematically, in a changing climate, the occurrence of a flood per year is still a Bernoulli trial Y with occurrence probability P, but P is an uncertain value rather than a constant. The uncertainty of P reflects the uncertainty in climate change and its impacts on flood probability.

Assuming P is a random variable with the expectation $\mu(P)$ and the standard deviation $\sigma(P)$, the expectation and variance of the Bernoulli variable Y can be given by

$$E(Y) = E(E(Y \mid P)) = \mu(P)$$

6-6

$$D(Y) = D_P[E(Y \mid P)] + E_P[D(Y \mid P)] = \mu(P) \cdot [1 - \mu(P)]$$

6-7

It is observed that

$$\sum_{i=1}^{\infty} \left(\frac{1}{1+r}\right)^i = \frac{1}{r}$$

6-8

$$\sum_{i=1}^{\infty}\left(\frac{1}{(1+r)^2}\right)^i = \frac{1}{(1+r)^2 - 1}$$

6-9

The above equations show that the expectation and variance of Y are determined by the expectation of P. Based on the above equations, the expectation and variance of total cost can be given by

$$\mu(C) = I_0 + I_1 \cdot X + \frac{\mu(P) \cdot S}{r}$$

6-10

$$\sigma^2(C) = \frac{\mu(P) \cdot [1 - \mu(P)] \cdot S^2}{(1+r)^2 - 1}$$

6-11

where $\mu(C)$ is the mean of total cost, $\sigma(C)$ is the standard deviation of total cost, S is the damage caused by flooding, and r is the discount rate. The cost is discounted on a very long time horizon.

Apart from the uncertainty introduced by climate change, there is also variance in the estimations of investment and damage costs which is caused by the shortage of information. The uncertainty in the costs of investment and damage can be considered by assuming the corresponding cost parameters in Equation 6-1 as normal distributed variables. Assuming the Bernoulli variable Y and the variable S are independent, the variance of the product of Y and S can be written as

$$\begin{aligned} Var(Y \cdot S) &= Var(Y) \cdot Var(S) + E^2(Y) \cdot Var(S) + Var(Y) \cdot E^2(S) \\ &= \mu(P) \cdot (1 - \mu(P)) \cdot \sigma^2(S) + \mu^2(P) \cdot \sigma^2(S) + \mu(P) \cdot (1 - \mu(P)) \cdot \mu^2(S) \\ &= \mu(P) \cdot \left[\sigma^2(S) + (1 - \mu(P)) \cdot \mu^2(S) \right] \end{aligned}$$

6-12

The expectation and standard deviation of total cost can be calculated as

$$\mu(C) = \mu(I_0) + \mu(I_1) \cdot X + \frac{\mu(P) \cdot \mu(S)}{r}$$

6-13

$$\sigma^2(C) = \sigma^2(I_0) + \sigma^2(I_1) \cdot X^2 + \frac{\mu(P) \cdot [\sigma^2(S) + (1 - \mu(P)) \cdot \mu^2(S)]}{(1+r)^2 - 1}$$

6-14

where $\mu(I_0)$ is the mean of initial investment, $\sigma(I_0)$ is the standard deviation of initial investment, $\mu(I)$ is the mean of variable investment, $\sigma(I)$ is the standard deviation of variable investment, $\mu(S)$ is the mean of damage, $\sigma(S)$ is the standard deviation of damage, and r is the discount rate. The added dike height X and the flood probability P are related through the height of the dike. X is the difference between the dike heights before and after

heightening. *P* is equal to the probability of a river water level exceeding the dike height; it is determined by Equation 6-5 with the assumption that only the failure mechanism of overflowing is considered.

The following question is how to calculate $\mu(P)$, the expectation of *P*. Since variable *P* is estimated by the probabilistic model, the parameters in the model are also random variables in this case. The uncertainty of *P* can then be described by the parameter uncertainty of the probabilistic model. Assuming the parameters *A*, *B* and *C* in the GEV probabilistic model (Equation 6-5) are independent normally distributed variables, the expectation of *P* can be calculated by

$$\mu(P) = \int_{-\infty}^{\infty}\int_{0}^{\infty}\int_{Climit}^{\infty}\left(1-e^{-\left[1+C\left(\frac{H-A}{B}\right)\right]^{-\frac{1}{C}}}\right)f(C)f(B)f(A)\,dC\,dB\,dA, \quad H > A \quad Climit = \frac{B}{A-H}$$

$$\mu(P) = \int_{-\infty}^{\infty}\int_{0}^{\infty}\int_{-\infty}^{Climit}\left(1-e^{-\left[1+C\left(\frac{H-A}{B}\right)\right]^{-\frac{1}{C}}}\right)f(C)f(B)f(A)\,dC\,dB\,dA, \quad H < A \quad Climit = \frac{B}{A-H} \qquad 6\text{-}15$$

$$\mu(P) = \int_{-\infty}^{\infty}\int_{0}^{\infty}\left(1-e^{-\left[1+C\left(\frac{H-A}{B}\right)\right]^{-\frac{1}{C}}}\right)f(B)f(A)\,dB\,dA, \qquad C = 0$$

where *f(A)*, *f(B)* and *f(C)* are the probabilistic density functions of *A*, *B* and *C*. The GEV distribution function is defined on the set {*H*: 1+*C*(*H-A*)/*B*>0}, and the shape parameter *C* determines the type of the GEV family of distribution. Thus, the expectation of *P* is calculated using the different functions shown above.

The above method of $\mu(P)$ calculation implies that no model uncertainty is considered as only one type of probabilistic model (GEV) is used. The uncertainty of *P* is described only by the uncertainty in the parameters of probabilistic model, which leads to the assumption that the uncertainty in the parameters of probabilistic model represents the uncertainty in climate change and its impact on future flood probability. The calculation of $\mu(P)$ is similar to the method introduced by Van Gelder (1996) which copes with the statistical (parameter) uncertainty caused by the limited historical observation distribution in a stationary environment. In his study, the statistical uncertainty in the parameters of probabilistic model was integrated out (or marginalised out) to determine the 'predictive' probabilistic. By doing this, it is avoided that 'using point estimators for uncertain parameters underestimates the variance in the random variable'. In contrast to Van Gelder's method, the proposed approach in this paper integrates out the uncertainty in climate change impacts on flood probability; the parameter uncertainty is quantified from the hydrological simulations driven by projected future climate conditions rather than from historical observations in Van Gelder's method. The approach of quantifying the parameter uncertainty will be described in Section 6.4.

6.4 The applicable approach for deriving future flood probability of the Huai River

The Huai River basin is highly regulated by flood control projects including reservoirs, sluices, and water retention area. The modelling framework of assessing climate change impacts on flood frequency described in Chapter 5 could be generally carried out over the rivers without hydraulic structures. However, the hydrological model calibrated with the daily observed discharge in this modelling framework could not well simulate the future discharge series influenced by the flood control measures.

To guarantee the reliable results of the economic optimisation, an approach of deriving future flood frequency taking account of the influences of flood control measures was used here. A data set of the historical natural monthly runoff was reconstructed by the Huai River basin authority based on the observed discharge and the operation of the upstream hydraulic structures. The hydrological model was calibrated with the reconstructed historical natural runoff data at monthly scale; it was then used to project future monthly runoff. Thus, the output of the hydrological model is considered as the future runoff without the influence of the hydraulic structures. To bridge the outputs of the hydrological model and river stages, the empirical relationship based on the historical data was employed; and the derivation of this empirical relationship will be explained in the following paragraphs.

Since historical records cannot foresee the future climate, multi-GCM ensembles under different scenarios have been widely used to take account of the uncertainty in climate change and its impact. The GCMs selected from the IPCC AR4/ CMIP3 archives are taken as an example of the multi-GCM ensemble to describe the approach of quantification of the uncertainty introduced by climate change in this chapter. The period of 2070-2099 (2080s) is set as the future target period. For this period, the future world is described by different plausible scenarios, and GCMs were driven to provide climate projections (precipitation and temperature) under each scenario. These scenarios are IPCC SRES A1B, A2 and B1 scenarios that represent the median, high and low GHG emissions, respectively (Nakicenovic et al. 2000). The period of 1961-1990 is set as the baseline period that represents the historical climate, and each GCM provides the retrospection of historical climate during the baseline period. The monthly GCM projections of precipitation and air temperature are used here.

The parameter sets *A*, *B* and *C* of the GEV distribution from the projection of one GCM under one future scenario is obtained in five steps (as shown in Figure 6.1):

Step 1 The monthly runoff volume (m^3/month) series was calculated from the Xinanjiang monthly hydrological model driven by the outputs from one GCM for both the baseline period and the future period, respectively.
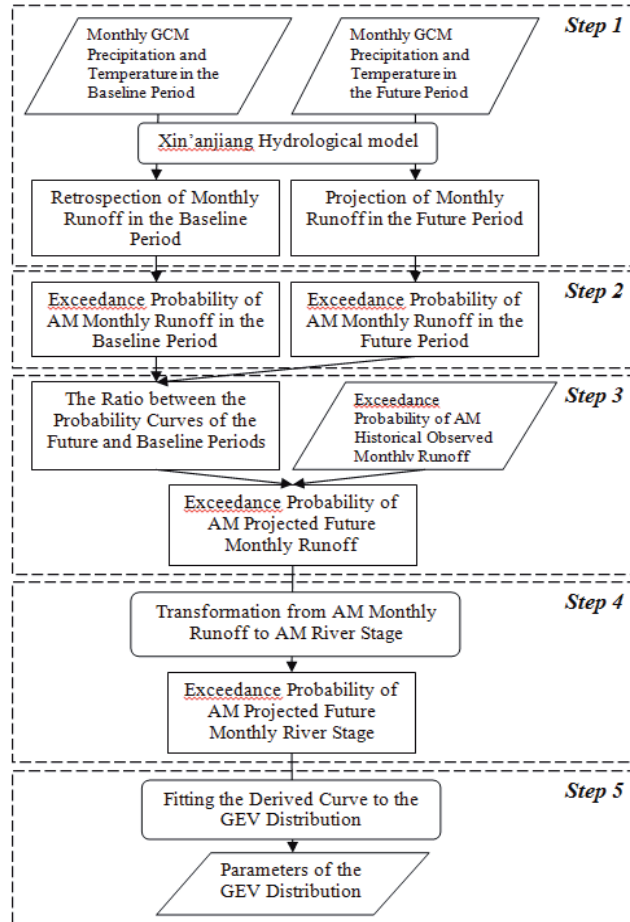
Figure 6.1 Flowchart of the derivation of the parameters of the Generalised Extreme Value probabilistic distribution of the future river stage. In this figure, annual maximum is denoted as AM.

Step 2 The curve of exceedance probability of annual maximum monthly runoff was determined for both periods based on the above time series (see Figure 6.2: the red solid line for the baseline period and the red dashed line for the future period).

Step 3 The ratio between the curve of the future period and that of the baseline period was calculated at each percentile. Then the future probability curve of runoff was projected by scaling the present-status curve derived from observations (the black line in Figure 6.2) by the ratio at each percentile.

$$R_{Future,p} = R_{present,p} \; ratio_p \qquad\qquad\qquad 6\text{-}16$$

$$ratio_p = \frac{R_{future...GCMs,p}}{R_{baseline-GCMs,p}} \qquad\qquad\qquad 6\text{-}17$$

where, $R_{future,p}$ is the future annual maximum monthly runoff at the percentile of p; $R_{present,p}$ is the historical observed annual maximum monthly runoff at the percentile of p under present climate; $ratio_p$ is the relative change between the baseline and future periods at percentile p; $R_{baseline-GCMs,p}$ is the annual maximum monthly runoff projected by the GCM under present climate; $R_{future-GCMs,p}$ is the annual maximum monthly runoff projected by the GCM under future climate.
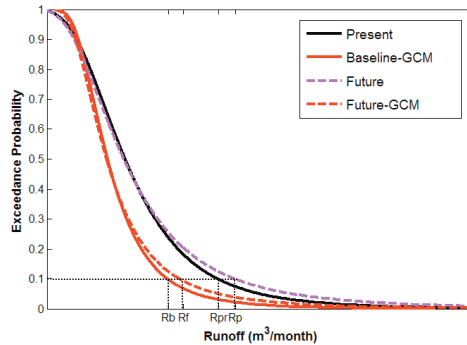
Figure 6.2 Projection of future probability - runoff curve (This figure is only used for indication)

Step 4 Then the projected exceedance probability of annual maximum monthly runoff was converted to the river stage-probability relationship through an empirical relationship (Subfigure a in Figure 6.3). The derivation process of this empirical relationship is shown in Subfigure b-d of Figure 6.3. This process is employed to take account of the influence of the flood control measures (in subfigure b) and to solve the problem of lacking long-term stage records (in subfigure c and d). The relationships (solid curves) in subfigure b-d were derived based on the historical records (circles). The derivation of the relationships is described below:

First, the relationship between *annual maximum actual (observed) monthly runoff* and *annual maximum natural monthly runoff* (Subfigure b) was used to obtain the future annual maximum monthly runoff regulated by the hydraulic structures. It is assumed that the operation of the flood control measures in the future remains the same as the present. Secondly, the relationship between *annual maximum observed instantaneous discharge* and *annual maximum actual monthly runoff* (Subfigure c) was used to obtain the future annual maximum discharge. The underlying assumption is that this relationship between peak discharge and monthly water volume stay unchanged in the future. Then the relationship between the *river stage* and the *discharge* during the high-discharge event in 2007 (Subfigure d) was used to transform the discharge to river stage. It is assumed that the present stage-discharge relationship stays unchanged in the future. The relationship between the *instantaneous river stage* and *annual maximum natural monthly runoff* (Subfigure a) was finally derived through the three relationships described above. This stage-

natural monthly runoff relationship was used to transform the future annual maximum natural monthly to the corresponding river stage.
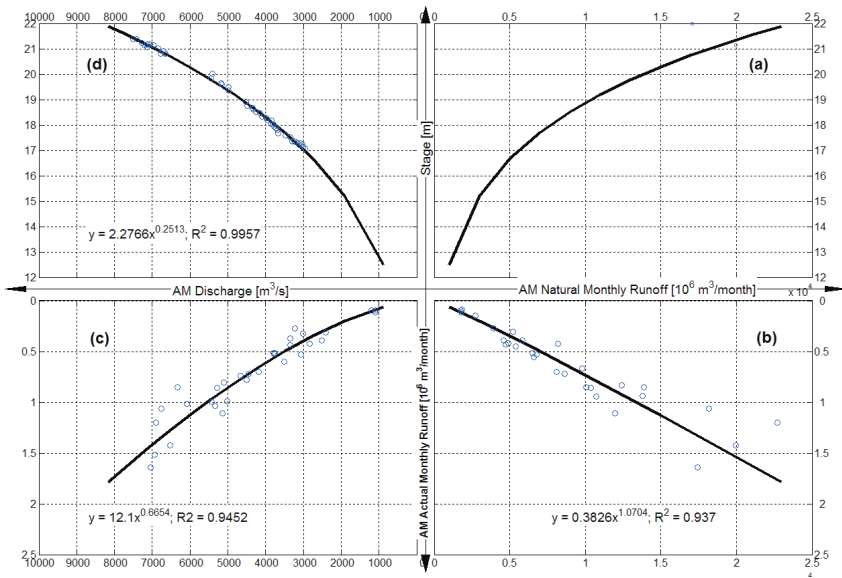
Figure 6.3 Conversion from monthly runoff to river stage

(From bottom right to top right in the counter clockwise direction)

Step 5 The parameter set of *A*, *B* and *C* was obtained by fitting the derived river stage-probability relationship to the GEV cumulative distribution function using the least square method.

Repeating the above five steps, the parameter sets from the projections of all GCMs for all scenarios can be obtained. The distribution of each parameter can be derived by equally weighting the participating GCMs; and it is then used to determine the expected predictive probability $\mu(P)$ (Equation 6-15).

The key assumption of the proposed approach is that the uncertainty of future climate change is represented by the uncertainty in GCM projections and is then quantified by the parameter uncertainty of the probabilistic model of the river stage. The derivation of future runoff-probability relationship is essentially similar to the commonly used delta change downscaling method which perturbs the observation by the projected difference from GCMs between the future and baseline period. The hydrological modelling of monthly runoff and its following conversion to river stage is more suitable to be applied over a large basin where floods are generally caused by seasonal rainfall than over a small catchment.

6.5   *Application to the Old Dike Ring*

The proposed approach was applied to the Old Dike Ring area in Bengbu, China. The Old Dike Ring was built to protect the most urbanized part of Bengbu city on the south bank of the Huai River. The Old Dike Ring is a reverse U-shape dike with the length of 12.6 km (see Figure 1.6), and it protects an area of 49 km^2. The mean elevation of the dike crest is 25.5m (Chinese Height Datum 1985), which was designed to withstand the greatest historical flood in1954, with a return period of about 40 years. The mean elevation of the bottom of the dike is 21.0m. The elevation of mean river water level in non-flood season is 13.65 m. Here, the failure probability of the dike is assumed to be equal to the exceedance probability of the dike crest, which means only the failure mechanism of overflowing is considered. The failure mechanism of overtopping, which is important for see dikes, can be neglected in the design of river dikes.

6.5.1 Uncertainty in flood probability under climate change

For the sake of simplicity, the projections of future climate from two GCMs from IPCC AR4 data sets, CSIRO-Mk3.0 (CSMK3) and GFDL-CM2.0 (GFCM20), were selected based on their performances of simulating the historical climate. Both of the GCMs provided the retrospections of the historical climate from 1960 to 1990 representing the present climate and the future projections from 2070 to 2099 under three GHG emission scenarios representing the future climate (see Figure 6.4).

Figure 6.4 Timeline of the GCMs projections

Since the long-term record of the historical river stage is not available, through Step 4 and 5 in Section 6.4, the parameters of the present-status probabilistic model of river stage were derived based on the historical records of runoff from 1956 to 2000. According to the derived probabilistic model, the return period of river stage in 1954 is 60 years and the return period of the river stage at the present dike height is about 1600 years. Compared to the return period of the flood in 1954 (40 years) provided by the authority, the calculated return period of river stage is higher. This discrepancy could be attributed to the difference in the record lengths used and the bias in the derivation of river stage based on river runoff (Step 4 and 5 in Section 6.4).

Through the five steps in Section 6.4, the parameters of the GEV probabilistic distribution of future river stage resulted from two GCMs under three scenarios were obtained, respectively (see Table 6.1). The spread of the probability curves is large (see Figure 6.5). The

shape parameters from the GCM projections have much larger variation (with variance coefficient of 185%) than the scale and shift parameters. The GCM ensemble projected a higher flood probability than the present status except the projection of GFCM20 under low emission scenario (B1). The high emission scenario (A2) leads to a higher probability than the other scenarios. CSMK3 generally projected a higher flood probability than GFCM20.

Table 6.1 Parameter sets of the present status and from GCM projections

GCMs-scenarios	Parameters of GEV distribution		
	Shape parameter (C)	Scale parameter (B)	Shift parameter (A)
Present Status	-0.0169	0.9705	18.7568
CSMK3-A1B	0.0124	1.3305	17.475
GFCM20-A1B	0.0564	1.1302	17.301
CSMK3-A2	0.0878	1.7044	16.3553
GFCM20-A2	0.0613	1.4385	18.5171
CSMK3-B1	0.0483	1.4745	16.9612
GFCM20-B1	-0.0767	0.7247	18.9283
Predictive_Mean	0.0316	1.30	17.59
Predictive_S.D	0.0584	0.339	0.97
Variance Coefficient	185%	26.1%	5.5%

Here the projections from both of the GCMs under three scenarios were treated as equally weighted realizations. By assuming the parameters obey a normal distribution, the expected predictive flood probability in the future, $\mu(P)$, was calculated using Equation 6-15 (shown as blue solid curve in Figure 6.5).
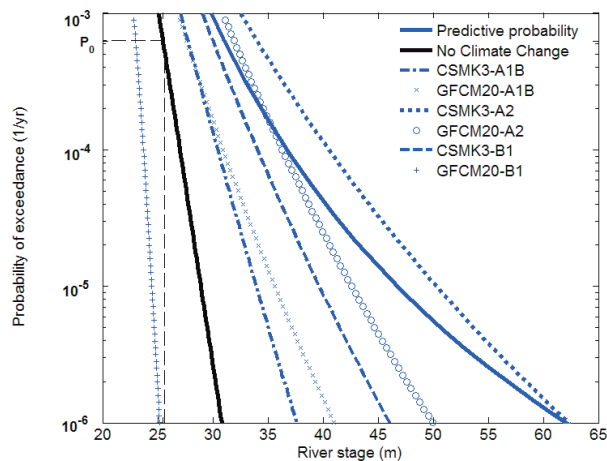
Figure 6.5 Exceedance probability of river stage under present climate and future climate. P_0 is the failure probability at current dike height

The expected predictive flood probability, $\mu(P)$, is considered as the probability that integrates the uncertainty related to the future climate. As can be seen in Figure 6.5, the expected predictive flood probability is much larger than the present situation (no climate change occurs), which indicates that climate change will lead to increased flood probability. The predictive probability curve has an upward trend towards the low exceedance probability end compared to the present-status curve, which is caused by the increased spread of the flood probabilities of the GCM ensemble at the lower end. Larger uncertainty in the projections of GCM ensemble leads to a higher expected predictive flood probability.

Compared to the present flood probability P_0, the river stages suggested by the GCM ensemble would be up to 10m higher than the present level. The drastic increase can be explained by the physical reasons underlying the hydrological responses to climate change and the extrapolation uncertainty in deriving the river stage-probability relationship, which is explained in detail in the following paragraphs.

The river basin in this study is a rainfall dominated basin with a large area (about 120000 km^2). The increase in river flow can be attributable to the absolute increase in the rainfall and the changes in the spatial and temporal distribution of the rainfall. According to the analysis on the historical records, annual runoff coefficient increases when the amount of annual rainfall is larger. This implies that the increase rate of runoff is greater than that of rainfall. If a GCM projects a drastic increase in rainfall, more drastic increase would be resulted in river flow. Moreover, long-duration rainfall events affecting large areas could cause simultaneous high flows in the tributaries, which leads to drastic high flow in the main stream of the Huai River. Thus, future changes suggested by GCMs in the spatial and temporal distribution of the rainfall may lead to more extreme high flows.

As shown in the beginning of this section, the approach of deriving the river stage based on the runoff underestimated the flood probability at the present dike height. When being used to derive future stage, the empirical relationships employed in the derivation need to be extrapolated, which could bring additional uncertainty. For example, the rating curve used to derive the stage-discharge relationship was determined based on the historical records. The result would be less reliable if the hydraulic characteristics of the control section change beyond the measured range. The relationship between annual maximum actual (observed) monthly runoff and annual maximum natural monthly runoff is used to represent the influence of the upstream flood control measures based on the historical records. This relationship cannot accurately foresee the possible flood control measures in the future for the river flows that are much greater than the present level. Moreover, the flood frequency was determined from the 30-year river flow time series; thus, considerable uncertainty occurs when extrapolating the frequency curves to lower probability. To reduce these uncertainties, it is recommended to take account of the operations of hydraulic structures in the hydrological models, to determine the rating curve by computational hydraulic modelling and to use the resampling methods in order to obtain longer time series.

6.5.2 The effect of climate change on risk-averse economic optimization

To prevent floods in a changing climate, the assumed precautionary adaptation measure is to build a flood wall on the top of the dike in the year 2013 to increase the crest height. It is assumed that the flood wall is robust enough to resist the potential water loads. The effect of the uncertainty of climate change on the economic optimization was compared with the effect of the uncertainty of damage. Three situations were analysed:

S1: The climate stays unchanged in the future. Only uncertainty in damage is included (the standard deviation is assumed as 30% of the expected damage). The mean and standard deviation of the total cost were calculated as

$$\mu(C) = I_0 + I_1 \cdot X + \frac{P_0 \cdot \mu(S)}{r} \qquad\qquad 6\text{-}18$$

$$\sigma^2(C) = \frac{P_0 \cdot \left[\sigma^2(S) + (1 - P_0) \cdot \mu^2(S)\right]}{(1+r)^2 - 1} \qquad\qquad 6\text{-}19$$

where P_0 is the present flood probability; the definitions of other symbols are the same as those in the previous equations.

In this situation, if the risk-aversion index is taken as 0, the results would be the basic outcomes of the economic optimisation under the present climate in a risk-neutral condition.

S2: The climate will change. Only uncertainty in the flood probability caused by climate change is included. The mean and standard deviation of the total cost were calculated as

$$\mu(C) = I_0 + I_1 \cdot X + \frac{\mu(P) \cdot \mu(S)}{r} \qquad\qquad 6\text{-}20$$

$$\sigma^2(C) = \frac{\mu(P) \cdot (1 - \mu(P)) \cdot \mu^2(S)}{(1+r)^2 - 1} \qquad\qquad 6\text{-}21$$

S3: The climate will change. Both uncertainties in damage and climate change are included. The mean of the total cost was calculated in the same way as in S2 (Equation 6-20), and the standard deviation was calculated as

$$\sigma^2(C) = \frac{\mu(P) \cdot \left[\sigma^2(S) + (1 - \mu(P)) \cdot \mu^2(S)\right]}{(1+r)^2 - 1} \qquad\qquad 6\text{-}22$$

The values of the parameters in above equations are shown in Table 6.2

Table 6.2 The values of the parameters used in the risk-averse economic optimisation

Variables	Values	Method and Reference
I_0	10 million RMB	Calculated based on Regulations of Budget Quotas and Unit Value of the Hydraulic Construction in Anhui Province, China.
I_x	11 million RMB	
$\mu(S)$	14.8 billion RMB	Estimated based on the economic assessment carried out by Xu and Chen (1999)
$\sigma(S)$	30%* $\mu(S)$	Recommended by Slijkhuis et al. (1997)
r	8%	Recommended in Economic Evaluation Methods and Parameters about Construction Project (the 3rd Version), Published by National Development and Reform Commission and Ministry of Construction of China

For all three situations, the uncertainty in the investment cost was not considered for simplicity. Because the flood probability is estimated as a function of the dike height, the added dike height is set as the decision variable. The objective function is to minimize $\mu(C)+k\cdot\sigma(C)$, where $\mu(C)$ and $\sigma(C)$ were respectively calculated by Equations 6-18 – 6-22 corresponding to each situation. The risk-aversion index, k, was respectively taken as 0, 0.5, 1 and 1.5 for each situation. The costs ($\mu(C)$, $\sigma(C)$ and $\mu(C)+k\cdot\sigma(C)$) at different added dike height is shown in Figure 6.6. Figure 6.7 is similar to Figure 6.6, but the horizontal axis is the return period corresponding to the added dike height. It is notable that for the same added dike height, the corresponding return period in the no-climate-change situation is different from that in the climate-change situation.
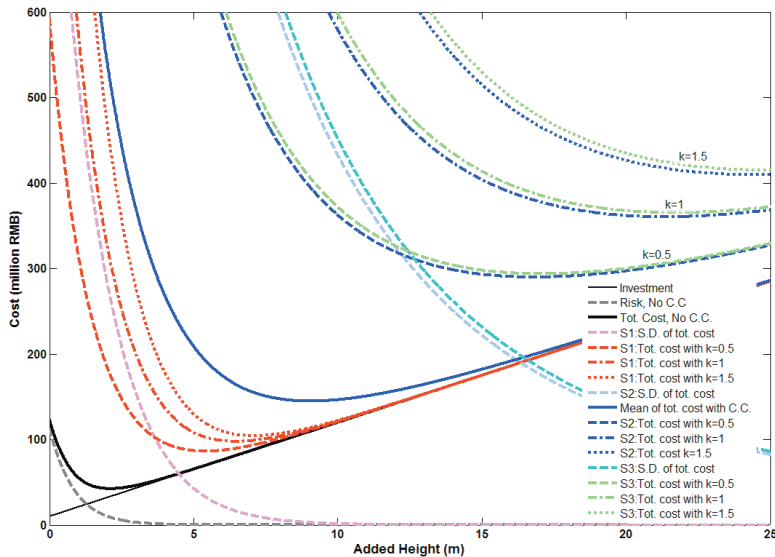
Figure 6.6 Costs V.S. Height for three situations with different risk-aversion indexes.

The black thin line and grey dashed curve show the investment and risk under the present climate, respectively. The black solid curve show the total cost under a no-climate-change situation. The total cost with varied risk-aversion indexes corresponding to situation S1, S2 and S3 are represented by red, blue and green curve clusters, respectively. The dashed curves that monotonously decrease with heights are standard deviation of total costs.
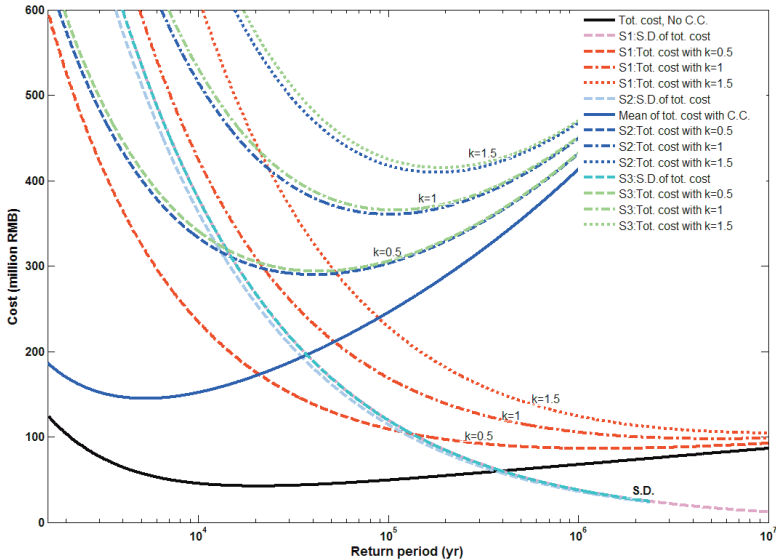
Figure 6.7 Costs V.S. Return period for three situations with different risk-aversion indexes. The legend is the same as in Figure 6.6

Generally speaking, the more uncertainties are included and the larger the risk-aversion index is, the more investment and the higher the dike should be to reach the economic optimum. The effect of the uncertainty in climate projections is much larger than that of the uncertainty in damage, which can be seen in Figure 6.6, the curves of S3 (both uncertainties are included) are close to the curves of S2 (the uncertainty caused by climate change is included), but deviate obviously from S1 (the uncertainty in damage is included).

It is also observed that the uncertainty in climate change causes an obvious increase in the standard deviation of the total costs, which leads to a higher optimal height. In terms of the safety level, the effect of climate change reduces the optimal return period (blue solid curve in Figure 6.7), which is due to the increase in the flood probability (as shown in Figure 6.5), while the effect of including the uncertainty in damage leads to an increased optimal safety level (red curves in Figure 6.7).

The optimal results of three situations are summarized in Table 6.3, in which the columns correspond to the risk-aversion index k from 0 to 1.5 with an interval of 0.5. The index value of 0 represents a risk-neutral condition when the optimisation is based only on mean values. The risk-aversion level increases with the value of k as more proportion of uncertainty (standard deviation) of total costs is included to determine a safer optimisation. S1 with k equals to 0 represents the optimum under the present climate without uncertainty in damage, which is the basic risk-neutral economic optimisation. It can be seen that when the risk-aversion index increases, its influence decreases. For instance, for S1, the optimal height increases by 3.3m when k increases from 0 to 0.5, but only by 0.62m when k increases from

1 to 1.5. There are similar results in terms of optimal total costs and safety level. The effect of climate change leads to wild results on optimal heightening and total cost: increase by 325% and 240%, respectively. Meanwhile, the optimal safety level is reduced dramatically from one in 20620 to one in 5263. However, if the decision maker is more risk averse (*k*=0.5), the optimal safety level is higher than the risk-neutral optimum under the present climatic conditions.

Table 6.3 The optimal results of three situations

Optimal added height (m)				
k	0	0.5	1	1.5
S1: U in Damage	2.13	5.42	6.48	7.1
S2: U in C.C.	9.06	16.83	21.35	24.55
S3: D &C.C.	9.06	17.07	21.67	24.91
Optimal total costs (million RMB)				
k	0	0.5	1	1.5
S1: U in Damage	42.4	86.3	97.7	104.3
S2: U in C.C.	144.8	289.8	360.4	409.4
S3: D &C.C.	144.8	293.7	365.3	415.0
Optimal safety level (1/yr)				
k	0	0.5	1	1.5
S1: U in Damage	20620	1.3E+06	5.3E+06	1.2E+07
S2: U in C.C.	5263	40000	100000	166667
S3: D &C.C.	5263	43478	111111	200000

6.5.3 The influence of the timing of climate change

The above analysis only considers the extreme timing pattern that the climate will change right after the construction of the flood wall, which may be criticised as unrealistic. In reality, climate change is a gradually evolving process. To analyse the influence of the timing of climate change, a pattern of gradual climate change and an extreme pattern of a sudden change in 2070 (as shown in Figure 6.8) are compared with the results of S2 in Section 6.5.2.

Pattern 1: The climate suddenly changes after heightening (2013). Discounting time horizon: 2014~very long

Pattern 2: The climate gradually changes until 2070 and stays stationary after 2070. Discounting time horizon is from 2014 to far future (2200). The flood probability during 2014~2069 is assumed to increase exponentially, which is given by:

$$P_i = P_0 \cdot e^{\gamma \cdot i} \qquad\qquad 6\text{-}23$$

$$\gamma = \frac{\ln \mu(P) - \ln P_0}{m} \qquad\qquad 6\text{-}24$$

where P_i is the flood probability in the year i, P_0 is the present flood probability, $\mu(P)$ is the future probability in 2070 and later, γ is the increasing rate of flood probability, and m is the number of years during 2014~2069.

Pattern 3: The climate stays stationary until the sudden change in 2070. Discounting time horizon: 2014~ very long
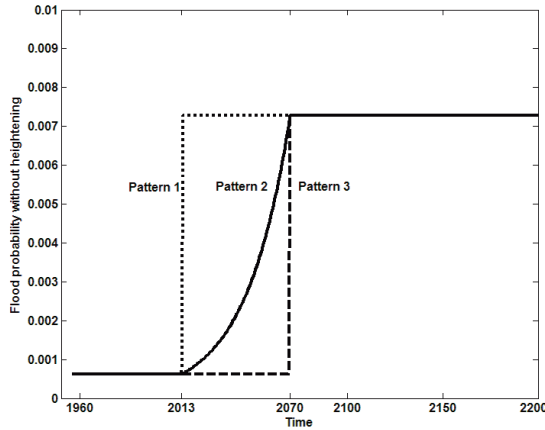
Figure 6.8 Flood probabilities over time without heightening the dike in three timing patterns

The case of Pattern 1 is equivalent to the situation S2 in Section 6.5.2, and the calculation is the same as presented above (Equation 6-20 - 6-21).

For the case of Pattern 2, the total cost consists of the investment of construction, the risk under the transient climate (2014-2069) and the risk under the changed climate (after 2070). The mean and standard deviation of total cost can be given by

$$
\begin{aligned}
\mu(C) &= E(I_{total}) + E(R_{before\,2070, Pattern2}) + E(R_{after\,2070}) \\
&= I_0 + I_1 \cdot X + S \cdot \sum_{i=1}^{56} P_i \cdot \left(\frac{1}{1+r}\right)^i + \mu(P) \cdot S \cdot \sum_{i=57}^{187} \left(\frac{1}{1+r}\right)^i
\end{aligned}
\qquad 6\text{-}25
$$

$$
\begin{aligned}
\sigma^2(C) &= Var(R_{before\,2070, Pattern2}) + Var(R_{after\,2070}) \\
&= S^2 \cdot \sum_{i=1}^{56} P_i \cdot (1-P_i) \cdot \left(\frac{1}{(1+r)^2}\right)^i + \mu(P) \cdot \left(1-\mu(P)\right) \cdot S^2 \cdot \sum_{i=57}^{186} \left(\frac{1}{(1+r)^2}\right)^i
\end{aligned}
\qquad 6\text{-}26
$$

For the case of Pattern 3, the total cost consists of the investment of construction, the risk under the present climate (2014-2069) and the risk under the changed climate (after 2070). The mean and standard deviation of the total cost can be given by:

$$\mu(C) = E(I_{total}) + E(R_{before2070,Pattern3}) + E(R_{after2070})$$

$$= I_0 + I_1 \cdot X + P_0 \cdot S \cdot \sum_{i=1}^{56}\left(\frac{1}{1+r}\right)^i + \mu(P) \cdot S \cdot \sum_{i=57}^{\infty}\left(\frac{1}{1+r}\right)^i$$

6-27

$$\sigma^2(C) = Var(R_{before2070,Pattern3}) + Var(R_{after2070})$$

$$= P_0 \cdot (1-P_0) \cdot S^2 \cdot \sum_{i=1}^{56}\left(\frac{1}{(1+r)^2}\right)^i + \mu(P) \cdot \left(1-\mu(P)\right) \cdot S^2 \cdot \sum_{i=57}^{\infty}\left(\frac{1}{(1+r)^2}\right)^i$$

6-28

where I_{total} is the investment cost, $R_{before2070}$ and $R_{after2070}$ are the risk under the present climate and under a changed climate, respectively.

The optimal risk-neutral results for the three timing patterns are summarized in Table 6.4. If the sudden change in climate occurs right after the construction of heightening (Pattern 1), more investment is required to reach the optimal safety standard. For the pattern of a gradually changing climate, the required investment of the heightening is much lower than for Pattern 1; the optimal safety level is lower as well. In Pattern 3 where climate will not change until 2070, the optimal dike heightening is further decreased and is close to the results for the no climate change case. However, the corresponding optimal safety level of Pattern 3 is dramatically lower than that of the present due to the increase in the flood probability after the sudden change in climate. It is notable that the expected predictive flood probability integrates the uncertainty in climate change projections, thus the future safety level is an inference into the future based on the available predictions at present. The real future flood probability could be lower or higher than the expected predictive level. Whether further heightening is needed in 2070 depends on the information obtained in the future.

Table 6.4 Optimal results of different climate patterns (risk neutral)

Pattern	Added Height (m)	Costs (million RMB)	Return period
No climate change	2.13	42.4	20620
Pattern1: Sudden change in 2013	9.06	144.8	5263
Pattern2: Gradual change until 2070	3.37	62.6	662
Pattern3: Sudden change in 2070	2.34	48.5	422

The optimal added dike height with risk aversion is shown in Table 6.5. The greater the risk-aversion, the higher the dike should be. The influence of the risk-aversion index decreases when its value increases.

Table 6.5 Optimal added height (m) with different risk-aversion indexes

Pattern	Risk- aversion index: k			
	0	0.5	1	1.5
No climate change	2.13	5.42	6.48	7.1
Pattern1: Sudden change in 2013	9.06	16.83	21.35	24.55
Pattern2: Gradual change until 2070	3.37	6.3	7.48	8.23
Pattern3: Sudden change in 2070	2.34	5.4	6.38	6.93

Figure 6.9 shows the flood probabilities with time corresponding to the optimal dike height with risk-aversion levels of 0, 0.5 and 1 for the gradual climate change pattern. The flood probability is lowered immediately after dike heightening for each risk-aversion level. With the change of climate, the flood probability gradually increases until the assumed stationary condition of climate in 2070. Following the assumption mentioned above, the flood probability in the transition period increase exponentially with a constant increasing rate.
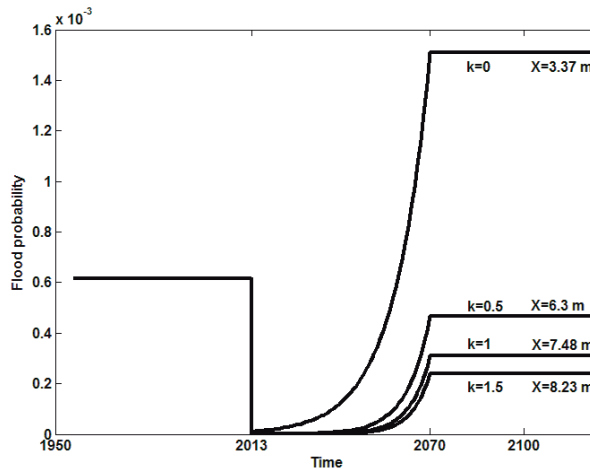
Figure 6.9 Flood probabilities over time with heightening the dike under Climate Change Pattern 2. The optimal dike heightening for each risk-aversion level is also shown

It can be seen that with no risk aversion, the optimal heightening leads to much higher flood probability in the future. If the risk-aversion index is taken as 0.5, the optimal safety level will be higher than the present safety level, even when climate change occurs. The difference in optimal safety levels gets smaller when risk-aversion index gets larger.

6.6   Discussion

In this chapter, the uncertainty in GCM projections was assumed to represent the uncertainty in future climate change. Actually, the variance in the projections of the future climate only represents the agreement of the climate models rather than the true uncertainty in climate change. There hasn't been a way to fully explain and accurately quantify the true uncertainty in future climate change. Using a GCM ensemble and quantifying its uncertainty helps better understand the uncertainty in climate change. The agreement of GCM projections represents the ability of climate models describing the real world. The more uncertainty in the projections, the less confidence can be had in climate models; thus, the more risk-aversion attitude should be held in the decision making in order to guarantee a safe flood defence.

In a risk-aversion economic optimisation, extra cost beyond the economic optimal cost is paid to reduce the uncertainty and to guarantee a safer flood defence. The extra money is quantified by the product of the standard deviation of total cost and the risk aversion index. The risk aversion index reflects the willingness of the decision makers to invest more in order to achieve a safer flood defence structure. A high value of the risk aversion index implies a high willingness to avoid the risk. This method may be criticized to be subjective and ambiguous in the selection of the risk-aversion index (Aven and Flage 2009). However, it is a way to turn it into a quantifiable index when a "subjective" attitude has to be incorporated. The selection of the risk aversion index value is dependent on the choice of the decision maker and the specific application. As shown in Figure 6.9 an increasing risk-aversion level does not always leads to significant improvement of safety. It is recommended to the decision makers that an appropriate risk aversion index would be the value that most effectively improves the safety.

The decision problem here is: what is the economic-optimal precautionary adaptation to climate change by the way of dike heightening. The practical difficulty in making adaptations is the timing of the action, because we cannot know the exact timing of change in climate and the resulting change in river flows. Whether a precautionary adaptation is necessary to be made now in order to cope with the impacts in the future is a question to be answered. It can be seen from Table 6.4 that there is a large variability in the required investments of dike heightening for different timing patterns of climate change. If an adaptation to cope with the anticipating climate change in the near future is made while the climate actually changes in a far future, the cost of "unnecessary" dike heightening would be up to 84 million RMB (Patten 1 vs. Patten 3). Thus it might be wiser to adopt an alternative "wait and see" adaptation strategy if the climate will change in an unknown future. In this strategy, one could wait for a couple of decades to see if there are changes in the statistics of river flows and the influence factors such as rainfall. The preference between "take action now" and "wait and see" depends on the costs of these options. If the calculated optimal dike heightening requires more total costs than the cost of risk for doing nothing, it would be economically optimal to stick to the present safety level and wait until more information is available. Assuming the present-climate-status optimal dike heightening has been achieved, the remaining flood risk is around 9 million RMB. The initial investment cost to make an adaptation is 10 million RMB, which is even more than the remaining flood risk. If the climate will change in a very far future, the optimal precautionary adaptation would require more total costs than the risk of sticking to the present-status optimal safety level due to the relatively high initial investment cost. Thus, the "wait and see" strategy may be better than the "take action now" strategy from an economic point of view if the climate will change in the far future.

The drastic increase in the future river stage can be physically explained by the projected increase in rainfall amount and the changes in the spatial and temporal distribution of rainfall. The reality of the calculated river stage is thus dependent on the reality of the projected rainfall by the GCMs. Additional uncertainty could arise from extrapolating the

empirical relationships used in deriving the stage-probability relationship. The physical based methods are recommended to be used instead of the empirical relationships in order to reduce the extrapolation uncertainty.

It is notable that the resulted dike heightening of 9m-24m for a sudden climate change is enormous and beyond physical reality. This is understandable as this results was obtained based on an extreme hypothesis that the climate will change very soon and the flood wall is robust to resist the future water load. The expected predictive flood probability is an inference of the future flood probability based on the present available information, which integrates the uncertainty in climate projections. It is rather an indication of the uncertainty in climate projections than an actual future flood probability. Using the expected predictive flood probability in an extreme situation with a sudden climate change helps us understand what the cost is when taking action right now in order to cope with the deep uncertainty in climate change based on the available information. Apart from the extrapolation uncertainty mentioned in the last paragraph, the cheap adaptation considered in this study also partly accounts for these great values. Since the adaptation analysed here is aimed at taking a precautionary action, a cheap measure of constructing a flood wall is assumed rather than a heightening of the whole dike, which requires more initial and variant investment. If a permanent heightening is considered in the analysis, the optimal dike heightening would be lowered to some degree.

Theoretically, a lower discount rate leads to a higher optimal dike height. The value of the discount rate r was assumed to be constant in this study. As a long-term time period is considered in this thesis, the uncertainty associated with the economic growth may be as large as the uncertainty related to climate change. The uncertainty related to the discount rate can also be modelled by a normal distribution. An example can be seen in the study of Slijkhuis et al. (1997) who compared the use of a normally distributed discount rate (with a variation coefficient of 10%) with the case of a fixed discount rate when estimating the total costs of optimal dike heightening and the corresponding damage over a 100-year horizon using Monte-Carlo simulation. Their analysis showed that the use of a normally distributed discount rate leads to comparable result from the use of a constant discount rate.

Chapter 7 Conclusions and recommendations

7.1 Conclusions

A framework of analysing the uncertainty in assessing climate change impacts on river floods has been presented in this thesis. To take account of this uncertainty, a decision-making method of adapting river dikes to climate change has been proposed based on the risk-averse economic optimization. The Huai River Basin in China was selected as a case study to implement the uncertainty analysis framework, and a city dike ring located along the midstream of the Huai River was selected to test the proposed decision-making method. The framework of uncertainty analysis and the proposed method of risk-reverse economic optimization could also be applied to other river basins and flood defenses.

7.1.1 Future climate projections

According to the GCM ensemble from the CMIP5 data set, the future temperature over the study area is suggested to increase by 4^oC to 8^oC at the end of this century under the high emission scenario without mitigation measures. The standard deviation of precipitation intensity is also suggested to increase especially in summer, which may lead to floods of a

larger magnitude in the future. The GCMs have a better agreement in reproducing the present-day temperature. However, large variation was found in the simulation of precipitation, which emphasizes the importance of bias-correcting and downscaling the climate model outputs. The variability among the climate model outputs can be attributed among other factors to the physics used by the models and the model resolution. Higher resolution does not grant better model performances. The use of multi-GCM ensembles is necessary to take account of the uncertainty in the future climate change projections.

7.1.2 Uncertainty in downscaling methods

Chapter 3 was under taken with the overarching aim of assessing the uncertainty in the empirical statistical methods for downscaling daily GCM outputs and providing the basis for using these downscaling methods in climate change impact assessments. Empirical statistical downscaling methods were classified based on calibration strategies (bias correction and change factor) and statistical transformations (mean based, variance based, quantile mapping, quantile correcting and transfer function methods). The performances of ten downscaling methods resulting from the combinations of calibration strategies and transformation methods were assessed using a 16-GCM ensemble over the Huai River basin in China.

The approach of inter-model cross validation was employed to measure the skill of the downscaling methods in a pseudo-observed climate. The results show that the change factor based methods outperform the bias correction based methods in projecting the probability distribution of downscaled daily temperature. In downscaling daily precipitation, the choice of the transformation methods dominates total uncertainty compared to the choice of the calibration strategies. When implementing the change factor calibration strategy, simply adding (for temperature) or multiplying (for precipitation) the mean change factor is sufficient to represent the relative changes projected by GCMs. More sophisticated bias correction based methods are needed to remove the biases in the higher-order statistics of the raw GCM outputs. Non-parametric transformation methods perform better than the simple parametric methods used in this study.

The two calibration strategies lead to fundamentally different temporal structures and spatial variability in the downscaled future climatic variables. The bias correction based methods produced larger uncertainty bounds of inter-annual variability than the change factor methods. The bias correction based methods also resulted in relatively more uncertainty than the change factor based methods with regards to the probability distributions of the downscaled variables. The downscaling method uncertainty was comparable to the GCM uncertainty for downscaled precipitation. More uncertainty was introduced by the calibration strategies than the statistical transformation methods.

7.1.3 Hydrological modelling in the context of climate change

Chapter 4 assessed the uncertainties associated with the parameter calibration of the lumped Xinanjiang hydrological model when assessing the climate change impacts on river flow of a large basin in China. The transferability of model parameters was tested in the context of historical climate variability using the differential split-sample test. The uncertainties in projected future river flow stemming from the choice of calibration period and parameter equifinality were compared.

The transferability of the parameters calibrated from a wet period to a dry period was poorer than the other way around. The model error increased with the increase of the difference in rainfall between the calibration and validation periods. The variability in the simulation due to equifinality also increased with the rainfall difference. The annual maximum 30 day discharge may be overestimated when the parameters were transferred to a period that is wetter than the calibration period.

When projecting future streamflow, the uncertainty due to the choice of calibration periods is not negligible in the assessments where the mean hydrological condition is analysed. The uncertainty stemming from the equifinal parameter sets should be considered when the assessment is focused on the extreme floods. When forcing the hydrological model with a future climate that is much wetter than the calibration period, unrealistic extreme discharge may be generated. It is recommended to calibrate the hydrological model over the period with similar climatic conditions compared to the future climate. The results presented are dependent on the hydrological mode used and the climatic and geographic properties of the basin. The uncertainty evaluation of the performance of the hydrological models should routinely be carried out on a case by case basis.

7.1.4 The overall uncertainty assessment and the reflections

In Chapter 5, an uncertainty assessment was carried out by comparing the contribution of each component in the modelling framework. Five sources of uncertainty were analysed, i.e. GCM structure, greenhouse gas emission scenario, downscaling method, the choice of period for calibrating hydrological model, and the equifinality effect of hydrological parameters. The results show that the future flood magnitude is expected to increase not only due to the increase in mean precipitation but also due to the increase in the variation of precipitation. Nonetheless, there is still a small likelihood that the flood quantiles with a high return period (above 20 years) will decrease in the future. The uncertainty comparison suggests the following order of component significance (greatest to least): GCM > emission scenario > (empirical) downscaling method > hydrological modelling (choice of calibration period and equifinality.

Since the models used in impact assessments are not able to perfectly simulate the real world, it has been generally recommended to use multiple methods or models for each

component of the modelling framework and to analyse the associated uncertainties. Chapters 2-5 in this thesis gave an example of the uncertainty assessment framework which consists of the analysis on the uncertainty associated with each component and the assessment of the overall uncertainty. The aim is not to reduce uncertainty but to gain knowledge by exploring uncertainty, and uncertainty need to be identified from errors. Implementing the proposed uncertainty assessment framework will help obtain reliable impact assessments by employing appropriate approaches with computational efficiency. Specifically, the preliminary analysis on the GCM ensemble helps better analyse the physical reasons underlying the hydrological responses to climate change; the inter-model cross validation approach can be used to measure the performances of the downscaling methods, based on which, the underperforming downscaling methods should be discarded; the differential split-sampling method helps assess the transferability of hydrological models to differing climatic conditions based on the available historical records; the relative contributions of different sources of uncertainty can be recognised by the analysis of variance and the key uncertainties should be focused on in the following impact assessment.

Detailed reflections can also be drawn from the application of the uncertainty assessment framework in the case study. Multiple GCMs and multiple emission scenarios have to be employed to describe the plausible change of the climate. For the empirical downscaling methods, the choice of calibration strategies should be considered as a source of uncertainty in addition to other uncertainties in impact assessments especially where the change in the temporal sequence of climate variables is a key factor. The simplest mean-based change factor (the so-called delta change method) can be used in preliminary impact assessments, especially those requiring multiple projections of GCMs and scenarios, due to its ease of use and more or less similar performance compared to more sophisticated methods. For the hydrological modelling, the parameter uncertainty has less influence on the impact assessments compared to the uncertainties associated with GCMs and emission scenarios. However, the additional uncertainty arising from transferring the model to a future climate that is much different from the present climate should gain more attentions.

7.1.5 Adaptation to climate change under uncertainty

A risk-averse economic optimization method for river dike adaptation to climate change was proposed in this thesis. This method provides a way of coping with climate change uncertainty in economic optimization by adjusting the level of risk-aversion attitude. A case study of the Old Dike Ring in Bengbu was carried out by using the proposed method. The conclusions are drawn as follows:

The proposed approach enables decision makers to make trade-offs between the confidence in the climate projections and the risk-aversion attitude. Introducing the risk-aversion attitude in the adaptation of river dikes can help cope with the uncertainty in climate change and reach a safer decision, but simply increasing the level of risk-aversion does not always

lead to a significant improvement of safety. As can be seen in the timing pattern of gradual climate change, the efficiency of the influence of the risk-aversion index on optimisation decreases when its value increases.

The uncertainty related to climate change increases the optimal dike height and decreases the optimal safety level in case of risk aversion. The uncertainty introduced by climate change has a much more significant influence on the optimal decision than an uncertainty in damage assumed as 30%. The uncertainty in damage was not further analysed in this thesis. It is likely that this uncertainty could be much larger especially in the long term due to the land use change and the economic development.

Timing of climate change is also an influential factor in adaptation decision makings. The sooner climate change is expected, the more uncertainty in the flood probability caused by climate change is taken into account in the economic optimisation. The practical questions in adaptation decision making is when and to what extent should the dikes be strengthened, considering the uncertainty in climate change impacts. The results of the case study suggest that taking the "wait and see" strategy is more economic optimal than a precautionary adaptation taken right now.

A flood wall with the height of 8 m or more is enormous and unfeasible in reality. This implies that simply building a flood wall as a precautionary adaptive measure cannot sufficiently reduce the impacts of climate change in a near future, and the integrated adaptation including regulating reservoirs, using water retention areas and secondary levees should be carried out.

Even though this study is focused on a "hard" measure of river dike heightening, the proposed methods could be used in guiding adaptation decisions for other sectors implementing both engineering and non-engineering measures.

7.2 Recommendations

Some parts of this thesis can be improved for the future work, and on the basis of this thesis several recommendations are made below:

- Even though empirical statistical downscaling methods are computationally efficient and easy to implement, further research is required to overcome their limitations. For example, these downscaling methods do not address the reproduction of the inter-annual variability of the climatic variables. Similarly, the difference in the temporal sequence resulting from the choice of calibration strategies requires more attention in impact assessments especially in those where the temporal structure of climatic variables is a critical issue, e.g. design storm estimation and crop yield prediction. The lack of spatial variability in the bias correction based methods is another issue that warrants attention in future studies.

- Dynamical downscaling methods and more sophisticated statistical downscaling methods were not used in the analysis due to their high computational cost. Including more downscaling methods would lead to more robust results. For instance, using a stochastic weather generator to generate time series of future precipitation could provide information on future climate variability.

- The hydrological model structure is also an important source of uncertainty in impact assessments. Only one lumped hydrological model structure was used in this thesis. It is recommended to include model structures with different assumptions in order to explore the uncertainty envelope. Moreover, uncertainty could also arise from the configuration of models, e.g., lumped vs distributed. With consideration of the simulative ability of climate models, the appropriate model configuration should be investigated on a case by case basis.

- The commonly used linear relationship between cost and dike height has been used to estimate the investment cost of dike construction. The underlying assumption of this linear approximation is that the added height X is considered to be relatively small. If a larger change in height is required, the assumed linear approximation may no longer be valid due to the required broader base of the dike associated with the higher height. In practical decision problems under a stationary climate, the linear approximation is able to fulfil the requirement of the analysis. However, in the decision problem under a changed climate, the large uncertainty in future flood probability increases the risk, which leads to an increasing range of the possible value of X. The use of a linear function tends to underestimate the dike costs, which explains the high optimal dike height found in this thesis. If a more realistic function is used, the optimal dike height may be lower.

- Here, only the failure mechanism of overflowing was taken into account and a linear relationship between damage and river stage was assumed. Damage estimation based on inundation modelling is recommended to be used. Climate change could impact on the future flood hydrographs which may complicate the estimation of damage. The scenarios of possible flood hydrographs suggested by GCM ensembles are recommended to be used as boundary conditions for the inundation models. In addition, economic growth also plays an important role in the damage estimation. It is thus recommended that varied economic growth rates should be used in correspondence with the greenhouse gas emission scenarios.

References

Alcamo, J., A. Bouman, J. Edmonds, A. Grübler, T. Morita and A. Sugandhy (1995). "An evaluation of the IPCC IS92 emission scenarios." RESEARCH REPORT-INTERNATIONAL INSTITUTE FOR APPLIED SYSTEMS ANALYSIS IIASA RR.

Arnell, N. W., M. J. L. Livermore, S. Kovats, P. E. Levy, R. Nicholls, M. L. Parry and S. R. Gaffin (2004). "Climate and socio-economic scenarios for global-scale climate change impacts assessments: characterising the SRES storylines." Global Environmental Change 14(1): 3-20.

Aven, T. and R. Flage (2009). "Use of decision criteria based on expected values to support decision-making in a production assurance and safety setting." Reliability Engineering & System Safety 94(9): 1491-1498.

Bae, D.-H., I.-W. Jung and D. P. Lettenmaier (2011). "Hydrologic uncertainties in climate change from IPCC AR4 GCM simulations of the Chungju Basin, Korea." Journal of Hydrology 401(1-2): 90-105.

Bastola, S. (2013). "Hydrologic impacts of future climate change on Southeast US watersheds." Regional Environmental Change.

Bastola, S., C. Murphy and J. Sweeney (2011). "Evaluation of the transferability of hydrological model parameters for simulations under changed climatic conditions." Hydrol. Earth Syst. Sci. Discuss. 8(3): 5891-5915.

Bastola, S., C. Murphy and J. Sweeney (2011). "The role of hydrological modelling uncertainties in climate change impact assessments of Irish river catchments." Advances in Water Resources 34(5): 562-576.

Bastola, S., C. Murphy and J. Sweeney (2011). "The sensitivity of fluvial flood risk in Irish catchments to the range of IPCC AR4 climate change scenarios." Science of the Total Environment 409(24): 5403-5415.

Bell, V. A., A. L. Kay, R. G. Jones and R. J. Moore (2007). "Development of a high resolution grid-based river flow model for use with regional climate model output." Hydrol. Earth Syst. Sci. 11(1): 532-549.

Bell, V. A., A. L. Kay, R. G. Jones and R. J. Moore (2007). "Use of a grid-based hydrological model and regional climate model outputs to assess changing flood risk." International Journal of Climatology 27(12): 1657-1671.

Beven, K. and A. Binley (1992). "The future of distributed models: model calibration and uncertainty prediction." Hydrological processes 6(3): 279-298.

Beven, K. and J. Freer (2001). "Equifinality, data assimilation, and uncertainty estimation in mechanistic modelling of complex environmental systems using the GLUE methodology." Journal of hydrology 249(1): 11-29.

Blaney, H. and W. Criddle (1950). Determining water requirements in irrigated area from climatological irrigafon dat. Soil Conservation Service, Tech, US Department of Agriculture: 96:48.

Boé, J., L. Terray, F. Habets and E. Martin (2007). "Statistical and dynamical downscaling of the Seine basin climate for hydro-meteorological studies." International Journal of Climatology **27**(12): 1643-1655.

Booij, M. J. (2005). "Impact of climate change on river flooding assessed with different spatial model resolutions." Journal of Hydrology **303**(1-4): 176-198.

Bouwer, L. and J. Aerts (2004). "Coterlet van de GM, Giesen van de N, Gieske A, Mannaerts C.(2004), Evaluating Downscaling Methods for preparing Global Circulation Model (GCM) Data for Hydrological Impact Modelling." Aerts JCJH, Droogers P (eds).

Brath, A., A. Castellarin and A. Montanari (2002). "Assessing the effects of land-use changes on annual average gross erosion." Hydrology and Earth System Sciences Discussions **6**(2): 255-265.

Brath, A., A. Montanari and G. Moretti (2006). "Assessing the effect on flood frequency of land use change via hydrological simulation (with uncertainty)." Journal of Hydrology **324**(1-4): 141-153.

Brigode, P., L. Oudin and C. Perrin (2013). "Hydrological model parameter instability: A source of additional uncertainty in estimating the hydrological impacts of climate change?" Journal of Hydrology **476**: 410-425.

Bultot, F., G. L. Dupriez and D. Gellens (1990). "Simulation of land use changes and impacts on the water balance — A case study for Belgium." Journal of Hydrology **114**(3–4): 327-348.

Cameron, D., K. Beven and P. Naden (1999). "Flood frequency estimation by continuous simulation under climate change (with uncertainty)." Hydrology and earth system sciences **4**(3): 393-405.

Carter, T. R., R. N. Jones, X. Lu, S. Bhadwal, C. Conde, L. O. Mearns, B. O'neill, M. D. Rounsevell and M. B. Zurek (2007). "New assessment methods and the characterisation of future conditions."

Chen, J., F. P. Brissette, D. Chaumont and M. Braun (2013). "Performance and uncertainty evaluation of empirical downscaling methods in quantifying the climate change impacts on hydrology over two North American river basins." Journal of Hydrology **479**: 200-214.

Chen, J., F. P. Brissette and R. Leconte (2011). "Uncertainty of downscaling method in quantifying the impact of climate change on hydrology." Journal of Hydrology **401**(3-4): 190-202.

Chen, J., F. P. Brissette, A. Poulin and R. Leconte (2011). "Overall uncertainty study of the hydrological impacts of climate change for a Canadian watershed." Water Resources Research **47**(12): W12509.

Chiew, F. H. S., J. Teng, J. Vaze, D. A. Post, J. M. Perraud, D. G. C. Kirono and N. R. Viney (2009). "Estimating climate change impact on runoff across southeast Australia: Method, results, and implications of the modeling method." Water Resources Research **45**(10): W10414.

Coron, L., V. Andréassian, C. Perrin, J. Lerat, J. Vaze, M. Bourqui and F. Hendrickx (2012). "Crash testing hydrological models in contrasted climate conditions: An experiment on 216 Australian catchments." Water Resources Research **48**(5): n/a-n/a.

Das, T., A. Bárdossy, E. Zehe and Y. He (2008). "Comparison of conceptual model performance using different representations of spatial variability." Journal of Hydrology **356**(1-2): 106-118.

Das, T., M. Dettinger, D. Cayan and H. Hidalgo (2011). "Potential increase in floods in California's Sierra Nevada under future climate projections." Climatic Change **109**(1): 71-94.

Deque, M. (2007). "Frequency of precipitation and temperature extremes over France in an anthropogenic scenario: Model results and statistical correction according to observed values." Global and Planetary Change **57**(1-2): 16-26.

Déqué, M., S. Somot, E. Sanchez-Gomez, C. M. Goodess, D. Jacob, G. Lenderink and O. B. Christensen (2011). "The spread amongst ENSEMBLES regional scenarios: regional climate models, driving general circulation models and interannual variability." Climate Dynamics **38**(5-6): 951-964.

Dessai, S. and M. Hulme (2004). "Does climate adaptation policy need probabilities?" Climate Policy **4**(2): 107-128.

Dessai, S. and M. Hulme (2007). "Assessing the robustness of adaptation decisions to climate change uncertainties: A case study on water resources management in the East of England." Global Environmental Change **17**(1): 59-72.

Diaz-Nieto, J. and R. L. Wilby (2005). "A comparison of statistical downscaling and climate change factor methods: impacts on low flows in the River Thames, United Kingdom." Climatic Change **69**(2-3): 245-268.

Dosio, A. and P. Paruolo (2011). "Bias correction of the ENSEMBLES high-resolution climate change projections for use by impact models: Evaluation on the present climate." Journal of Geophysical Research: Atmospheres **116**(D16): D16106.

Finger, D., G. Heinrich, A. Gobiet and A. Bauder (2012). "Projections of future water resources and their uncertainty in a glacierized catchment in the Swiss Alps and the subsequent effects on hydropower production during the 21st century." Water Resources Research **48**(2): n/a-n/a.

Fowler, H. J., S. Blenkinsop and C. Tebaldi (2007). "Linking climate change modelling to impacts studies: recent advances in downscaling techniques for hydrological modelling." International Journal of Climatology **27**(12): 1547-1578.

Gudmundsson, L., J. B. Bremnes, J. E. Haugen and T. Engen-Skaugen (2012). "Technical Note: Downscaling RCM precipitation to the station scale using statistical transformations – a comparison of methods." Hydrology and Earth System Sciences **16**(9): 3383-3390.

Gutjahr, O. and G. Heinemann (2013). "Comparing precipitation bias correction methods for high-resolution regional climate simulations using COSMO-CLM." Theoretical and Applied Climatology.

Hawkins, E., T. M. Osborne, C. K. Ho and A. J. Challinor (2013). "Calibration and bias correction of climate projections for crop modelling: An idealised case study over Europe." Agricultural and Forest Meteorology **170**: 19-31.

Haylock, M. R., G. C. Cawley, C. Harpham, R. L. Wilby and C. M. Goodess (2006). "Downscaling heavy precipitation over the United Kingdom: a comparison of dynamical and statistical methods and their future scenarios." International Journal of Climatology **26**(10): 1397-1415.

Hemer, M., K. McInnes and R. Ranasinghe (2012). "Climate and variability bias adjustment of climate model-derived winds for a southeast Australian dynamical wave model." Ocean Dynamics **62**(1): 87-104.

Ho, C. K., D. B. Stephenson, M. Collins, C. A. T. Ferro and S. J. Brown (2012). "Calibration Strategies: A Source of Additional Uncertainty in Climate Change Projections." Bulletin of the American Meteorological Society **93**(1): 21-26.

Hollis, G. (1975). "The effect of urbanization on floods of different recurrence interval." Water Resources Research **11**(3): 431-435.

Houghton, J. T., B. A. Callander and S. K. Varney (1992). Climate change 1992: the supplementary report to the IPCC scientific assessment, Cambridge University Press.

Hu, W. (2012). "The Influence of Bengbu Sluice and Upstream Dams and sluices on the Natural Hydrologic Regimes of the Huaihe River (in Chinese) 蚌埠闸及上游闸坝对淮河自然水文情势的影响." SCIENTIA GEOGRAPHICA SINICA **32**(8): 1013-1019.

Hurkmans, R. T. W. L., W. Terink, R. Uijlenhoet, E. J. Moors, P. A. Troch and P. H. Verburg (2009). "Effects of land use changes on streamflow generation in the Rhine basin." Water Resources Research **45**(6): n/a-n/a.

Ines, A. V. M. and J. W. Hansen (2006). "Bias correction of daily GCM rainfall for crop simulation studies." Agricultural and Forest Meteorology **138**(1-4): 44-53.

IPCC (2001). Climate change 2001: impacts, adaptation, and vulnerability: contribution of Working Group II to the third assessment report of the Intergovernmental Panel on Climate Change, Cambridge University Press.

Jarosch, A. H., F. S. Anslow and G. K. Clarke (2012). "High-resolution precipitation and temperature downscaling for glacier models." Climate dynamics **38**(1-2): 391-409.

Jiang, T., Y. D. Chen, C.-y. Xu, X. Chen, X. Chen and V. P. Singh (2007). "Comparison of hydrological impacts of climate change simulated by six hydrological models in the Dongjiang Basin, South China." Journal of Hydrology **336**(3-4): 316-333.

Jonkman, S. N., P. H. A. J. M. van Gelder and J. K. Vrijling (2003). "An overview of quantitative risk measures for loss of life and economic damage." Journal of Hazardous Materials **99**(1): 1-30.

Jung, I.-W., H. Moradkhani and H. Chang (2012). "Uncertainty assessment of climate change impacts for hydrologically distinct river basins." Journal of Hydrology **466-467**: 73-87.

Kay, A., H. Davies, V. Bell and R. Jones (2009). "Comparison of uncertainty sources for climate change impacts: flood frequency in England." Climatic Change **92**(1-2): 41-63.

Kidson, J. W. and C. S. Thompson (1998). "A comparison of statistical and model-based downscaling techniques for estimating local climate variations." Journal of Climate **11**(4).

Kingston, D. G., J. R. Thompson and G. Kite (2011). "Uncertainty in climate change projections of discharge for the Mekong River Basin." Hydrology and Earth System Sciences **15**(5): 1459-1471.

Klemeš, V. (1986). "Operational testing of hydrological simulation models." Hydrological Sciences Journal **31**(1): 13-24.

Krause, P., D. P. Boyle and F. Bäse (2005). "Comparison of different efficiency criteria for hydrological model assessment." Adv. Geosci. **5**: 89-97.

Kuijper, B. and M. Kallen (2010). "The impact of risk aversion on optimal economic decisions."

Kuijper, B. and M. Kallen (2012). "Uncertainty in optimal decisions for dike maintenance." Structure and Infrastructure Engineering **8**(4): 317-327.

Kundzewicz, Z., Y. Hirabayashi and S. Kanae (2010). "River Floods in the Changing Climate— Observations and Projections." Water Resources Management **24**(11): 2633-2646.

Lambert, S. J. and G. J. Boer (2001). "CMIP1 evaluation and intercomparison of coupled climate models." Climate Dynamics **17**(2-3): 83-106.

Lauer, A. and K. Hamilton (2012). "Simulating Clouds with Global Climate Models: A Comparison of CMIP5 Results with CMIP3 and Satellite Data." Journal of Climate **26**(11): 3823-3845.

Leander, R. and T. A. Buishand (2007). "Resampling of regional climate model output for the simulation of extreme river flows." Journal of Hydrology **332**(3–4): 487-496.

Leander, R., T. A. Buishand, B. J. van den Hurk and M. J. de Wit (2008). "Estimated changes in flood quantiles of the river Meuse from resampling of regional climate model output." Journal of Hydrology **351**(3): 331-343.

Leggett, J., W. J. Pepper, R. J. Swart, J. Edmonds, L. Meira Filho, I. Mintzer and M. Wang (1992). "Emissions scenarios for the IPCC: an update." Climate change: 71-95.

Lempert, R. J. and D. G. Groves (2010). "Identifying and evaluating robust adaptive policy responses to climate change for water management agencies in the American west." Technological Forecasting and Social Change **77**(6): 960-974.

Lenderink, G., A. Buishand and W. v. Deursen (2007). "Estimates of future discharges of the river Rhine using two scenario methodologies: direct versus delta approach." Hydrology and Earth System Sciences **11**(3): 1145-1159.

Li, C. Z., L. Zhang, H. Wang, Y. Q. Zhang, F. L. Yu and D. H. Yan (2012). "The transferability of hydrological models under nonstationary climatic conditions." Hydrol. Earth Syst. Sci. **16**(4): 1239-1254.

Li, H., J. Sheffield and E. F. Wood (2010). "Bias correction of monthly precipitation and temperature fields from Intergovernmental Panel on Climate Change AR4 models using equidistant quantile matching." Journal of Geophysical Research **115**(D10).

Li, J. L. F., D. E. Waliser, W. T. Chen, B. Guan, T. Kubar, G. Stephens, H. Y. Ma, M. Deng, L. Donner, C. Seman and L. Horowitz (2012). "An observationally based evaluation of cloud ice water in CMIP3 and CMIP5 GCMs and contemporary reanalyses using contemporary satellite data." Journal of Geophysical Research: Atmospheres **117**(D16): D16105.

Lopez, A., F. Fung, M. New, G. Watts, A. Weston and R. L. Wilby (2009). "From climate model ensembles to climate change impacts and adaptation: A case study of water resource management in the southwest of England." Water Resources Research **45**(8): n/a-n/a.

Maraun, D. (2013). "Bias Correction, Quantile Mapping, and Downscaling: Revisiting the Inflation Issue." Journal of Climate **26**(6): 2137-2143.

Masson, D. and R. Knutti (2011). "Spatial-Scale Dependence of Climate Model Performance in the CMIP3 Ensemble." Journal of Climate **24**(11): 2680-2692.

Maurer, E. and H. Hidalgo (2008). "Utility of daily vs. monthly large-scale climate data: an intercomparison of two statistical downscaling methods." Hydrology and Earth System Sciences **12**(2): 551-563.

Maurer, E. P. (2007). "Uncertainty in hydrologic impacts of climate change in the Sierra Nevada, California, under two emissions scenarios." Climatic Change **82**(3-4): 309-325.

Mearns, L., I. Bogardi, F. Giorgi, I. Matyasovszky and M. Palecki (1999). "Comparison of climate change scenarios generated from regional climate model experiments and statistical downscaling." Journal of Geophysical Research: Atmospheres (1984–2012) **104**(D6): 6603-6621.

Merz, R., J. Parajka and G. Blöschl (2011). "Time stability of catchment model parameters: Implications for climate impact analyses." Water Resources Research **47**(2): n/a-n/a.

Middelkoop, H., K. Daamen, D. Gellens, W. Grabs, J. C. J. Kwadijk, H. Lang, B. W. A. H. Parmet, B. Schädler, J. Schulla and K. Wilke (2001). "Impact of Climate Change on Hydrological Regimes and Water Resources Management in the Rhine Basin." Climatic Change **49**(1-2): 105-128.

Milly, P. C. D., R. T. Wetherald, K. A. Dunne and T. L. Delworth (2002). "Increasing risk of great floods in a changing climate." Nature **415**(6871): 514-517.

Monirul Qader Mirza, M. (2002). "Global warming and changes in the probability of occurrence of floods in Bangladesh and implications." Global Environmental Change **12**(2): 127-138.

Montanari, A. (2007). "What do we mean by 'uncertainty'? The need for a consistent wording about uncertainty assessment in hydrology." Hydrological Processes **21**(6): 841-845.

Moriasi, D., J. Arnold, M. Van Liew, R. Bingner, R. Harmel and T. Veith (2007). "Model evaluation guidelines for systematic quantification of accuracy in watershed simulations." Trans. ASABE **50**(3): 885-900.

Moss, R. H., J. A. Edmonds, K. A. Hibbard, M. R. Manning, S. K. Rose, D. P. van Vuuren, T. R. Carter, S. Emori, M. Kainuma, T. Kram, G. A. Meehl, J. F. Mitchell, N. Nakicenovic, K. Riahi, S. J. Smith, R. J. Stouffer, A. M. Thomson, J. P. Weyant and T. J. Wilbanks (2010). "The next generation of scenarios for climate change research and assessment." Nature **463**(7282): 747-756.

Mpelasoka, F. S. and F. H. S. Chiew (2009). "Influence of Rainfall Scenario Construction Methods on Runoff Projections." Journal of Hydrometeorology **10**(5): 1168-1183.

Murphy, J. (1999). "An evaluation of statistical and dynamical techniques for downscaling local climate." Journal of Climate **12**(8).

Murphy, J. (2000). "Predictions of climate change over Europe using statistical and dynamical downscaling techniques." International Journal of Climatology **20**(5): 489-501.

Murphy, J. M., D. M. Sexton, D. N. Barnett, G. S. Jones, M. J. Webb, M. Collins and D. A. Stainforth (2004). "Quantification of modelling uncertainties in a large ensemble of climate change simulations." Nature **430**(7001): 768-772.

Naef, F., S. Scherrer and M. Weiler (2002). "A process based assessment of the potential to reduce flood runoff by land use change." Journal of Hydrology **267**(1): 74-79.

Najafi, M. R., H. Moradkhani and I. W. Jung (2011). "Assessing the uncertainties of hydrologic model selection in climate change impact studies." Hydrological Processes **25**(18): 2814-2826.

Nakicenovic, N., J. Alcamo, G. Davis, B. De Vries, J. Fenhann, S. Gaffin, K. Gregory, A. Griibler, T. Y. Jung and T. Kram (2000). "Emissions scenarios."

Nakicenovic, N., J. Alcamo, G. Davis, B. de Vries, J. Fenhann, S. Gaffin, K. Gregory, A. Grubler, T. Y. Jung and T. Kram (2000). Special report on emissions scenarios: a special report of Working Group III of the Intergovernmental Panel on Climate Change, Pacific Northwest National Laboratory, Richland, WA (US), Environmental Molecular Sciences Laboratory (US).

New, M., A. Lopez, S. Dessai and R. Wilby (2007). "Challenges in using probabilistic climate change information for impact assessments: an example from the water sector." Philos Trans A Math Phys Eng Sci **365**(1857): 2117-2131.

Panofsky, H. A. and G. W. Brier (1958). Some applications of statistics to meteorology, Pennsylvania State University University Park, PA.

Piani, C., J. O. Haerter and E. Coppola (2009). "Statistical bias correction for daily precipitation in regional climate models over Europe." Theoretical and Applied Climatology **99**(1-2): 187-192.

Piani, C., G. P. Weedon, M. Best, S. M. Gomes, P. Viterbo, S. Hagemann and J. O. Haerter (2010). "Statistical bias correction of global simulated daily precipitation and temperature for the application of hydrological models." Journal of Hydrology **395**(3-4): 199-215.

Price, K., S. T. Purucker, S. R. Kraemer and J. E. Babendreier (2012). "Tradeoffs among watershed model calibration targets for parameter estimation." Water Resources Research **48**(10): n/a-n/a.

Prudhomme, C., N. Reynard and S. Crooks (2002). "Downscaling of global climate models for flood frequency analysis: where are we now?" Hydrological Processes **16**(6): 1137-1150.

Prudhomme, C., R. L. Wilby, S. Crooks, A. L. Kay and N. S. Reynard (2010). "Scenario-neutral approach to climate change impact studies: Application to flood risk." Journal of Hydrology **390**(3-4): 198-209.

Quan, D., C. Xing, C. Tiexi and C. Xing-Wu (2009). "Relationship between extremes of precipitation and discharge in the Huaihe River Basin." Journal of Nanjing University (Natural Science) **45**(6): 790-801.

Raff, D., T. Pruitt and L. Brekke (2009). "A framework for assessing flood frequency based on climate projection information." Hydrology & Earth System Sciences **13**(11).

Räisänen, J. (2007). "How reliable are climate models?" Tellus A **59**(1): 2-29.

Räisänen, J. and T. Palmer (2001). "A probability and decision-model analysis of a multimodel ensemble of climate change simulations." Journal of Climate **14**(15): 3212-3226.

Räisänen, J. and O. Räty (2012). "Projections of daily mean temperature variability in the future: cross-validation tests with ENSEMBLES regional climate simulations." Climate Dynamics: 1-16.

Reynard, N. S., C. Prudhomme and S. M. Crooks (2001). "The Flood Characteristics of Large U.K. Rivers: Potential Effects of Changing Climate and Land Use." Climatic Change **48**(2-3): 343-359.

Rojas, R., L. Feyen, A. Dosio and D. Bavera (2011). "Improving pan-European hydrological simulation of extreme events through statistical bias correction of RCM-driven climate simulations." Hydrol. Earth Syst. Sci. **15**(8): 2599-2620.

Salathe, E. P. (2005). "Downscaling simulations of future global climate with application to hydrologic modelling." International Journal of Climatology **25**(4): 419-436.

Schmidli, J., C. Frei and P. L. Vidale (2006). "Downscaling from GCM precipitation: a benchmark for dynamical and statistical downscaling methods." International Journal of Climatology **26**(5): 679-689.

Seiller, G., F. Anctil and C. Perrin (2012). "Multimodel evaluation of twenty lumped hydrological models under contrasted climate conditions." Hydrology and Earth System Sciences **16**(4): 1171-1189.

Shabalova, M., W. van Deursen and T. Buishand (2003). "Assessing future discharge of the river Rhine using regional climate model integrations and a hydrological model." Climate Research **23**(3): 233-246.

Shi, P., X. Ma, Y. Hou, Q. Li, Z. Zhang, S. Qu, C. Chen, T. Cai and X. Fang (2012). "Effects of Land-Use and Climate Change on Hydrological Processes in the Upstream of Huai River, China." Water Resources Management **27**(5): 1263-1278.

Slijkhuis, K. A. H., P. H. A. J. M. Van Gelder and J. Vrijling (1997). "Optimal dike height under statistical-construction-and damage uncertainty." Structural Safety and Reliability **7**: 1137-1140.

Solomon, S. (2007). Climate change 2007-the physical science basis: Working group I contribution to the fourth assessment report of the IPCC, Cambridge University Press.

Sorooshian, S. and V. K. Gupta (1983). "Automatic calibration of conceptual rainfall‐runoff models: The question of parameter observability and uniqueness." Water Resources Research **19**(1): 260-268.

Sperber, K. R., H. Annamalai, I. S. Kang, A. Kitoh, A. Moise, A. Turner, B. Wang and T. Zhou (2012). "The Asian summer monsoon: an intercomparison of CMIP5 vs. CMIP3 simulations of the late 20th century." Climate Dynamics **41**(9-10): 2711-2744.

Stainforth, D. A., T. Aina, C. Christensen, M. Collins, N. Faull, D. J. Frame, J. A. Kettleborough, S. Knight, A. Martin and J. Murphy (2005). "Uncertainty in predictions of the climate response to rising levels of greenhouse gases." Nature **433**(7024): 403-406.

Surfleet, C. G. and D. Tullos (2013). "Uncertainty in hydrologic modelling for estimating hydrologic response due to climate change (Santiam River, Oregon)." Hydrological Processes **27**(25): 3560-3576.

Surfleet, C. G., D. Tullos, H. Chang and I.-W. Jung (2012). "Selection of hydrologic modeling approaches for climate change assessment: A comparison of model scale and structures." Journal of Hydrology **464-465**: 233-248.

Tabor, K. and J. W. Williams (2010). "Globally downscaled climate projections for assessing the conservation impacts of climate change." Ecological Applications **20**(2): 554-565.

Taylor, K. E., R. J. Stouffer and G. A. Meehl (2012). "An Overview of CMIP5 and the Experiment Design." Bulletin of the American Meteorological Society **93**(4): 485-498.

Teutschbein, C. and J. Seibert (2012). "Bias correction of regional climate model simulations for hydrological climate-change impact studies: Review and evaluation of different methods." Journal of Hydrology **456–457**(0): 12-29.

Themeßl, M. J., A. Gobiet and G. Heinrich (2011). "Empirical-statistical downscaling and error correction of regional climate models and its impact on the climate change signal." Climatic Change **112**(2): 449-468.

Themeßl, M. J., A. Gobiet and A. Leuprecht (2011). "Empirical-statistical downscaling and error correction of daily precipitation from regional climate models." International Journal of Climatology **31**(10): 1530-1544.

Tian, Y., M. J. Booij and Y.-P. Xu (2013). "Uncertainty in high and low flows due to model structure and parameter errors." Stochastic Environmental Research and Risk Assessment **28**(2): 319-332.

Van Dantzig, D. (1956). "Economic decision problems for flood prevention." Econometrica: Journal of the Econometric Society: 276-287.

Van Gelder, P. H. A. J. M. (1996). How to deal with wave statistical and model uncertainties in the design of vertical breakwaters. Probabilistic Design Tools for Vertical Breakwaters; Proceedings Task 4 Meeting, Hannover, Germany.

Van Gelder, P. H. A. J. M. and J. K. Vrijling (1998). Sensitivity analysis of reliability-based optimization in sea dike designs. Sensitivity Analysis of Model Output**:** 313-315.

Vaze, J., D. A. Post, F. H. S. Chiew, J. M. Perraud, N. R. Viney and J. Teng (2010). "Climate non-stationarity – Validity of calibrated rainfall–runoff models for use in climate change studies." Journal of Hydrology **394**(3-4): 447-457.

Vrijling, J. K., W. Van Hengel and R. Houben (1995). "A framework for risk evaluation." Journal of Hazardous materials **43**(3): 245-261.

Vrugt, J. A., C. J. Ter Braak, H. V. Gupta and B. A. Robinson (2009). "Equifinality of formal (DREAM) and informal (GLUE) Bayesian approaches in hydrologic modeling?" Stochastic environmental research and risk assessment **23**(7): 1011-1026.

Wang, J. and Z. Zhang (2005). The calculation and analysis of flood volume in 2003 (in Chinese). Proceedings of Youth Forum of Huai River Regulation 青年治淮论坛论文集, China Water & Power Press.

Wemelsfelder, P. J. (1939). Wetmatigheden in het optreden van stormvloeden, Koninklijk Instituut van Ingenieurs.

Wilby, R., S. Charles, E. Zorita, B. Timbal, P. Whetton and L. Mearns (2004). "Guidelines for use of climate scenarios developed from statistical downscaling methods."

Wilby, R. L. (2005). "Uncertainty in water resource model parameters used for climate change impact assessment." Hydrological Processes **19**(16): 3201-3219.

Wilby, R. L., C. W. Dawson and E. M. Barrow (2002). "SDSM—a decision support tool for the assessment of regional climate change impacts." Environmental Modelling & Software **17**(2): 145-157.

Wilby, R. L. and I. Harris (2006). "A framework for assessing uncertainties in climate change impacts: Low-flow scenarios for the River Thames, UK." Water Resources Research **42**(2): n/a-n/a.

Wilby, R. L., L. E. Hay, W. J. Gutowski, R. W. Arritt, E. S. Takle, Z. Pan, G. H. Leavesley and M. P. Clark (2000). "Hydrological responses to dynamically and statistically downscaled climate model output." Geophysical Research Letters **27**(8): 1199-1202.

Wood, A. W. (2002). "Long-range experimental hydrologic forecasting for the eastern United States." Journal of Geophysical Research **107**(D20).

Wood, A. W., L. R. Leung, V. Sridhar and D. Lettenmaier (2004). "Hydrologic implications of dynamical and statistical approaches to downscaling climate model outputs." Climatic change **62**(1-3): 189-216.

Xia, J., H. Du, S. Zeng, D. She, Y. Zhang, Z. Yan and Y. Ye (2012). "Temporal and spatial variations and statistical models of extreme runoff in Huaihe River Basin during 1956–2010." Journal of Geographical Sciences **22**(6): 1045-1060.

Xu, C.-y. (1999). "From GCMs to river flow: a review of downscaling methods and hydrologic modelling approaches." Progress in Physical Geography **23**(2): 229-249.

Xu, C.-y., E. Widén and S. Halldin (2005). "Modelling hydrological consequences of climate change—progress and challenges." Advances in Atmospheric Sciences **22**(6): 789-797.

Xu, H., R. G. Taylor and Y. Xu (2011). "Quantifying uncertainty in the impacts of climate change on river discharge in sub-catchments of the Yangtze and Yellow River Basins, China." Hydrology and Earth System Sciences **15**(1): 333-344.

Xu, Y. and P. Chen (1999). "Economic assessment of flood defense system Bengbu City (In Chinese)." Journal of Economics of Water Resources **5**: 30-33.

Yang, C., Z. Lin, Z. Yu, Z. Hao and S. Liu (2010). "Analysis and Simulation of Human Activity Impact on Streamflow in the Huaihe River Basin with a Large-Scale Hydrologic Model." Journal of Hydrometeorology **11**(3): 810-821.

Yang, C., Z. Yu, Z. Hao, J. Zhang and J. Zhu (2012). "Impact of climate change on flood and drought events in Huaihe River Basin, China." Hydrology Research **43**(1-2): 14-22.

Yew Gan, T., E. M. Dlamini and G. F. Biftu (1997). "Effects of model complexity and structure, data quality, and objective functions on hydrologic modeling." Journal of Hydrology **192**(1–4): 81-103.

Zhang, X. C. (2005). "Spatial downscaling of global climate model output for site-specific assessment of crop production and soil erosion." Agricultural and Forest Meteorology **135**(1-4): 215-229.

Zhang, Y., J. Xia, T. Liang and Q. Shao (2010). "Impact of water projects on river flow regimes and water quality in Huai River Basin." Water resources management **24**(5): 889-908.

Zhao, R.-J. (1992). "The Xinanjiang model applied in China." Journal of Hydrology **135**(1–4): 371-381.

List of Symbols

Symbol	Description	Unit
X_O	the observed climatic variable during the baseline period	mm/^{o}C
X'_O	the downscaled climatic variable during the future period	mm/^{o}C
X_M	the climate model simulations for the baseline period	mm/^{o}C
X'_M	the climate model simulations for the future period	mm/^{o}C
T_{BC}	the statistical transformation functions for the BC based methods	
T_{CF}	the statistical transformation functions for the CF based methods	
WT_M	the modelled wet-day threshold	
WT_O	the observed wet-day threshold	
F	empirical cumulative distribution function	
F^{-1}	reversed empirical cumulative distribution function	
MRE_p	a factor of Mean Relative Error (MRE) at percentile p	
ABS	the absolute value	
X'_p	the pth percentiles of the downscaled distributions	mm/^{o}C
X_p^O	the pth percentiles of the pseudo-observed distributions	mm/^{o}C
X_p^{Raw}	the pth percentile of raw GCMs projection	mm/^{o}C
PET	potential evapotranspiration	mm
k	a monthly consumptive use coefficient	
p	the percentage of the daytime hours for each day out of total daytime hours of the year	
T	daily mean temperature	^{o}C
R	Runoff	mm
P	Rainfall	mm
Q	discharge at the basin outlet	m^3/s
F	the total area of a sub-basin	m^2
f	the pervious area of F	m^2
K	ratio of potential evapotranspiration to pan evaporation	
UM	tension water storage capacity of the upper layer	mm
LM	tension water storage capacity of the lower layer	mm
C	evaporation coefficient of the deep layer	
WM	areal mean tension water storage capacity	mm
B	exponential parameter of the soil moisture storage capacity curve	
IM	the percentage of the impervious area of the sub-basin	
SM	areal mean free water capacity of the surface soil layer	mm
EX	exponent of the free water capacity curve	
KG	outflow coefficient of the free water storage to groundwater	
KI	outflow coefficient of the free water storage to interflow	

CI	recession constant of the interflow storage	
CG	recession constant of the groundwater storage	
CS	recession constant in the Lag and Route method	
L	the lag parameter in the Lag and Route method	
M_i	the modelled monthly flow at the month i	m^3/s
O_i	the observed monthly flow at the month i	m^3/s
$\bar{O}$	the observed mean values of the flow character	m^3/s
$\bar{M}$	the modelled mean values of the flow character	m^3/s
SS_{tot}	the total sum of squares	
SS_{cali}	the sum of squares resulted from the choice of the calibration periods	
SS_{equi}	the sum of squares resulted from equifinal parameter sets	
$\bar{\Delta}_i$	the group mean of the results from the calibration period i	
Δ_{ij}	the projected relative change using the parameter set j calibrated from the calibration period i	
$\bar{\Delta}$	the grand mean of the results from all the parameter sets	
C	the total cost	Million RMB
I_0	the initial investment	Million RMB
I_1	the variable investment	Million RMB
S	the damage	Million RMB
r	the discount rate	
p	the annual flood probability	1/year
X	the height which the dike is raised by	m
h_0	the current dike crest height	m
A	the location parameter of the probabilistic distribution	
B	the scale parameter of the probabilistic distribution	
C	the shape parameter of the probabilistic distribution	
$f(A)$	the distribution of the location parameter	
$f(B)$	the distribution of the scale parameter	
$f(C)$	the distribution of the shape parameter	
μ	mean	
σ	standard deviation	
$\mu(P)$	the expected predictive flood probability	1/year
P_0	the present flood probability	1/year
P_i	the flood probability in the year i	1/year
γ	the increasing rate of flood probability	
k	the index of the level of risk aversion	
Y	a Bernoulli variable	

List of Abbreviations

GCM	General Circulation Model/Global Climate Model
CDF	cumulative distribution function
PDF	probabilistic density function
GEV	Generalized Extreme Value
IPCC	Intergovernmental Panel on Climate Change
AR	assessment report
CMIP	Coupled Model Intercomparison Project
WCRP	World Climate Research Programme
WGCM	Working Group on Couples Modeling
WMO	World Meteorological Organization
UNEP	United Nations Environment Programme
GHG	greenhouse gas
SERS	Specral Report on Emissions Scenarios
RCP	representative concentration pathways
BC	bias correction
CF	change factor
MB	mean based
VB	variance based
QM	quantile mapping
QC	quantile correcting
TF	transfer function
Obs	observation
Mod	model simulation
wd	wet day
S.D.	standard deviation
NSE	Nash-Sutcliff efficiency
PVE	percentage volume error

List of Tables

List of Figures

Acknowledgement

On the evening of 16th December 2009, I arrived at Amsterdam Schiphol Airport. It was my first time to be in a foreign land, and it was also the start of a challenging period of my life. This thesis book is a memorial to this period of my life, and it is, of course, a happy ending of my PhD study. It is my pleasure to express my gratitude to the people who made this thesis possible.

First, I would like to thank my promotors: Prof. Han Vrijling and Prof. Pieter van Gelder. Thank you for giving me the opportunity to do my PhD study in a country famous for its flood defenses and provided valuable guidance on my study. Prof. Vrijling, thank you for your inspiring advices which open my mind. I am happy to talk with you about my study as well as the hot events in China and the Netherlands. My Chinese colleagues and I will always remember the nice tour on your boat. We enjoyed it very much. Prof. van Gelder, thank you so much for your guidance during my PhD study. You were always encouraging and patient, which greatly improved my confidence and helped me challenge the difficulties in my study.

I also would like to express my gratitude to Prof. Roshanka Ranasinghe and Assoc. Prof. Shreedhar Maskey, who gave me very valuable suggestions in the aspects of downcaling and hydrological modeling, respectively. Thank you very much for your advices which greatly helped me finish this thesis. I cherish our inspiring discussions a lot.

My special thanks are extended to Prof. Bas Jonkman, Prof. Paolo Reggiani and Dr. Jan Verkade who offered me great help when I was looking for the research topic at the beginning of my PhD study.

The China Scholarship Council (CSC) is acknowledged for its financial support for this study. Stichting Het Lamminga Fonds is also acknowledged for partly financing this study. I would like to thank Prof. Marcel Stive for his approval of Stichting Het Lamminga Fonds and his efforts in making the Chinese students feel at home.

Thanks are also addressed to Ms. Franca Post and Mr. Cees Timmers from CICAT for their arrangement before and during my stay in the Netherlands. I am very grateful to Ms. Mariette van Tilburg, who offered me great help in checking the English language and translating the propositions and summary of this thesis. Assistance provided by our secretaries, Ms. Judith Schooneveld, Ms. Agnes Groenestein and Ms. Inge van Rooij is greatly appreciated.

I wish to thank many people in the Netherlands I met who make my life interesting and help me survive my PhD life. I do not know where the future will take us, and I would like to list your names here and keep you in my memory: Mei Xuefei, Gong Xun, Ke Qian, Xu Zijin, Meng Wei, Li Fan, Dang Xiangxiang, Li Mingliang, Wu Dongju, Zhao Gensheng, Zhong Hua, Cui Haiyang, An Ran, Wang Haiqiang, Wu Qi, Zhang Xiaoyu, Shi Huajie, Zhang Lu, Cui Hao, Shang Ran, Hu Jingyi, Zhang Xuedong, Li Sheng, Lu Jie, Cai Huayang, Chen Bishuang, Dong Congli, Jacqueline Isabella Anak Gisen and Mr. Lin, Wang Ling, Fei Cui, Tang Jiaqi, Wang Jing, Zhu Shouen, Zhou Yang, Chen Linying and Huang Yamin, Hu Zhan, Su Min, Yao Peng, Chu Ao, Li Wei, Chen Xuexue, Niu Lixia, Yan Hong, Lu Jie, Gong Jiakun, Zhao Xiaoyan, Huang Haoliang, Deng Qiwen, Jiang Xu, Qiang Xuhong, Jasna Duricic, Saulo Meirelles Nunes Da Rocha and Mini, Myron van Damme, Wiebke Jaeger, Vana Tsimopolou, Dominik Paprotny, Le Hai Trung, Cong Van Mai, Poonam Taneja, Peter Quist, Ms. Wang Xiali, Wei Xiaoyan, Vera, Alida, Maarten Mulder… Due to the limited space, it is not possible to list all the names, but I would like to express my humble thanks to all the people I know.

Last but not the least, I would like to express my deep sense of gratitude and appreciation to my family. Sorry that I have been on the run to explore the world outside and not being with you everyday. To my husband, Wang Shuzheng, thank you for keeping us together wherever I go. Thank you for being the one who listens to my problems and wipes my tears away. I am grateful to have you in my life. To my parents, you are my role models for my future professional career. I am not me without you. Thank you for always believing in me and encouraging me to do my best. Thank you for the support and unconditional love you've been giving me.

Lu Wang

April 2015 in Delft

Curriculum Vitae

Lu Wang was born in the Handan City, Hebei Province, China, on September 25, 1984. From 2003 to 2007, she studied Hydrology and Water Resources Engineering at Hohai University, Nanjing, China. She continued to do her MSc study at Hohai University in 2007 and obtained the MSc degree in Hydrology and Water Resources in 2009. During her MSc study, she participated in a couple of research projects: Project of the Technology of Warning and Risk Management on Extreme Floods and Droughts in China and Project of the Regional Water Cycle Model and Uncertainty Analysis in the Headstream Region of Yellow River under Climate Change. In December 2009, she started her PhD study at the Section of Hydraulic Structures and Flood Risk, Delft University of Technology, the Netherlands. This PhD study was financially supported by the Chinese Scholarship Council (CSC) and partially supported by Stichting Het Lamminga Fonds. In July 2010, she got trained in the Erasmus Intensive Programme: Integrated Multidisciplinary Approach to Flood Risk Analysis. Lu Wang's future research interests are climate change impact assessment and adaptation decision-making, statistical downscaling, and flood risk analysis.

Peer-reviewed publications

L. Wang, R.W.M.R.J.B. Ranasinghe, S. Maskey, P.H.A.J.M. Van Gelder, J.K. Vrijling. Comparison of empirical statistical methods for downscaling daily climate projections from CMIP5 GCMs: a case study of the Huai River Basin, China. International Journal of Climatology, 2015 (In press). DOI: 10.1002/joc.4334

L. Wang, P.H.A.J.M. Van Gelder, J.K. Vrijling, S. Maskey, and R.W.M.R.J.B. Ranasinghe. Risk-averse economic optimization in the adaptation of river dikes to climate change. Water Resources Management, 2014: 1-19.

Yueguan Zhang, Fengge Su, Zhenchun Hao, Chongyu Xu, Zhongbo Yu, Lu Wang, Kai Tong. Impact of projected climate change on the hydrology in the headwaters of the Yellow River Basin. Hydrological Processes. (Accepted)

Qin Ju, Zhenchun Hao, Lu Wang and Weijuan Jiang. Evaluation of IPCC AR4 global climate model simulation over Yangtze River Basin. Cold Region Hydrology in a Changing Climate, 2011, IAHS Publ.346: 144-149.

Conferences

L. Wang, P.H.A.J.M. Van Gelder, J.K. Vrijling, R.W.M.R.J.B. Ranasinghe, and S. Maskey (2013, June). Coping with the uncertainties in the climate change adaptation of river dikes

using risk-aversion economic optimization. In 8th International Conference of EWRA" Water Resources Management in an Interdisciplinary and Changing Context", Porto, Portugal, 26-29 June 2013. European Water Resources Association (EWRA). (Oral presentation).

L. Wang, P.H.A.J.M. Van Gelder and J.K. Vrijling. A preliminary analysis of climate change effect on long-term risk-based design of flood defense. Proceedings of EGU General Assembly 2012 (22-27 April, Vienna, Austria) Geophysical Research Abstracts Vol. 14, EGU2012-2079, 2012 EGU General Assembly 2012. (Poster presentation)

L. Wang, P. Reggiani, P.H.A.J.M. Van Gelder and J.K. Vrijling. GCMs simulative ability on climatic and extreme hydrologic conditions over Chinese Huai River Basin. Proceedings of EGU General Assembly 2011 (April 3-8 2011, Vienna, Austria) Geophysical Research Abstracts Vol. 13, EGU2011-1068, 2011. (Oral presentation)

Lu Wang, Zhenchun Hao, Pieter Van Gelder, P.Reggiani, J.K.Vrijling. Scenario-Based Prediction of Extreme Floods in the Chinese Huai River Basin under Climate Change. The 8th International Probabilistic Workshop, Maritime University of Szczecin, (2010), pp (377-400). ISBN 978-83-89901-49-1. (Oral presentation)